Research Square

Preprints are preliminary reports that have not undergone peer review.
They should not be considered conclusive, used to inform clinical practice,
or referenced by the media as validated information.

Seed-applied multi-kingdom synthetic communities selectively reshape bacterial communities and highlight key criteria for strain selection

Logan Suteau

logan.suteau@gmail.fr

Univ Angers, Institut Agro, INRAE, IRHS, SFR QUASAV, F-49000 Angers, France

Claire Campion

Univ Angers, Institut Agro, INRAE, IRHS, SFR QUASAV, F-49000 Angers, France

Coralie Marais

Univ Angers, Institut Agro, INRAE, IRHS, SFR QUASAV, F-49000 Angers, France

Martial Briand

Univ Angers, Institut Agro, INRAE, IRHS, SFR QUASAV, F-49000 Angers, France

Anaïs Hardouin

Univ Angers, Institut Agro, INRAE, IRHS, SFR QUASAV, F-49000 Angers, France

Kaat Hellyn

Univ Angers, Institut Agro, INRAE, IRHS, SFR QUASAV, F-49000 Angers, France

Kenji Maurice

Univ Angers, Institut Agro, INRAE, IRHS, SFR QUASAV, F-49000 Angers, France

Muriel Marchi

Univ Angers, Institut Agro, INRAE, IRHS, SFR QUASAV, F-49000 Angers, France

Marie Simonin

Univ Angers, Institut Agro, INRAE, IRHS, SFR QUASAV, F-49000 Angers, France

Natalia Guschinskaya

Univ Angers, Institut Agro, INRAE, IRHS, SFR QUASAV, F-49000 Angers, France

---

Research Article

Keywords: Seedling microbiota, Fungi, Yeasts, Bacteria, Transmission, Microbiota engineering, Defined microbial communities

Posted Date: August 3rd, 2026

DOI: https://doi.org/10.21203/rs.3.rs-10369696/v1

License: This work is licensed under a Creative Commons Attribution 4.0 International License.
Read Full License

Additional Declarations: No competing interests reported.

Title page

Seed-applied multi-kingdom synthetic communities selectively reshape bacterial communities and highlight key criteria for strain selection

Authors: Logan Suteau, Claire Campion, Coralie Marais, Martial Briand, Anaïs Hardouin, Kaat Hellyn, Kenji Maurice, Muriel Marchi, Marie Simonin, Natalia Guschinkaya

Logan Suteau logan.suteau@gmail.com
Claire Campion claire.campion@univ-angers.fr
Coralie Marais coralie.marais@inrae.fr
Martial Briand martial.briand@inrae.fr
Anaïs Hardouin anais.hardouin@inrae.fr
Kaat Hellyn kaat.hellyn@inrae.fr
Kenji Maurice kenji.maurice@inrae.fr
Muriel Marchi muriel.marchi@inrae.fr
Marie Simonin marie.simonin@inrae.fr
Natalia Guschinskaya natalia.guschinskaya@univ-angers.fr

Affiliation :
Univ Angers, Institut Agro, INRAE, IRHS, SFR QUASAV, F-49000 Angers, France

Corresponding author :
Logan Suteau logan.suteau@gmail.com
Natalia Guschinskaya natalia.guschinskaya@univ-angers.fr

Abstract:

Defined microbial communities (also known as synthetic communities) are showing promising results for plant health but are lacking an efficient lab to field transition. This is the due to limited knowledge on how to efficiently modulate plant microbiota by considering complex environments and multi-kingdom interactions. In this study, we aimed to better understand the transmission and impact of multi-kingdom synthetic communities (SynComs) from the seed to seedling stage. We constructed 20 different SynComs using both *a priori* and random approaches, from pool of diverse strains including 24 bacteria, 11 yeasts and 10 filamentous fungi. SynComs were inoculated on *Brassica napus* seeds and we monitored both transmission and impact on the microbiota of 15-day-old seedlings grown in non-sterile soil. Optimization of the inoculation protocol showed that alginate coating improved

bacterial, yeast and filamentous fungi concentrations by more than 2 log compared with other approaches. With this inoculation method, we observed contrasted seedling colonization profiles, with SynComs members representing between 1.1-45.7% of bacterial community and 3.2-36.6% of fungal community. Our multiple SynCom design revealed that strain selection is a more critical determinant of SynCom performance than assembly strategy. Even randomly assembled communities performed well, as long as they are drawn from a pool of ecologically relevant, well-adapted taxa. Based on these evidences, we identified key bacterial and fungal traits explaining efficient seedling colonization such as high abundance on inoculated seed and low *in vitro* lag-time. Despite low colonization levels, we observed that SynCom inoculation altered seeding bacterial community assembly in 14 SynComs. A total of 82 native bacterial ASVs were identified as responsive to SynCom inoculation, most likely originating from the soil. This shift indicates that SynComs influence community assembly by modulating the recruitment of environmental taxa, especially when SynCom strains were more integrated in multi-kingdom network structures. Finally, we identified four distinct SynComs profiles which either colonized strongly or not seedlings while shifting of not native microbiota. Altogether, these findings provide actionable directions for improving SynCom design, suggesting that leveraging ecological processes such as host adaptation, optimal inoculation density, and network integration could enhance both colonization efficiency and plant phenotypic outcomes.

Keywords:

Seedling microbiota, Fungi, Yeasts, Bacteria, Transmission, Microbiota engineering, Defined microbial communities.

Background:

An increasing number of studies use defined microbial communities [1] also known as synthetic communities (SynComs) [2] on plants to modulate plant phenotype [3] and protect against biotic and abiotic stressors [4, 5]. While having beneficial effects in controlled conditions, these methods are not as performant in the field and suffer a lack of efficient transfer from lab to more realistic conditions [6, 7]. With most studies mainly focusing on phenotypic effect and neglecting colonization dynamics of the SynCom, low performance can be often attributed to a weak establishment of the inoculant [7]. Furthermore, the lasting effects of these inoculants on the native microbiota is still underestimated despite the ecological risks they imply [8]. These knowledge gaps highlight the needs for a better monitoring of the colonization process of microbial inoculants on plants.

Microbial interactions play an important role in the assembly and dynamics of plant and soil microbiota. When inoculated, SynCom encounters native communities (e.g. soil, seed), triggering community coalescence described as the joining of previously separate communities into a new entity

[9]. During this event, both inoculated and native strains will compete for similar resources [10, 11] and engage in molecular dialogue [12]. Pioneer studies on SynCom inoculation suggest that both the number of organisms (i.e. propagule size [13]) and the timing of arrival (i.e. priority effects [14]) are key drivers of the successful establishment within communities [15]. Thus, a better understanding and consideration of the ecological processes at play during SynCom inoculation is key to improve inoculation success [16].

One way to harness these ecological processes is also to target specific "critical windows" during plant development that could be more favorable for inoculant establishment. For instance, at the seed stage native plant microbiota is sparse, favoring inoculant establishment through priority effect and propagule pressure [14]. Improvement in seed technologies also allows the coating of seed for a more efficient delivery of microorganisms [17]. The inoculation and monitoring of bacterial communities in seed to seedling stages has shown promising results with high colonization [15, 18]. However, like most studies using SynComs inoculation experiments, the focus has primarily been on bacterial communities, while only a few studies consider both bacterial and fungal inoculation (4 out of 86 surveyed in Xu et al., 2025 [19]). Yet, interkingdom interactions between bacteria and fungi naturally occur within plant microbiota and modulate plant phenotype [20]. More recently, an increasing interest has grown in multi-kingdom inoculum as they enhance disease suppressiveness [21, 22] .Still, while we know that complex interactions occur between these kingdoms [23], limited knowledge on how to design and inoculate efficiently these multi-kingdom inoculants is available. An upgraded guideline for the use of multi-kingdom inoculant is then required to fully harness the beneficial effects mediated by these multi-kingdom interactions.

In this study, we aim to gain a deeper understanding of multi-kingdom SynCom inoculation to characterize their colonization success of seeds and seedling, and their impact on the native microbiome. To do so, 20 different SynComs were designed based on distinct criteria and inoculated onto *Brassica napus* L. seeds and grown for 15 days in non-sterile soil. We hypothesized that both fungal and bacterial strains inoculated onto seed would be transmitted to the seedling (H1).

As SynCom outperforms single strain inoculant in colonization and survival [24], a better understanding of efficient strain combination is required. That is why we hypothesized that SynCom designs based on specific assembly criteria would achieve higher colonization than those assembled randomly (H2). We aimed to find easily characterizable traits for an entire microbial collection such as natural abundance and prevalence in target habitat (here seed and seedling) as potential indicators of host adapation [25], taxonomic distance as indicator of reduced niche competition [26] and growth speed for quicker access to resources [27].

Even though SynCom composition should be a main driver of colonization through microbial interactions, specific strain traits might be linked to a higher colonization. Thus, identifying these traits could allow a future better selection of strains for SynCom composition. Here, we also hypothesized that strains traits could influence their colonization success but could differ between bacteria and fungi (H3). We investigated traits relative to the native abundance and prevalence of strains, their proportion in inoculant (relative abundance in inoculated seeds) as well as basic phenotyping traits (*in vitro* growth parameters).

Finally, plant microbiome assembly is a dynamic process that evolves throughout development [28]. In native conditions, seedling microbiota is mostly shaped by its environment [29, 30]. In this context, ecological processes such as priority effects [14] and community coalescence [9] are known to play key roles in shaping microbiome structure and dynamics. We therefore hypothesized that SynCom inoculation would alter the recruitment of both soilborne and native seedborne microbiota during seedling microbiota assembly, and that these shifts would be associated with specific inoculated strains or SynCom composition (H4)

Methods:

- **Biological material:**

Microbial strains:

The bacterial and fungal strains used in this study were obtained from Simonin *et al*., 2026 that aimed to create a diverse collection of seed-borne microorganisms [31]. Briefly, seeds from four *Brassica napus* L. (oilseed rape) genotypes (Jupiter, Aviso, Mohican, Milena), produced under two production modes (open-field vs self-pollinated cages), were used for isolation from both seeds and seedlings germinated under gnotobiotic conditions. The bacterial strains were isolated on Tryptic Soy Agar (TSA) 10% strength and fungal strains on Malt Agar (MA) medium. This collection resulted in a total of 636 bacterial and 188 fungal strains. A preliminary genotyping of all isolates was performed using metabarcoding of the *gyrB* bacterial marker gene (Illumina Miseq) or NS7/ITS4 + D1/D2 regions for yeasts (Sanger sequencing) and NS7-ITS4 for filamentous fungi (Sanger sequencing). The representativeness of the strain collection was assessed by comparing it to the bacterial and fungal community composition of the same seeds and seedlings used for strain isolation. It showed that 17% of the bacterial diversity and 6% of the fungal diversity detected by metabarcoding in seed lots was recovered through isolation. Even if these numbers appear to be low, the most prevalent and abundant taxa were isolated and the collection represented 69% (bacteria) and 75% (fungi) of the total relative abundance of the seed microbiota.

Plant material:

We used winter oilseed rape seeds of the Jupiter genotype produced under open-field conditions in 2020 at the IGEPP field station, Le Rheu, Bretagne (48.13916, -1.799776) and stored at 9°C. These seeds are from the same seed lot than the one used for the microbial collection.

Strain culture conditions and phenotyping:

Bacterial strains were routinely grown on 10% TSA medium at 18°C and fungal strains were grown on MA medium at 20°C. For growth rate assessment, bacterial strains were adjusted to an optical density of 600 nm (OD600) of 0.01 in 10% Tryptic Soy Broth (TSB) and monitored by spectrophotometry. Optical density was measured with a spectrophotometer over 72h at 25°C. Yeasts and filamentous fungi growth was also measured in liquid culture in Malt Broth (MB) at a final concentration of 10^5 cells.mL^{-1} using nephelometry [32] at 25°C over 72h.

- **SynCom strains selection:**

A subset of strains from the microbial collection was preselected for SynCom design. Further criteria have been used.

Taxonomy:

First, one representative strain per genus was selected to capture the phylogenetic diversity associated with oilseed rape seeds. For the highly abundant genera (*Pantoea*, Pseu*domonas, Vishniacozyma, Holtermaniella* and *Cladosporium*), multiple strains were selected. This resulted in a preliminary set of 23 filamentous fungi, 27 yeasts and 60 bacterial strains chosen.

Strain growth rate *in vitro* condition:

Each strain was cultured to verify purity and viability after conservation. Growth parameters were then assessed for all strains using liquid microplate cultures. When multiple strains shared the same unique Amplicon Sequence Variant (ASV), the strain with the highest growth rate was selected; when no differences were observed, one strain was randomly chosen.

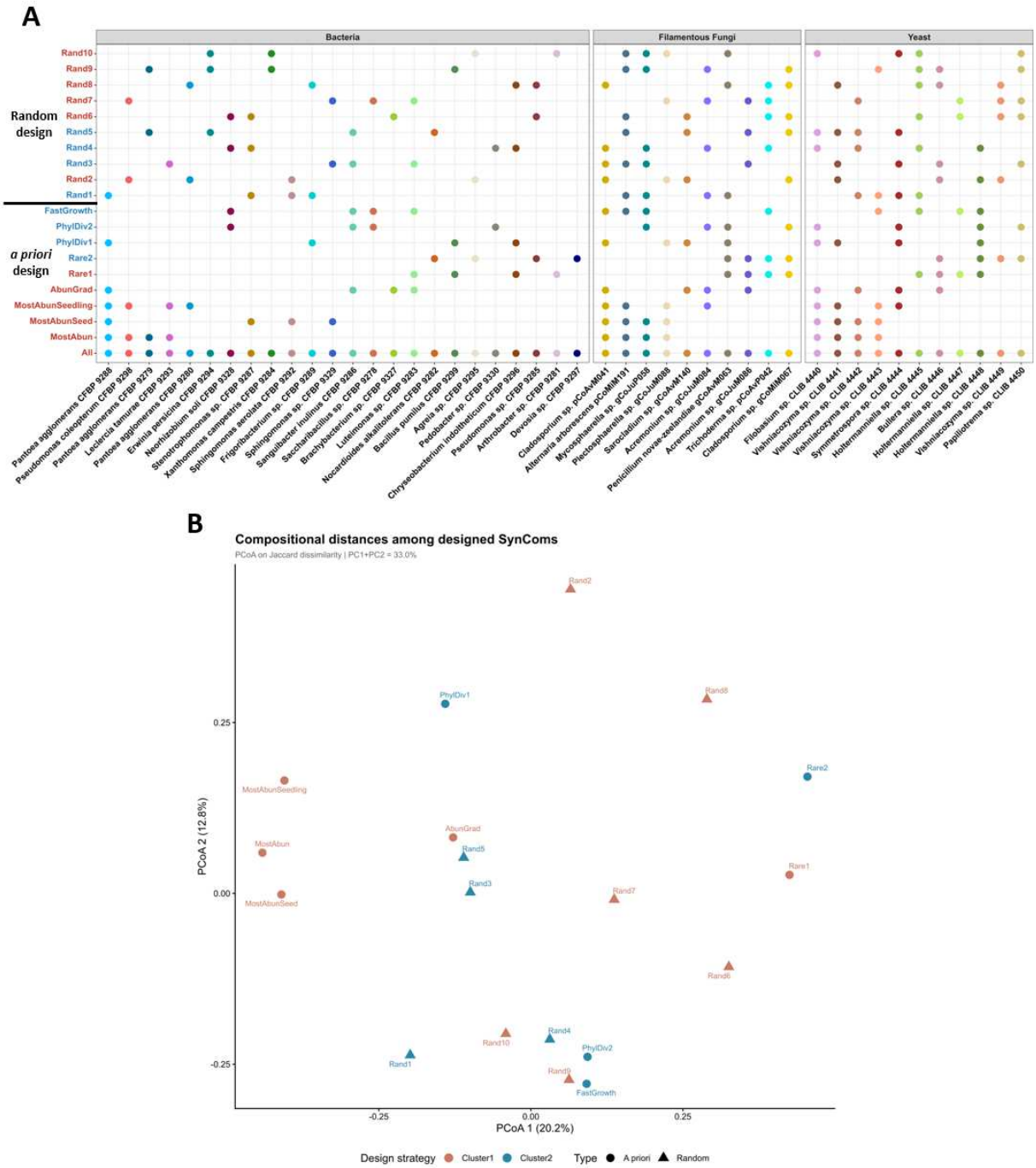
Sporulation:

For filamentous fungi, conidia production and spore viability were assessed, and strains unable to produce conidia were excluded as inoculation required conidia.

The final selection included 24 bacterial strains, 10 filamentous fungi and 11 yeasts with unique *gyrB* (bacteria) or ITS1 (fungi) ASV, enabling their detection in SynCom experiments *via* metabarcoding. Detailed information on all strains is provided in Table S1.

- **SynCom design:**

A total of 20 different SynComs were built, 10 of them using *a priori* criteria and 10 using random strain sampling. 19 out of 20 SynCom consisted of 12 strains: 4 bacteria, 4 yeast, and 4 filamentous fungi, to approach a low microbial richness typically observed in seeds [33]. Using metabarcoding data from Simonin *et al.* (2026) [31], we assessed the natural prevalence and relative abundance of each strain in the seed and seedling microbiota. Based on these data, seven SynComs were constructed: one containing the most abundant strains on seeds, one with the most abundant strains on seedlings, one with the most abundant strains overall, and two containing rare strains (*i.e.,* strains isolated but not detected by metabarcoding). One of them was designed to represent an abundance gradient, including the most abundant strains on seed and seedling, two strains with intermediate abundance, and one rare strain. Finally, a high richness SynCom was assembled by combining all selected strains (45 strains in total). In addition, two SynComs maximizing phylogenetic diversity were constructed by selecting strains from distinct families. One SynCom was composed of the fastest-growing strains in synthetic media. The remaining 10 SynComs were designed randomly by sampling with replacement between independent SynCom, while maintaining the composition of 4 bacteria, 4 filamentous fungi and 4 yeasts. In total, 20 SynComs were designed (Fig. 1A). Across these SynComs, each bacterial strain was included between 2 and 7 times, each yeast strain between 5 and 10 times, and each filamentous fungi strain between 6 and 11 times. The representativeness of the assembled SynComs out of all possible strain combinations was calculated and represented in a theoretical composition space (Supplementary material and methods). To assess the difference in SynCom composition, their compositional dissimilarity was assessed according to supplementary materials and methods (Fig. 1B). In brief, pairwise compositional dissimilarity between all communities (theoretical and effective) was quantified using the binary Jaccard distance and distance matrices were subjected to Principal Coordinates Analysis (PCoA).



186

187 Fig. 1: **SynCom composition**. (A) SynCom strain members and their distribution in the different SynComs used
188 during this study. Strains are divided between Bacteria (n = 24), Filamentous fungi (n = 10) and Yeast (n = 11).
189 SynComs are divided between Random and *a priori* constructions and colored to either Cluster 1 or Cluster 2
190 based on result presented later in the article. (B) Principal Coordinates Analysis (PCoA) of binary Jaccard distances
191 among the 19 experimentally designed 4B+4F+4Y SynComs, based on a 45-strain binary presence–absence
192 matrix (Cailliez correction). Points are shaped by design strategy and colored by cluster. Axis labels report the
193 percentage of total variance explained. Individual SynCom identifiers are annotated.

194

195 - **Seed inoculation optimization:**

To optimize the inoculation of SynComs on *Brassica napus* L. seeds, four inoculation methods were evaluated. The objectives were to increase microbial biomass on seeds, while maintaining a balanced proportion between bacteria, yeasts and filamentous fungi. In addition, we aimed to avoid negative effects on seed germination and to ensure reliable recovery of inoculated microorganisms for subsequent assessment of seed colonization. The four methods tested were seed soaking in different conditions (sterile water, 10mM $MgCl_2$, 2.4% glycerol) or seed coating in 2.4% sodium alginate. Each condition was applied to 120 seeds.

Each method was used to inoculate a bacterial strain (*Pantoea agglomerans* CFBP 9288) a yeast (*Filobasium* sp. CLIB 4440), the fungal strain *Cladosporium* sp. pCoAvM041, and a control condition using sterile water instead of microbial suspension resulting in a total of four independent inoculations. Seeds were inoculated at a 10^6 microorganisms.mL^{-1} concentration and dried for 10 min under a laminar flow hood. To assess seed colonization, eight seeds per each condition and per method were individually macerated in sterile water, or in 1% sodium citrate for alginate-coated seeds. Germination was evaluated by placing 100 seeds per condition on pleated paper, followed by incubation for 2 days in the dark at 20°C and 12 days under a 16h light and 8h dark photoperiod.

- **SynCom inoculation on *Brassica napus* seed**

The 20 SynComs were inoculated on *Brassica napus* seeds. Each strain was first prepared individually at a target concentration of 10^6 microorganisms.mL^{-1}, then mixed in equal proportions to assemble the SynComs. The resulting cultures were combined with sodium alginate to a final concentration of 2.4% method selected based on the previous experiment). Then, for each SynCom, 0.55 g of *Brassica napus* seeds (20 independent lots) were rinsed three times with sterile water and soaked in the SynCom suspensions for 30 min at 20°C under constant agitation. Seeds were then individually transferred into 10mM $CaCl_2$ to induce alginate encapsulation, dried, and 84 seeds were sown in non-sterile potting soil (Traysubstrat 092, Klassmann) per condition. Plants were grown in a greenhouse for 15 days and watered twice prior to harvest. To assess seedling phenotypes based on seed testing standards, we followed the International Seed Testing Association ISTA [34] guidelines. We classified each plant in three potential categories: non germinated, normal seedling, abnormal seedling to estimate the emergence and normality rates. Seedlings were considered abnormal when more than 50% of the cotyledons or leaves were necrotic or rotten, if the hypocotyl or epicotyl were deformed, or if the root system was absent, stunted, or rotten. For each condition, eight entire normal seedlings were collected and whole seedlings microbial communities were analyzed using metabarcoding. Roots were washed in sterile water prior to DNA extraction to minimize the presence of soil-associated organisms. Seedling hypocotyl length was measured on the remaining seedlings to assess the potential impact of SynCom inoculation on plant phenotypes.

- **DNA extraction, *gyrB* and ITS1 sequencing:**

The following metabarcoding approach was performed on the inocula, inoculated seeds and seedlings. For inocula, 200 µL of each fresh inoculum was instantly stored at −80˚C prior to DNA extraction. For inoculated seeds, eight seeds per condition were individually macerated in 1% sodium citrate and incubated overnight (∼16h) at 4°C under agitation (150 rpm). A 200µL aliquot from each suspension was plated to assess seed inoculation and then stored at -80°C. Control samples consisted of a pool of 30 seeds macerated in 1mL under the same conditions, and processed identically. Whole seedling samples were crushed using a roller, followed by the addition of 5mL of sterile water. Samples were then ground for 30s using a stomacher. DNA was extracted using 200 µL of the resulting suspension using the NucleoSpin® 96 Food kit (Macherey-Nagel, Düren, Germany), following the manufacturer's protocol. For potting soil, four replicates of 200 mg were sampled from control samples during seedling harvest and extracted using the DNeasy PowerSoil Pro kit (Qiagen), following the manufacturer's protocol.

For bacterial communities, the *gyrB* gene was amplified using gyrB_aF64 (5'-MGNCCNGSNATGTAYATHGG-3') and gyrB_aR353 (5'-ACNCCRTGNARDCCDCCNGA-3') primers [35]. PCR reactions were performed with Q5 High-Fidelity DNA Polymerase (NEB, Ipswich, Massachusetts, USA) in a 50 µL reaction volume containing 10 µL of 5X Reaction Buffer, 10 µL of 5X High GC Enhancer, 1 µL of 10mM dNTP mix, 1 µL of each forward and reverse primers (100 µM), 0.5 µL of polymerase, and 10 µL of DNA. Cycling conditions included an initial denaturation step at 98◦C for 3 min, followed by 25 cycles of amplification at 98˚C (30 s), 55˚C (45 s), and 72˚C (90 s), with a final elongation at 72˚C for 10 min. Fungal communities identification was based on the internal transcribed spacer (ITS) region amplification using primers ITS1F_Mi (5'-CTTGGTCATTTAGAGGAAGTAA-3') and ITS2_Mi (5'-GCTGCGTTCTTCATCGATGC-3') [36]. Amplification was performed using the same conditions as described for *gyrB* except a primer concentration of 10µM and a hybridation step at 50°C.

Amplicons were purified using magnetic beads (Sera-MagTM, Merck, Kenilworth, New Jersey). A second PCR was performed to add Illumina adapters and barcodes, with the following cycling conditions: denaturation at 98°C (1 min), followed by 10 cycles at 98°C (1 min), 55˚C (1 min), and 72°C (1 min), and a final elongation step at 72°C for 10 min. For ITS purification, an additional PCR product migration step on 1.8% agarose gel (70 V, 90 min) was performed to separate and recover fungal ITS (lower band, around 400 bp) from co-amplified plant ITS (higher band, >600 bp). The lower band was excised, extracted and purified using NucleoSpin Gel and PCR Clean up kit (Macherey-Nagel, Düren, Germany) and bead purified once more.

Library concentration was quantified using quantitative PCR (KAPA Library Quantification Kit, Roche, Basel, Switzerland). Libraries were mixed with 15% PhiX and sequenced using two MiSeq reagent kits

v2 500 cycles (Illumina). Quality controls included a blank extraction kit control, a PCR-negative control, PCR-positive control (*Lactococcus piscium* DSM6634, a fish pathogen that is not plant-associated or *Saccharomyces cerevisiae*, a yeast that is not plant-associated) and a bacterial mock community, included in each PCR plate. Raw amplicon sequencing data are available at the European Nucleotide Archive (ENA) under accession number PRJEB91662.

- **Long read genome extraction, sequencing, assembly and taxonomic affiliation:**

Genome extraction and sequencing:

High molecular weight bacterial DNA was extracted using the Wizard Genomic DNA Purification kit (Promega, A1120) with a slightly modified protocol. Cells were grown for 24 h in 10% TSB and washed three times with 50 mM EDTA. To preserve DNA integrity, no vortexing was applied and pipetting was minimized. Protein precipitation was performed twice to improve DNA purity. High molecular weight fungal DNA was extracted using a modified Möller protocol [37]. In brief, cultures were flash frozen and crushed, then washed three times with methanol-0,1%2-mercaptoethanol. Cells were resuspended in TES (100mM TRIS pH 8.0, 10mM EDTA, 2% SDS) and 100µg of proteinase K at 60°C for 1h for cell lysis. Washing steps included 1.4M NaCl and 1% CTAB, protein precipitation with SEVAG (Chloroform:Isoamyl Alcohol (24:1 V:V)) on ice and 1.6M NH_4Ac. DNA was precipitated with isopropanol and washed thrice with 70% ethanol before resuspension in water. DNA quality, concentration and fragment length were assessed using respectively a NanoDrop™ One Spectrophotometer, Qubit™ fluorometer and 1.5% gel electrophoresis. Afterwards, 1.5 µg of each strain's DNA was used for long-read sequencing with the Ligation sequencing gDNA - Native Barcoding Kit 24 V14 (SQK-NBD114.24) on the MinION Mk1D (Oxford Nanopore Technologies) sequencer using a FLO-MIN114 flow cell. The raw electrical signals obtained were then converted into a DNA sequence using the Dorado software, applying version of the high accuracy basecalling model available at the time the sequencing was carried out.

Genome assembly and taxonomic affiliation:

Bacterial genomes were assembled using Flye 2.9.5-b1801 [38]. Genomes that were not fully circularized were reassembled using different subsets of reads selected with filtlong. Checks for completeness and contamination were done with CheckM v1.2.2 [39] and taxonomic affiliation with gtdbtk v2.4.0 [40]. For fungal genomes, read filtering was done with NanoFilt 2.8.0, assembly with Flye 2.9.5-b1801, polishing with Racon v1.4.20 and biological completeness was estimated using BUSCO 6.0.0. Taxonomic affiliation was realized on the already known genus of the strain by using specific sequences detailed in Table S2. Each sequence used for comparison was obtained through *in silico* amplification on the assembled genome. For each specific gene, multiple sequence alignment was

done using MAFFT (v7) to obtain a same length sequence of the gene for all compared species. All trimmed genes were then aggregated to create a phylogenetic tree (Supplementary Fig.1 and Supplementary Fig.2) with IQ-TREEusing Ultrafast bootstrap (1000 iterations). For each investigated genus, the set of strains used for comparison and their sequence accession are available in Table S3 to S11. All assembled genome accession numbers can be found in Table S1.

- **Statistical and microbiota analyses:**

Bioinformatic processing of the amplicons was performed in R (v4.5.2). Primer sequences were removed using cutadapt v2.7 [41] and trimmed FASTQ files were processed with DADA2 v1.22.0 [39]. Reads were truncated at the first instance of a quality score ≤ 5, and chimeric sequences were identified and removed using the removeBimeraDenovo function. ITS1 sequences were processed using forward reads only, following Pauvert *et al.* (2019) [42], to maximize fungal diversity detection. ASVs were taxonomically assigned using a naïve Bayesian classifier with an in-house *gyrB* database (train_set_gyrB_v5.fa.gz, [43]) Unassigned sequences at the phylum level and *parE* sequences (a *gyrB* paralog) were removed. ITS1-derived ASVs were classified against the UNITE v.8 fungal database [44], and non-fungal ASVs were filtered out. All scripts are available at https://forge.inrae.fr/irhs-emersys/2026_logan_inoseed. Then, post-clustering curation was performed using LULU v0.1.0 [45] at a minimum threshold of 98% for *gyrB* and 99% for ITS. Contaminants were identified and removed using the decontam package v1.30.0, followed by manual curation. ASVs with fewer than 10 reads and detected in only one sample were removed from the dataset. Finally, samples with fewer than 1.000 reads after filtering were excluded from downstream analysis. To assess sequencing depth, rarefaction curves were generated using the rarecurve function of the vegan package (v2.7.2 [46]). Based on rarefaction curves, the *gyrB* dataset was rarefied at 3000 reads, and ITS dataset was rarefied at 2600 reads, resulting in 357 bacterial samples and 366 fungal samples. Rarefied ASV tables were then used to estimate species richness. For all other analyses, non-rarefied read counts were transformed into proportions (relative abundance) using the transform function from the microbiome R package. To estimate the effect of inoculation on species richness, observed richness was calculated on the rarefied dataset using the estimate_richness function of the phyloseq package (Version 1.54.0 ; [47]). To test the effect of SynCom inoculation on the microbiota, ordination analyses were performed using Bray-Curtis dissimilarity matrices computed on log(x+1) transformed non-rarefied data followed by Principal Coordinate Analysis (PCoA) using the ordinate function in phyloseq. To explore the percentage of variance explained by the factor SynCom on seed samples and seedling sample separately, permutational multivariate analysis of variance (PERMANOVA) was performed with 999 permutations using the adonis2 function from the vegan R package [46]. To further investigate the effect of SynCom on seedling microbiota, we used a clustering approach based on k-means clustering. The optimal

number of clusters was determined using the NbClust package in R by evaluating 26 distinct diagnostic indices. To assess SynCom colonization, inoculated strains were traced back by matching the already known *gyrB* and ITS sequence of the strain used in the dataset. Then, the cumulative contribution of the SynCom strain was quantified by summing the relative abundances of the inoculated ASVs in each condition.

Generalized Additive Models:

To elucidate the relationships between specific microbial traits and seedling colonization efficiency, we utilized Generalized Additive Models (GAMs) with the package mgcv [48] to explore both linear and non-linear traits correlations with colonization success, measured as the strain relative abundance in seedlings (response variable). A multivariate GAM was constructed using eight predictive variables: log10-transformed relative abundance on inoculated seeds, log10-transformed relative abundance in the initial inoculum, log10-transformed native relative abundance on seeds, native seed prevalence (defined as the proportion of occurrences across all sampled sites), genome size, growth rate, cumulative growth (Area Under the Curve, AUC), and lag phase duration. Relative abundance variables were log10-transformed to reduce the influence of highly abundant taxa. Independent multivariate models were fitted for bacterial and fungal datasets, with strain identity included as a random effect to account for phylogenetic structure. The relative importance of predictors within each model was quantified *via* hierarchical partitioning using the gam.hp package in R [49]. Model predictions were visualized using the ggplot2 package by extracting fitted GAM responses and plotting them against observed data.

Differential abundance analysis:

To gain insight into how SynCom inoculation reshaped seedling microbial communities, we identified differentially abundant ASVs between each individual SynCom treatment and the non-inoculated control group. To maximize the robustness of our differential abundance analysis and minimize algorithm-specific biases, we implemented a stringent consensus approach requiring an ASV to be significantly enriched or depleted in at least three out of four independent statistical methods. Seedling samples were first filtered using a prevalence threshold of 3% to retain low-prevalence taxa while allowing detection of SynCom-specific strains. Then, each SynCom was tested against the control (n = 16). Differential abundance testing was performed using the DAtest package (Version 2.8.0 [50]), which selects multiple statistical methods and ranks them based on performance metrics. For each method, the average performance score of each method was calculated for each condition, and the four best-performing methods were selected. For the *gyrB* dataset, the selected methods were LIMMA-ARL, EdgeR (exact test with TMM normalization), log-transformed t-test, and permutation tests. For ITS, the selected methods were EdgeR, Quasi-Poisson GLM, LIMMA - ALR and MgSeq Feature.

Multi-kingdom co-occurrence network:

To elucidate the ecological mechanisms underlying the distinct structural partitions observed with the clustering approach on the bacterial dataset, we constructed three multi-kingdom co-occurrence networks: (i) A global network including all bacterial and fungal ASVs detected across all seedling samples, (ii) a Cluster 1-specific, and (iii) a Cluster 2-specific network. The two clusters are based on SynCom impact on seedling native microbiota, Cluster 1 encompass SynComs inducing community shit and Cluster 2 SynCom with low or no impact. Although clustering was primarily defined by bacterial differential abundance profiles, the full fungal dataset was incorporated into each network to capture interkingdom associations, with particular emphasis on inoculated strains and differentially abundant bacteria. Networks were constructed using the multi domain SPIEC-EASI method [51], which is robust against compositional data by using clr-transformation to remove the unit-sum constraint of compositional data, as proposed by Aitchison [52]. Each network was constructed with a lambda ratio of $1x10^{-4}$, with 80 lambda values over 999 cross-validations, while neighborhood selection was performed using the Meinshausen and Bühlmann method ('mb'). Models were selected using the Stability Approach to Regularization Selection (StARS) algorithm with a stability threshold of 0.05, which was assessed for each network construction. The networks were visualized using Gephi [53] and their topological properties were calculated using the igraph package in R [54]. To allow comparison between networks with different numbers of nodes, nodes degree was normalized by dividing their degree by n-1, where n is the total number of nodes in each network. Betweenness centrality was normalized by its theoretical maximum in each graph using the igraph formula $B^n = \frac{2B}{(n-1)(n-2)}$ where B^n is the normalized betweenness, B is the absolute betweenness and n is the number of nodes.

In order to assess if inoculated strains preferentially interacted with each other or with non-inoculated strains, assortativity coefficients were calculated following Newman 2003 [55]. This coefficient ranges from -1 (disassortative mixing, where nodes preferentially connect to dissimilar nodes) and 1 (assortative mixing, where nodes preferentially connect to similar nodes). The assortativity coefficient was based on the inoculation status category of nodes (inoculated or not). We also calculated the proportion of connection each inoculated strain had with other inoculated strains to observe this interaction at node level. Seemingly, domain-specific interaction preferences were assessed by calculating, for each inoculated strain, the proportion of connections to bacterial *versus* fungal nodes.

Statistical analysis:

Statistical analysis was conducted after assessing data distribution using the Shapiro-Wilk test. None of the investigated data followed normal distribution, resulting in use of the Kruskal–Wallis test [56]

of R (BH; $\alpha = 0.05$). When multiple conditions were tested simultaneously, the non-parametric post-hoc test of Dunn (BH; $\alpha = 0.05$; [57]) was conducted.

Results:

1) Alginate encapsulation of synthetic microbial communities enhances seed colonization and outcompetes native microbiota

To ensure a sufficient propagule size for effective SynCom inoculation, we targeted a concentration of 10^5 microorganisms per seed for both bacterial and fungal taxa. This concentration was chosen to ensure a higher microbial biomass than non-inoculated seeds as well as its feasibility for fungal spore collection as part of inoculum preparation. Four distinct inoculation methods were evaluated on *Brassica napus* seeds: soaking in water, 10 mM $MgCl_2$, 5% glycerol, and coating with 2.4% sodium alginate. Among these, alginate coating consistently resulted in the highest microbial loads across all taxa (Fig. 2A). Bacterial load increased by approximately 2 logs (~85-fold), achieving $1.26x10^6$ bacteria per seed compared to $1.26x10^4$ bacteria per seed with water. Yeast abundance increased by almost 3 logs (~284-fold), from $4.0x10^2$ yeast per seed in water to 1.14×10^5 in alginate. The most pronounced effect was observed for filamentous fungi, with an increase of approximately 5-log (~74,475-fold), reaching 2.17×10^7 conidia per seed compared to 2.92×10^2 with water. In the absence of microbial inoculation, both alginate coating and glycerol treatments led to a slight but statistically significant increase in germination rate compared to the control (Fig. 2B; Dunn's test with Benjamini-Hochberg correction, $p < 0.05$). Dissolution of the alginate matrix enabled recovery of viable microorganisms, confirming its suitability for downstream assessment of seed colonization. Collectively, these results identify alginate encapsulation as an efficient and robust method for SynCom delivery onto seeds.

Following optimization of the inoculation method, a total of 20 distinct multi-kingdom SynComs were designed (Fig. 1A) and inoculated with alginate coating on seeds. Compositional distance calculations were used to assess the overall differences in SynCom composition (Fig. 1B). SynCom with expected similar composition (MostAbun, MostAbunSeed and MostAbunSeedling) clustered close to each other while randomly designed SynCom were disseminated along both axis. Post-inoculation, the total microbial load was quantified across eight individual seeds per condition to verify whether the target density of 10^5 cells per seed was reached (Fig. 2C). Non-inoculated control seeds (alginate only) exhibited a mean concentration of 3.13×10^3 microorganisms per seed. In comparison, 15 of the 20 SynComs reached significantly higher microbial load per single seed relative to non-inoculated controls, with mean concentrations ranging from 2.66×10^5 (MostAbunSeed) to 2.09×10^6 microorganisms per seed (Rare2). Conversely, the five SynComs PhylDiv1, PhylDiv2, Rare1, Rand4, and AbunGrad, yielded densities ranging from 1.58×10^3 to 2.72×10^5 microorganisms per seed, and did

not differ from controls. Overall, only four SynComs (PhylDiv1, PhylDiv2, Rare1, and Rand4) failed to reach the target inoculation threshold on seeds.

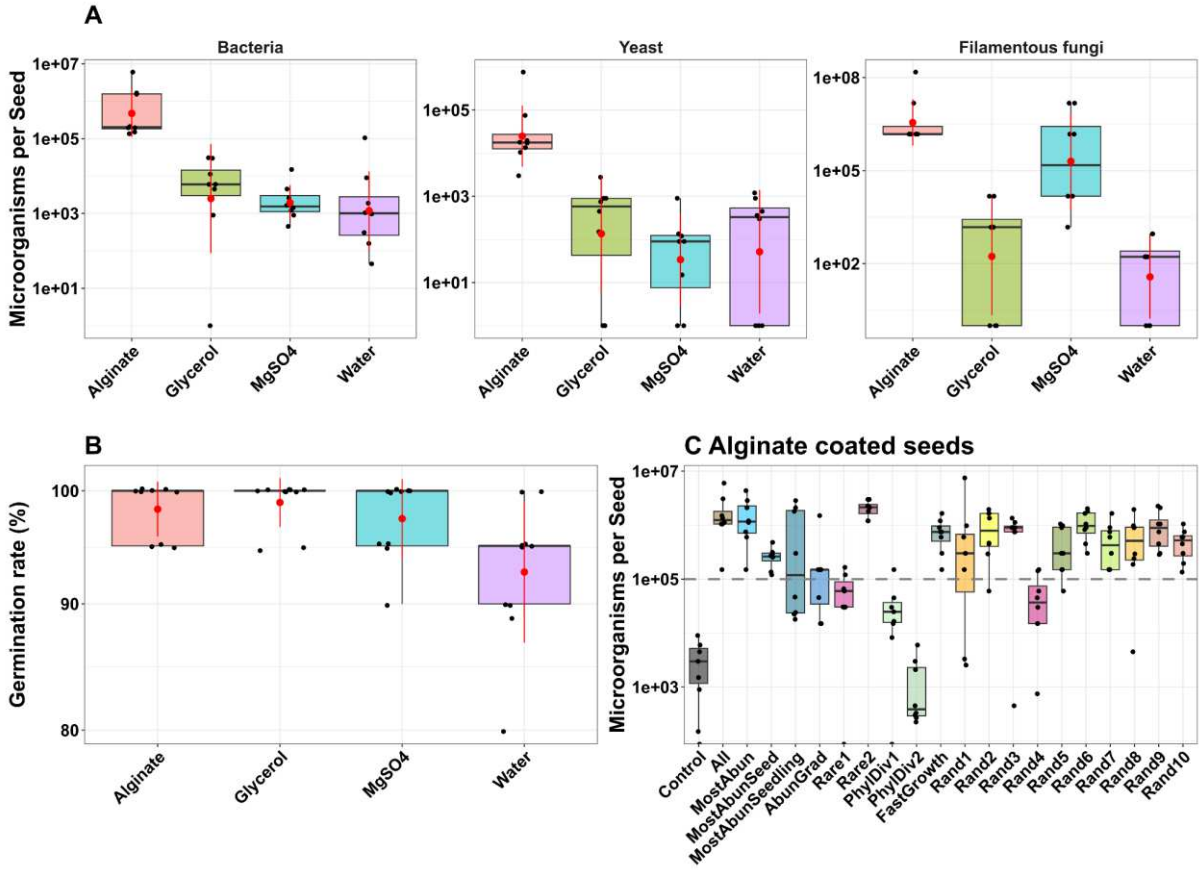


Fig. 2: **Evaluation of seed soaking and coating strategies and subsequent synthetic community (SynCom) colonization efficiency on *Brassica napus*.** (A) Impact of four inoculation methods on seed microbial population sizes using representative single bacterial, yeast, or filamentous fungal strains. (B) Influence of inoculation matrices on seed germination rates in the absence of microbial strain inoculation. For both (A) and (B), distinct letters indicate statistically significant differences between treatment groups (Dunn's post-hoc test with Benjamini-Hochberg correction, $p < 0.05$). (C) Total microbial population sizes recovered from individual seeds inoculated *via* sodium alginate encapsulation across 20 distinct SynCom design. Asterisks (*) indicate statistically significant differences compared to the non-inoculated control group (Pairwise comparisons using Dunn's many-to-one test with Benjamini-Hochberg correction, $p < 0.05$).

To determine whether the observed microbial richness reflected the initial inoculum or the persistence of native microbiota, we evaluated the number of ASVs across treatments (Observed richness). Because individual non-inoculated control seeds did not yield sufficient microbial DNA for robust metabarcoding amplification, we analyzed four replicates of 30 pooled seeds each to characterize the native microbiota. In these control pools, mean richness reached 63.25 bacterial ASVs and 33.50 fungal unique ASVs. For bacterial richness (Supplementary Fig.3A), nine SynComs (All, Rare1 and Rare2,

PhylDiv2, FastGrowth, Rand4, Rand5, Rand7, and Rand10) did not differ significantly from control conditions (Pairwise comparisons using Dunn's many-to-one test with BH correction, $p > 0.05$). Interestingly, although the "All" SynCom formulation included 24 bacterial strains in the initial inoculum, only 19 ASVs were detected on seeds after inoculation. In contrast, SynCom that significantly differed from the control pools exhibited reduced bacterial richness, with values ranging from 6.75 to 13 ASVs. Contrary to bacteria, fungal richness remained stable across all inoculated conditions (Supplementary Fig. 3B) and did not significantly differ from control pools (Pairwise comparisons using Dunn's many-to-one test with BH correction, $p > 0.05$). The highest mean fungal richness was observed in the SynCom All with 51.5 unique ASVs. Together, these results indicated that SynCom inoculation impacted bacterial richness of seeds but did not completely overtake native microbiota while fungal richness remained largely unaffected. The comparable fungal richness between inoculated seeds and pooled controls suggests that native fungal taxa persist following inoculation. This may be explained by the absence of seed surface sterilization prior to inoculation, which could allow native fungal communities, potentially more resistant to water rinsing than bacteria, to be maintained.

To determine whether SynCom inoculation altered seed microbial composition and structure and to assess its similarity with the initial inoculum profiles, we evaluated beta diversity using Bray-Curtis dissimilarity matrices. For bacterial communities (Fig. 3A), principal coordinate analysis (PCoA) revealed clear clustering by SynCom composition, with tight co-localization between each specific inoculum and its corresponding inoculated seeds. PERMANOVA confirmed that SynCom composition was the primary driver of bacterial beta diversity, accounting for 79% of the total community variance (PERMANOVA, 999 permutations, $R^2 = 0.79$, $p < 0.001$). For fungal communities (Fig. 3B), the initial inocula and the resulting inoculated seeds were separated along the first axis of the ordination. Nevertheless, SynCom treatment remained a significant factor, accounting for 35% of the variance (PERMANOVA, 999 permutations, $R^2 = 0.35$, $p < 0.001$). These results indicated that SynCom inoculation strongly modulated bacterial communities on seeds, whereas its effect on fungal communities is more moderate. Furthermore, partial overlap in fungal strains compositions across SynCom formulations may contribute to the reduced clustering observed between distinct SynCom treatments.

To quantify the extent to which the introduced SynComs successfully colonized the seed matrix, we tracked the specific ASVs assigned to the inoculated strains. Across all datasets, only two inoculated strains were not detected after inoculation: *Bacillus pumilus* CFBP 9299 and *Holtermanniella* sp. CLIB 4445, for which no sequence reads were recovered. The cumulative relative abundance of detected inoculum-derived ASVs was used to estimate the overall SynCom contribution to the seed microbiota (Fig. 3C). Non-inoculated control seeds already exhibited a high baseline abundance of SynCom-

associated taxa, representing 60.9% of the bacterial communities and 51.2% of the fungal communities. This finding is biologically consistent, as the strains selected for SynCom construction were originally isolated from this exact *B. napus* seed and seedling lot. Following inoculation, the average SynCom contribution increased to 93.7% for bacteria and 68.2% for fungi. This is further supported by taxonomic composition analyses of inoculum and seeds. In control seeds, bacterial communities were dominated by *Pantoea agglomerans* CFBP 9288 and *Erwinia persicina* CFBP 9294, with only minor contributions of other taxa such as *Pseudomonas coleopterum* CFBP 9298, *Neorhizobium soli* CFBP 9328, *Stenotrophomonas* sp. CFBP 9287, *Xanthomonas campestris* CFBP 9284 , *Sphingomonas aerolata* CFBP 9292 and *Sphingomonas* sp. CFBP 9329. Similarly, fungal communities were largely dominated by *Cladosporium* sp. pCoAvM041 and *Mycosphaerella* sp. gCoJuP058, alongside low-abundance taxa. In contrast, inoculated seeds showed a pronounced shift in taxonomic composition. For example, seeds inoculated with the SynCom "All" harbored 21 different bacterial and 18 fungal inoculated strains, with taxonomic profile closely mirroring those of corresponding inocula. Same patterns were observed for MostAbun and PhylDiv2, for both bacterial and fungal communities (Fig. 3D and Fig. 3E). Overall, seed taxonomic profiles matched their respective inoculum, a more pronounced effect for bacterial communities (Supplementary Fig.3 C and E) than for fungal communities (Supplementary Fig. 3D and Fig. 3E). This substantial enrichment demonstrates that the SynCom successfully outcompeted and displaced the remaining native microbiota. This effect is particularly pronounced for bacterial communities, whereas fungal communities, although influenced, retain a greater contribution from native taxa.

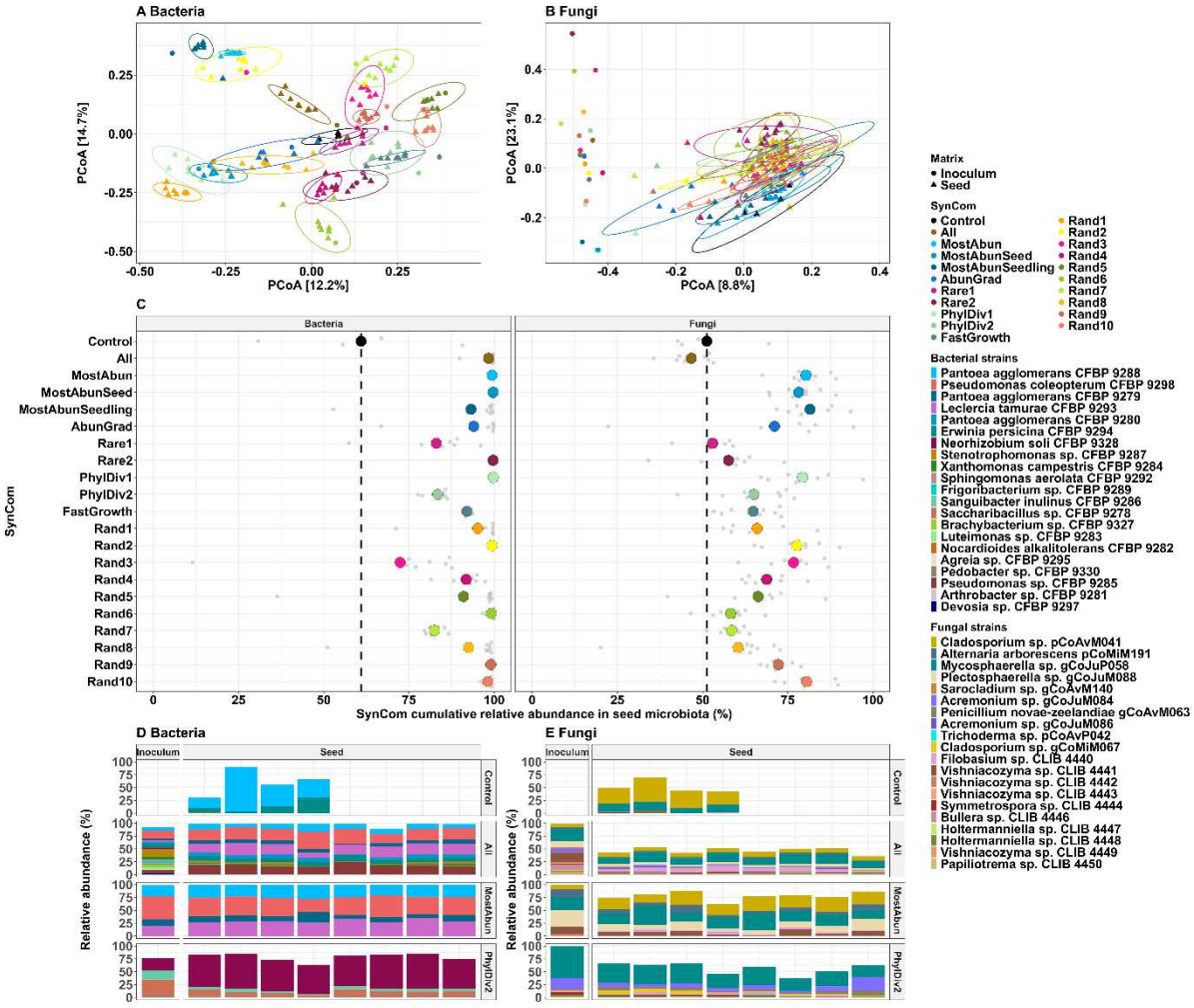


Fig. 3**: Beta diversity, community composition, and relative contribution of introduced SynComs to the *Brassica napus* seed microbiota.** (A–B) Principal Coordinate Analysis (PCoA) based on Bray-Curtis dissimilarity matrices (log(x+1) transformed) evaluating (A) bacterial and (B) fungal community structures across control and SynCom-inoculated seeds and their respective initial inocula. For SynCom treatments and inocula, individual points represent single seeds or independent inoculum samples, whereas control points represent pooled batches of 30 non-inoculated seeds. (C) Relative contribution (%) of inoculated SynCom strains to the total bacterial and fungal seed microbiota, calculated by summing the relative abundance of tracked inoculum-specific ASVs. (D–E) Taxonomic profiling of successfully tracked (D) bacterial and (E) fungal inoculum strains, illustrating relative abundances within the initial inocula and the resulting seed microbiota across the Control, All, MostAbun, and PhylDiv2 SynCom designs as example, all SynCom profiles are presented in Sup. Fig.3. Only inoculated strains are represented, thus blank space represent remaining non inoculated microbiota (i.e native taxa).

2) Seedling colonization is driven by SynCom composition

Following 15 days of growth in non-sterile potting soil, eight phenotypically normal seedlings seeds per condition (inoculated and control) were harvested to characterize the seedling microbiota. Concurrently, phenotypic effects of SynCom inoculation were evaluated across all remaining seedlings (n = 76) by monitoring germination rate, hypocotyl length, and the proportion of morphologically

normal seedlings. Seed germination was not significantly altered by SynCom inoculation (Supplementary Fig. 4A; Kruskal-Wallis rank-sum test, $p = 0.85$). However, hypocotyl length (Supplementary Fig.4B) was significantly reduced by four SynComs (Rare2, PhylDiv1, PhylDiv2, and FastGrowth) and significantly increased by five SynComs (MostAbun, Rand5, Rand7, Rand9, and Rand10; Pairwise comparisons using Dunn's many-to-one test with Benjamini-Hochberg [BH] correction, $p < 0.05$). The proportion of normal seedlings (Supplementary Fig. 4C) was significantly reduced in five SynComs (All, MostAbun, Rand6, Rand7 and Rand8; Pairwise comparisons using Dunn's many-to-one test with Benjamini-Hochberg [BH] correction, $p < 0.05$). Thus, the SynCom inoculation does not affect seed germination but significantly influences seedling phenotype, with both beneficial and detrimental effects depending on community composition.

The colonization of seedlings by inoculated strains was monitored by quantifying the cumulative relative abundance of the SynCom to the microbiota of emerged seedlings (Fig. 4A). In non-inoculated control seedlings, the baseline relative abundance of SynCom-associated taxa was low for both bacteria (6.9%) and fungi (2.6%), indicating limited natural transmission of these strains from seed to seedlings. Bacterial colonization of seedlings varied markedly depending on SynCom composition. Among the 20 SynComs tested, 14 exhibited higher colonization than control seedlings, including five *a priori* designed and nine randomly assembled SynComs. The highest colonization efficiencies were observed for SynCom Rand8 (45.7%) and Rand9 (42.0%), followed by the SynCom All (38.4%) and the three SynComs based on high natural abundance (MostAbun, MostAbunSeed and MostAbunSeedling) (Fig. 4A). Conversely, fungal colonization showed overall lower relative abundance compared to bacteria. However, all SynComs resulted in a higher fungal ASVs abundance than in control seedlings. The most effective SynComs for fungal colonization were Rand3 (36.6%) and Rand9 (26.3%), followed by PhylDiv1 (22.5%) and Rand1 (21.0%). A weak but statistically significant positive correlation was observed between bacterial and fungal colonization success within the same individual seedlings ($R^2 = 0.11$, $p = 2.8\times10^{-5}$; Supplementary Fig. 5A), suggesting limited co-dependence between kingdoms during colonization. To evaluate the impact of SynCom design strategies, we compared colonization efficiency between *a priori* and randomly assembled communities (Fig. 4B). For bacterial colonization, no significant difference was observed between the *a priori* (18.6%) and random (20.6%) design strategies (Wilcoxon-Mann-Whitney test, $p = 0.25$). In contrast, fungal colonization was significantly higher in randomly assembled SynCom (15.9%) compared to the *a priori* designed SynComs (11.6%) (Wilcoxon-Mann-Whitney test, $p < 0.05$). Overall, SynComs establishment remained partial for both bacterial and fungal communities. Nevertheless, colonization success was strongly influenced by SynCom composition, and notably, assembly based on high natural abundance outperformed the other designs.

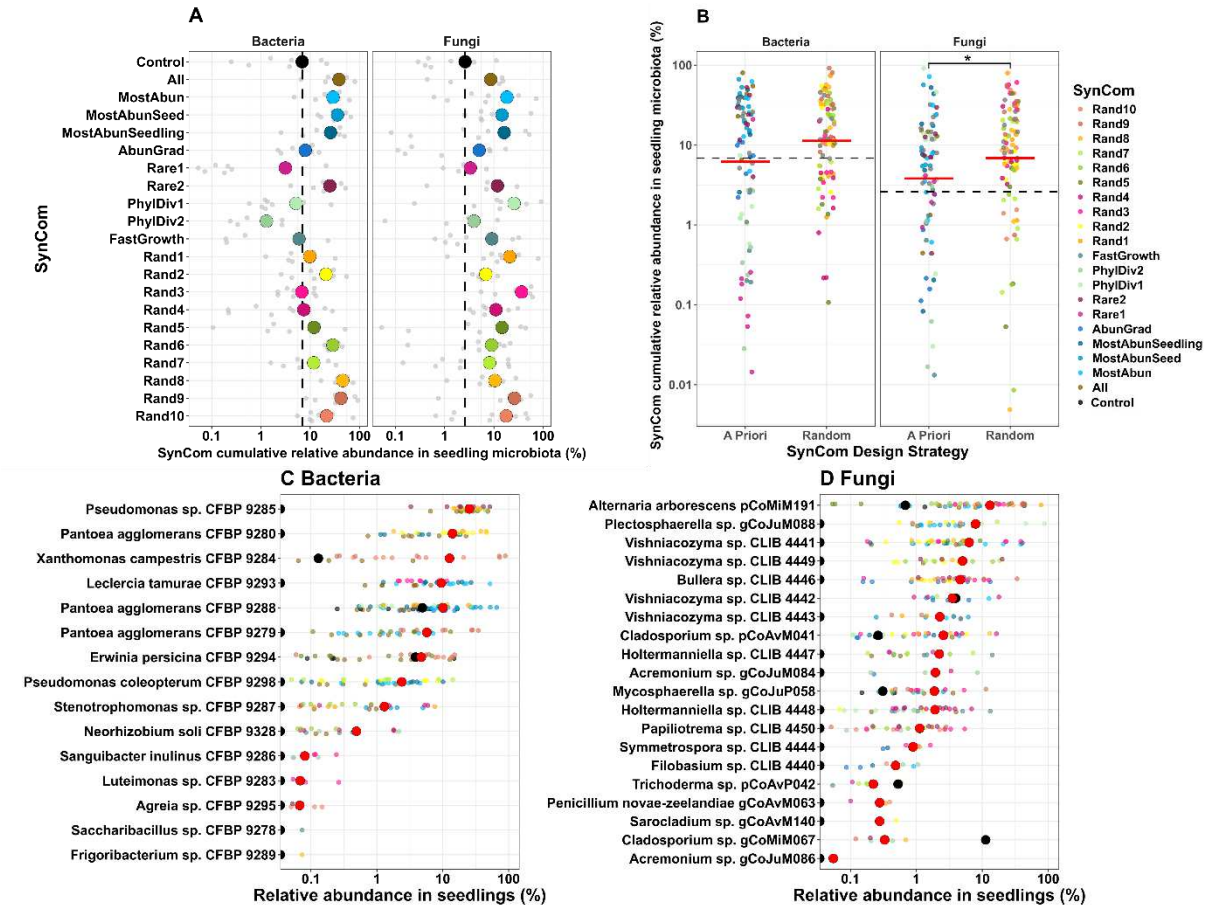


Fig. 4**: Characterization of SynCom colonization efficiency and strain-level relative abundances in the *Brassica napus* seedling microbiota.** (A) Cumulative relative abundance (%) of inoculated SynCom members to the bacterial and fungal communities of emerged seedlings. Light gray points indicate individual seedling replicates (n = 8), colored points designate treatment means, and the horizontal black dashed line indicates baseline recovery in the non-inoculated control group. (B) Comparative analysis of cumulative SynCom colonization between the *a priori* and random community-design frameworks. Solid red horizontal lines indicate group means, and black dashed lines indicate the mean baseline value of the control group. Asterisks (*) denote statistically significant differences between design strategies (Wilcoxon-Mann-Whitney test, $p < 0.05$). (C–D) Relative abundance profiles of successfully tracked (C) bacterial, (D) filamentous fungal and yeast strains within the seedling microbiota. Smaller colored points represent individual seedling values for each specific SynCom treatment. Red points indicate the mean relative abundance across all replicates for a given strain, while black points indicate its mean baseline abundance across eight non-inoculated control seedlings.

To evaluate the colonization potential of each inoculated strain, we quantified their relative abundance in emerged seedling. Among the bacterial strains (Fig. 4C), 16 out of 24 were successfully detected in seedling microbiota. Eight strains (CFBP 9292, CFBP 9327, CFBP 9282, CFBP 9299, CFBP 9330, CFBP 9296, CFBP 9281 and CFBP 9297) were not detected. Only three bacterial strains were found in control seedlings: CFBP 9284, CFBP 9288 CFPB 9294, explaining the low natural colonization of control seedlings. Strains affiliated to genera *Pseudomonas*, *Pantoea*, *Xanthomonas*, *Leclercia* and *Erwinia*

exhibited the highest colonization success. In particular, *Pseudomonas* sp. CFBP 9285 showed the greatest colonization, reaching a mean relative abundance of 21.4%. The remaining detected bacterial strains persisted at low abundances, ranging from 0.03% to 1.2%. For fungal strains (Fig. 4D), all filamentous fungi were successfully recovered from the seedlings, along 10 out of 11 yeast strains with six (five filamentous fungi and 1 yeast) found in control condition. Fungal colonization was primarily driven by filamentous taxa, notably *Alternaria arborescens* pCoMiM191 (10.6%) and *Plectosphaerella* sp. gCoJuM088 (7.5%), followed by the yeast *Vishniacozyma* sp. CLIB 4441 (5.7%). Tracking individual strain performance across multiple, compositionally distinct SynComs revealed that seed to seedling transmission success is strongly strain-dependent. A subset of strains consistently behaved as dominant colonizers across contexts, whereas others failed to establish or persisted only at marginal abundances.

3) Strain Traits Drive Seedling Colonization Success

To elucidate the relationships between specific microbial traits and seedling colonization efficiency, we used Generalized Additive Models (GAMs) to create a fungal and a bacterial multivariate model using eight predictive traits as fixed effects and strain identity as a random effect. The bacterial GAM explained 92.10% of the total deviance in log-transformed strain abundance in seedlings. The random effect of strain identity accounted for 43.67% of the model variance, indicating strong strain-specific differences in colonization, although it was not significant ($p = 0.085$), likely reflecting limited statistical power. Among the eight fixed predictors, three variables were significant. Strain abundance on inoculated seed (Fig. 5A, $p = 0.029$) and assembled genome size (Fig. 5B, $p < 0.001$) showed significant linear relationships with seedling colonization (edf = 1), contributing respectively to 20.08% and 14.88% of the explained deviance. Lag phase duration, exhibited a significant non-linear relationship with seedling establishment (Fig. 5C, edf = 4.37, $p < 0.001$) accounting for 5.42% of the total deviance in the model. The apparent offset between partial effect curves and raw data points reflects the conditional nature of prediction derived from multivariate GAMs, where predictors act simultaneously rather than independently. Overall, these results indicate that bacterial seedling colonization is primarily driven by high initial abundance on seeds and larger genome size, with shorter lag phase providing an additional but more limited advantage.

The fungal GAM explained 69.30% of the total deviance. In contrast to bacteria, the random effect of strain identity was statistically significant ($p = 0.027$) and accounted for the majority of the explained variance (59.77%). Three fixed effects significantly influenced fungal colonization. Relative abundance on inoculated seeds showed a strong non-linear relationship (Fig. 5D, $p < 0.001$, edf = 4.5) explaining 9.15% of the model deviance. Natural ASV prevalence on seeds also displayed a significant non-linear effect (Fig. 5E, $p = 0.022$, edf = 1.8), contributing 6.58%. Lag phase duration had a weaker but significant

non-linear effect (Fig. 5F, p = 0.016, edf = 2.5), explaining 1.17% of the deviance. Together, these results show that fungal colonization success is primarily associated with high abundance and prevalence on seeds, both following nonlinear relationships, while a shorter lag phase confering a moderate additional benefit.

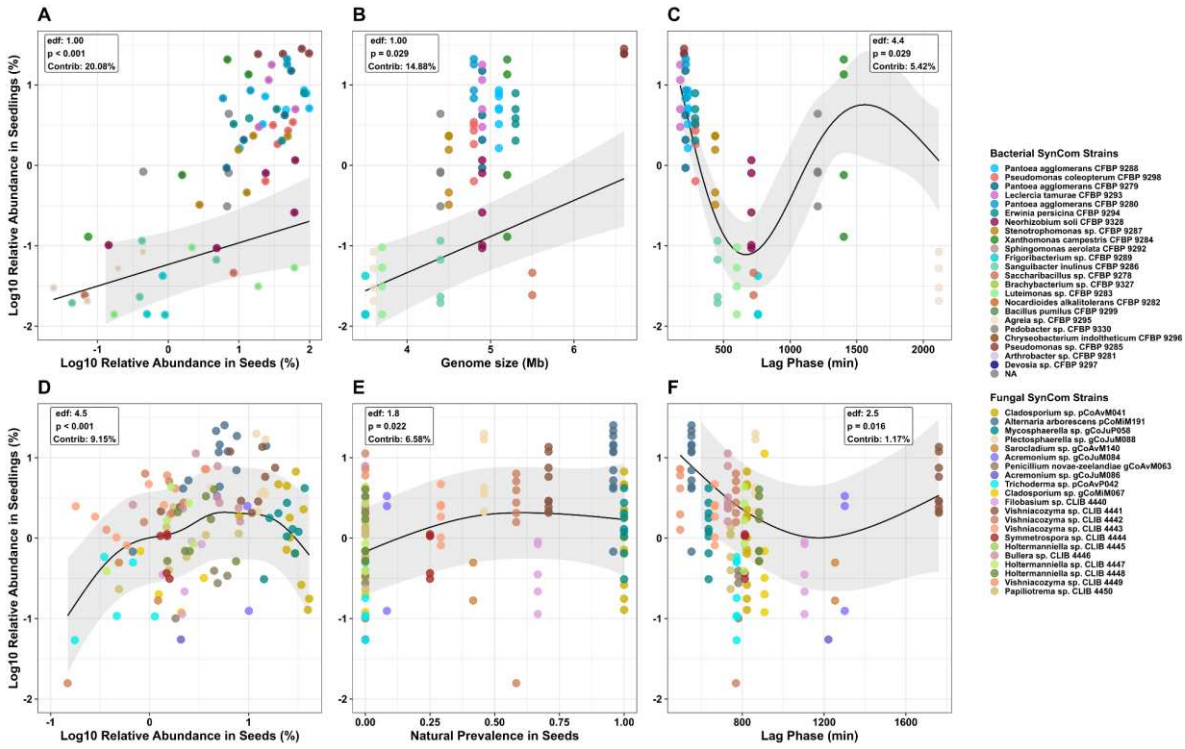


Fig. 5: **Generalized Additive Model (GAM) partial effects of significant phenotypic and ecological traits driving strain-level seedling colonization.** Predicted partial effects (solid blue lines) and corresponding 95% confidence intervals (shaded gray regions) of significant microbial traits predicting the log10-transformed relative abundance of inoculated strains in *Brassica napus* seedlings. For each parameter, the estimated degrees of freedom (edf), p, and relative deviance contribution (%) to the multivariate model are displayed. (A–C) Bacterial models predicting seedling log-abundance based on (A) log10 relative abundance on inoculated seeds, (B) assembled genome size, and (C) *in vitro* lag phase duration. (D–F) Fungal models predicting seedling log-abundance based on (D) log10 relative abundance on inoculated seeds, (E) native seed prevalence, and (F) *in vitro* lag phase duration.

4) SynCom inoculation modulates seedling microbiota assembly and community structure

To compare the microbial communities of the seedling between conditions, we analyzed beta diversity using Bray-Curtis dissimilarity matrices across seedling and bulk soil samples. Bacterial community composition was significantly driven by SynCom treatment (Fig. 6A), which explained 33% of the total variance (PERMANOVA, 999 permutations, $R^2 = 0.33$, $p < 0.001$), resulting in a clear clustering along the primary axis of the ordination. To objectively define the number and structure of these bacterial assemblages, k-means clustering was applied on the first two axes of the Principal Coordinate Analysis

(PCoA). The optimal number of clusters was determined using the NbClust package in R by evaluating 26 distinct diagnostic indices. A majority consensus of 10 indices supported k = 2 as the optimal partition (Table S12). This clustering significantly explained the variation observed in the bacterial community (PERMANOVA, 999 permutations, $R^2 = 0.17$, $p < 0.001$). The clustering approach was also tested on fungal communities (Supplementary Fig. 6) and revealed 3 overlapping clusters with a distribution of the same SynCom in multiple clusters. For these reasons, only bacterial community clusters were investigated.

For bacteria, Cluster 1 was clearly separated from non-inoculated control and included 12 SynComs: six randomly assembled communities (Rand2, Rand6, Rand7, Rand8, Rand9 and Rand10), and six *a priori* designs, including those based on high natural abundance (MostAbunSeedling, MostAbunSeed, MostAbun), the high richness community (All), the abundance gradient (AbunGrad), and one rare taxa community (Rare1). Conversely, Cluster 2 was positioned closer to the bulk soil samples and included the non-inoculated control, four random SynComs (Rand1, Rand3, Rand4, Rand5), the second rare SynCom (Rare2), both phylogenetic diversity based communities (PhylDiv1 and 2), and the fast-growing community (FastGrowth). Fungal community structure displayed weaker clustering (Fig. 6B), although SynCom treatment remained a significant driver of fungal community composition, explaining 22% of the variance (PERMANOVA, 999 permutations, $R^2 = 0.22$, $p < 0.001$). Bulk soil samples clustered independently and remained separated from all seedling samples. Pairwise comparisons revealed that only three SynComs significantly altered fungal community composition relative to the non-inoculated controls (Pairwise PERMANOVA, false discovery rate adjusted $p < 0.005$). Notably, all three belonged to the *a priori* design based on high native abundance: Most Abun ($R^2 = 0.13$), MostAbunSeedling ($R^2 = 0.16$), and AbunGrad ($R^2 = 0.22$). Taken together, these findings indicate that SynCom inoculation strongly reshapes bacterial community assembly, whereas fungal community assembly is less responsive to SynCom inoculation.

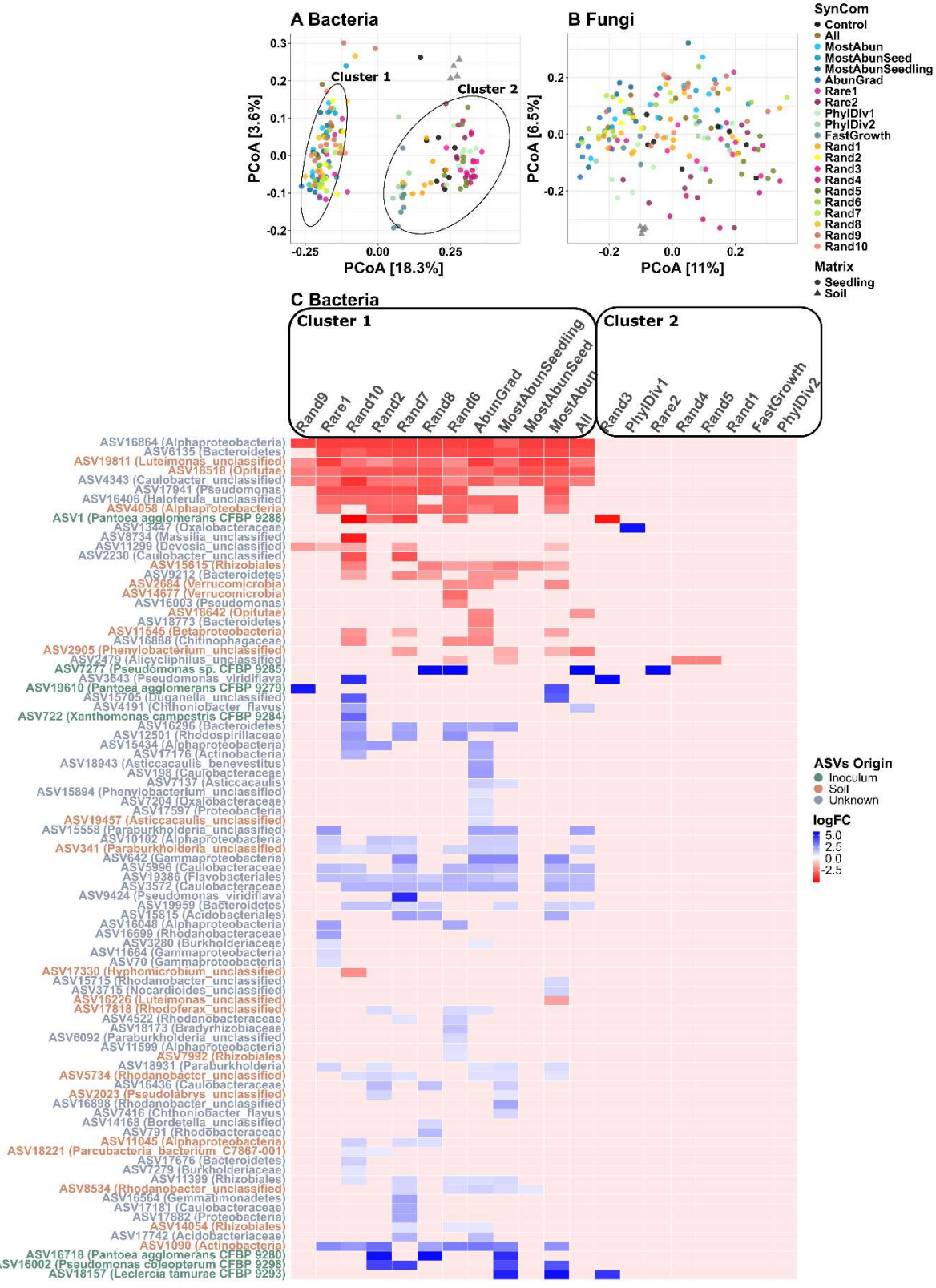


Fig. 6: **Community-level beta diversity and differential bacterial ASV recruitment in the *Brassica napus* seedling microbiota**. (A–B) Principal Coordinate Analysis (PCoA) based on Bray-Curtis dissimilarity matrices (log(x+1) transformed) for (A) bacterial and (B) fungal communities across bulk soil, non-inoculated control seedlings, and SynCom-inoculated seedlings. Cluster overlays are derived from k-means clustering partitioning using the NbClust package in R based on Euclidean distances. (C) Hierarchical clustering heatmap of differentially abundant

bacterial ASVs in inoculated seedlings relative to the non-inoculated control group, identified via a consensus of at least three out of four distinct statistical algorithms (LIMMA-ARL, EdgeR exact-TMM, log-transformed t-test, and permutation tests). Row annotations indicate the environmental or experimental origin of each ASV.

To identify which taxa were responsible for the community shift in seedlings, we used a differential abundance analysis between each SynCom treatment and the non-inoculated control group with four independent statistical methods, retaining ASVs being detected in at least 3 methods. No fungal ASV met the threshold, confirming that the seedling fungal microbiota remained resistant to specific SynCom-induced shifts. Conversely, 89 bacterial ASVs were identified as differentially abundant across 17 of the 20 SynCom treatments (Fig. 6C). Among these, seven corresponded inoculated strains: *Pantoea agglomerans* CFBP 9288*, Pseudomonas* sp. CFBP 9285, *Pantoea agglomerans* CFBP 9279, *Xanthomonas campestris* CFBP 9284*, Pantoea agglomerans* CFBP 9279*, Pseudomonas coleopterum* CFBP 9298*,* and *Leclercia tamurae* CFBP 9293. Most of these strains showed significant enrichment in the treatments in which they were introduced. In contrast, *Pantoea agglomerans* CFBP 9288 exhibited a unique pattern, being consistently depleted in treatments where it was not inoculated, likely reflecting its high natural abundance in control seedlings. The remaining 82 ASVs corresponded to non-inoculated native taxa. Taxonomic assignment revealed a strong dominance of *Pseudomonadota*, particularly within *Alphaproteobacteria* (35.4%; n= 29/82), *Gammaproteobacteria* (18.3%; n = 15/82), and *Betaproteobacteria* (17.1%; n = 14/82). Tracking their environmental origin indicated that only a minority of differentially abundant ASVs originated from bulk soil matrix (24.7%; n = 22) and non were identified a originating from native seed microbiota, whereas the majority could not be traced (67.4%; n = 60), suggesting recruitment from either unsampled source or rare seed or soil-derived taxa. Regression analyses revealed no significant correlation between the cumulative colonization efficiency of the inoculated strains and the number of differentially abundant native taxa, for either the bacteria (Supplementary Fig.5B, R^2 = 0.102, p = 0.171) or fungi (Supplementary Fig. 5C, R^2 = 0.063, p = 0.286). However, differential abundance profiles closely matched the k-means clusters established in Fig. 6A. This concordance indicates that community-level restructuring is not solely driven by the dominance of inoculated strains, but also depends on broader, SynCom-specific ecological interactions.

5) Interkingdom Co-occurrence Networks Reveal Structural Drivers of Community Clustering

To elucidate the ecological mechanisms underlying the distinct structural partitions observed between Cluster 1 (community shift) and Cluster 2 (no community shift), we constructed three multi-kingdom co-occurrence networks: (i) A global network including all bacterial and fungal ASVs detected across all seedling samples (Fig. 7A), (ii) a Cluster 1-specific (Fig. 7B), and (iii) a Cluster 2-specific network (Fig. 7C).

Although clustering was primarily defined by bacterial differential abundance profiles, the full fungal dataset was incorporated into each network to capture interkingdom associations, with particular emphasis on inoculated strains and differentially abundant bacteria.

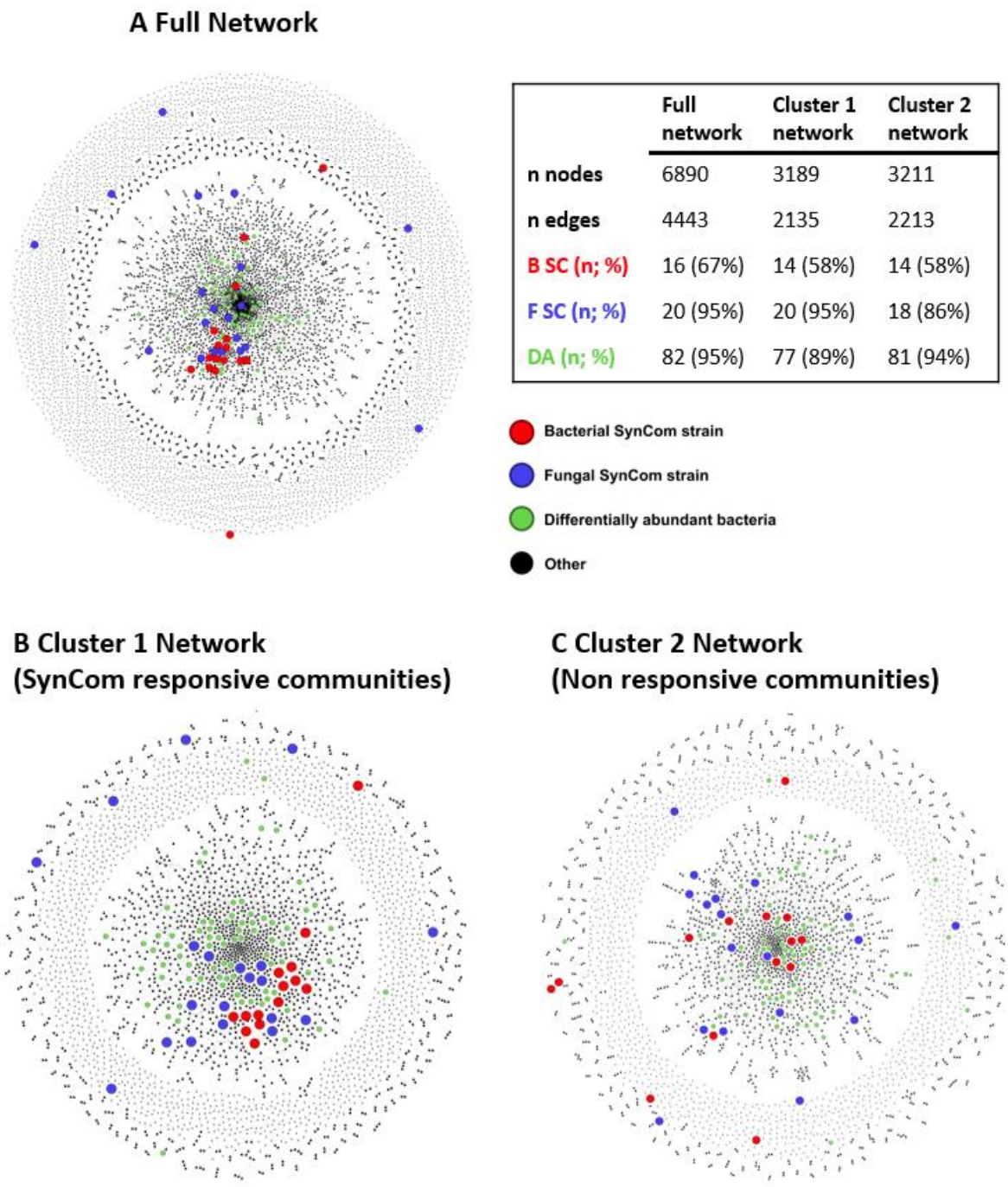


Fig. 7: **Topology of interkingdom co-occurrence networks in the *Brassica napus* seedling microbiota.** Visualizations represent microbial networks constructed across (A) the full dataset including all seedling samples, (B) seedling samples within Cluster 1, and (C) seedling samples within Cluster 2. Nodes represent unique bacterial or fungal ASVs, while edges denote statistically significant co-occurrence relationships. Node coloring distinguishes introduced SynCom bacterial (red) and fungal (blue) strains, differentially abundant native ASVs identified in consensus profiling (green), and background native microbiota (black). The table encompasses the

number of nodes and edges as well as the number and proportion of bacterial SynCom strain (B SC), fungal SynCom strain (F SC) and differentially abundant native ASVs (DA) across each network.

Even though the networks differed in size (n = 6890, 3189 and 3211 nodes for full, Cluster 1 and Cluster 2 networks), they showed similar density (1.87×10^{-4}, 4.2×10^{-4}, and 4.29×10^{-4} for full, Cluster 1 and Cluster 2 networks) and similar normalized numbers of connections among taxa (0.64, 0.67 and 0.69 normalized degree for full, Cluster 1 and Cluster 2 networks). This pattern was consistent when considering the full networks as well as their largest connected component (giant component) and peripheral nodes (Table S13).

We then investigated the position of SynCom strains within each network. The giant component of the Cluster 1 network included a higher proportion of inoculated strains than Cluster 2 (79%, n = 27 strains, versus 72%, n = 23 strains; Supplementary Fig. 7A), with 20 strains shared between both clusters. Network centrality metrics revealed marked differences in SynCom strain integration between the two clusters (Fig. 8A). SynCom strains exhibited significantly higher normalized degree in the Cluster 1 network (normalized node degree = 1.23 × 10-3) compared to both the global network (normalized node degree = 6.25 × 10-4) and Cluster 2 (normalized node degree = 6.81 × 10-4 Dunn's test with Benjamini-Hochberg correction, $p < 0.05$). This pattern was consistent with the analysis of the 100 most connected ASVs in each network (Supplementary Fig. 7C–E), where Cluster 1 network contained the highest number of SynCom strains (n = 10) and was the only network in which introduced fungal strains ranked among the most connected taxa. To assess whether inoculated strains acted as important connectors within the co-occurrence network, we calculated normalized betweenness centrality, which reflects how often a node lies on the shortest paths connecting other nodes (Fig. 8B). SynCom strains showed higher mean betweenness centrality in Cluster 1 (mean betweenness = 1.03 × 10-3) than in Cluster 2 (mean betweenness = 2.45 × 10-4; Dunn's test with BH correction, $p < 0.05$), while not differing significantly from the global network (mean betweenness = 3.35 × 10-4). These results suggest that SynCom strains are more integrated and play a greater structural role in Cluster 1 network than in Cluster 2. To further characterize SynCom integration in seedling microbiota, we examined assortativity coefficients to test whether inoculated strains preferentially connected with each other rather than with native taxa. The Cluster 1 network showed the highest assortativity (r = 0.36), followed by the global (r = 0.28) and Cluster 2 (r = 0.25) networks, indicating a general tendency for SynCom strains to co-associate. However, node-level analysis (Fig. 8C) revealed that SynCom strains shared a lower proportion of their edges with other introduced strains in Cluster 1 (percentage of connections between inoculated strains = 7.3%) and in the global network (9.3%) than in Cluster 2 (28%; Dunn's test with BH correction, $p < 0.05$). Across all networks, SynCom strains had a higher number of connections with native bacteria than with fungi (Fig. 8D). Notably, connections with fungi

were significantly less frequent in Cluster 2 compared to the other networks (Dunn's test with BH correction, $p < 0.05$).

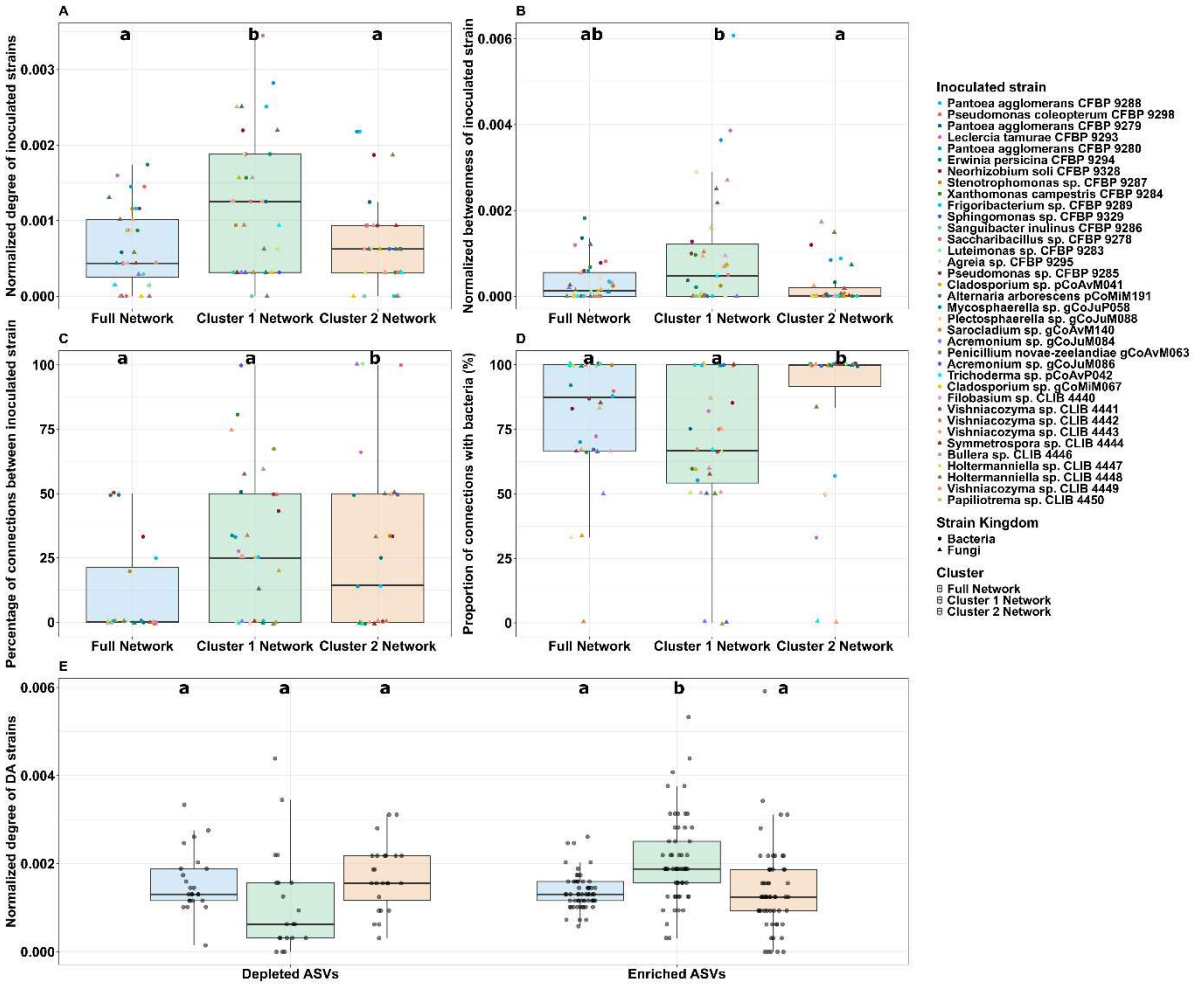


Fig. 8: **Network topological integration of introduced SynCom strains and differentially abundant native taxa.** (A–B) Characterization of SynCom strain centrality metrics using (A) normalized degree centrality (Edges/(Nodes - 1)) and (B) normalized betweenness centrality across the full, Cluster 1, and Cluster 2 network frameworks. (C) Proportion (%) of assortative interactions, defined as the percentage of topological edges linking an inoculated SynCom strain directly to another introduced strain. (D) Proportion of connections of introduced strains with bacterial ASVs. (E) Normalized degree centrality of responding native taxa, partitioned by their differential abundance profiles (depleted vs. enriched ASVs) across the three network configurations. Different lowercase letters denote statistically significant differences among network types within each abundance group (Dunn's test with Benjamini-Hochberg correction, $p < 0.05$).

Since SynComs strains integration modified the abundance of specific taxa, we investigated how the 82 identified differentially abundant (DA) native bacterial ASVs were behaving in these networks. These taxa were previously classified as enriched (n = 58) or depleted (n = 24, Fig. 6C). Within the global network, all 82 DA bacterial ASVs were exclusively located within the giant component. Within the cluster-specific networks, 77 DA ASVs were detected in Cluster 1, and 81 in Cluster 2, with the majority

(79.30%, n = 65 ASVs) shared between the giant components of all three networks. The normalized degree (Fig. 8E) of Cluster 1 network DA strains (2.08×10^{-3}) was higher than in the Cluster 2 (1.39×10^{-3}) and global (1.36×10^{-3}) networks (Dunn's test with BH correction, $p < 0.05$). Conversely, depleted ASVs showed reduced connectivity in Cluster 1 (1.13×10^{-3}) relative to Cluster 2 (1.70×10^{-3}; Dunn's test with BH correction, $p = 0.062$), while remaining comparable to the global network (1.57×10^{-3}). To test whether these connectivity shifts were driven by interactions with inoculated SynCom members, we quantified the proportion of edges linking SynCom strain to DA strains. This proportion was consistent across all three networks, with no significant differences (Kruskal-Wallis test, $p = 0.590$), indicating that global connectivity changes were not directly attributable to SynCom-DA interactions. However, strain-level analysis revealed a notable exception: *Pantoea agglomerans* CFBP 9280. In the Cluster 2 network, 85.7% of its interactions (6 out of 7 edges) involved DA native taxa, evenly distributed between enriched and depleted ASVs. In contrast, in the Cluster 1 network, only 11.1% of its interactions (1 out of 9 edges) targeted DA taxa. Overall, DA bacterial strains displayed network-specific connectivity patterns, with increased connectivity correlated to enriched ASVs and decreased connectivity correlated with depleted ASVs. These modifications were not explained by overall interaction frequency with SynCom strains, although the distinct connections of *Pantoea agglomerans* CFBP 9280 suggests the presence of strain-specific interaction dynamics that may contribute to community restructuring.

Identification of four SynCom profiles based on bacterial community shift and fungal colonization

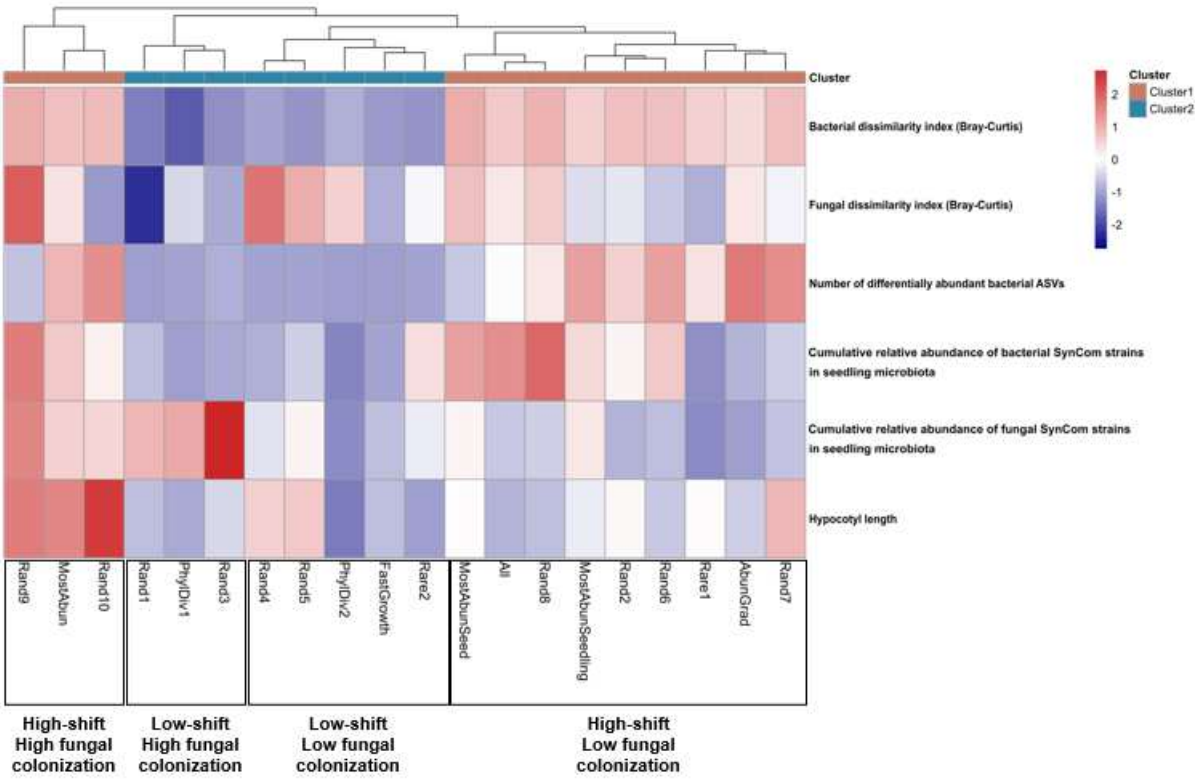


Fig. 9: **Main characteristics of SynComs' impacts. Hierarchical clustering heatmap summarizing the SynCom effects on seedling microbiota and phenotype**: Bacterial and fungal Bray-Curtis dissimilarity index compared to control condition, number of differentially abundant bacterial taxa, Cumulative relative abundance of bacterial and fungal SynCom strains and hypocotyl length. All displayed values are Z-score. SynComs belong to either Cluster 1 (Orange) or Cluster 2 (Blue) and are grouped in 4 distinct profiles.

The main characteristics of SynComs impact on seedlings are summarized in Fig. 9.

While clustering primarily separated SynComs based on their ability to modulate seedling bacterial microbiota (Cluster 1: community shift, Cluster 2: no community shift), this more integrative approach revealed four distinct SynCom profiles defined by two criteria: bacterial community shift and fungal colonization. 3 SynComs (Rand10, Rand9, and MostAbun) combined bacterial community shift with high fungal colonization and were termed "High shift - High fungal colonization". SynComs that modulated bacterial communities but had low fungal colonization were termed "High shift - Low fungal colonization." The remaining SynComs with limited community impact were further split by colonization levels into "Low shift - High fungal colonization" and "Low shift - Low colonization". The other criteria assessed (fungal community shift, bacterial colonization, hypocotyl length) did not clearly structure these profiles. Still, we can note that the "high shift - high colonization" SynComs displayed greater hypocotyl length than the other profiles. While comparing the four SynCom profiles with their composition (Fig. 1A) and compositional distance (Fig. 1B), no specific strain or SynCom composition matched with these profiles.

Discussion:

Tailored seed inoculation enables successful seed microbiota modulation

In this study, we provide new insights on the transmission and impact of multiple multi-kingdom SynComs on the seedling microbiota of an important crop species. In line with our first hypothesis (H1), we successfully inoculated *Brassica napus* seeds with 20 distinct multi-kingdom SynComs and demonstrated their partial transmission to the seedlings. By comparing four inoculation methods, we identified alginate coating as a robust method for high microbial load inoculation and transmission of multi-kingdom SynComs. This optimization highlights the importance of tailoring inoculation strategies to the target plant model to achieve a sufficient propagule pressure, a key factor to enhance seedling colonization [15]. Such methodological considerations are particularly critical given the diversity of plant models used in SynCom studies [19], and the fact that relatively few studies directly monitor the fate of introduced communities [6]. With efficient seed inoculation, we show that bacterial communities are more easily modified than fungal ones, likely reflecting the higher resistance and stability of native fungal communities [58]. Despite successful inoculation, only a small fraction of

809 inoculated strains persisted in 15-day old seedlings grown in non-sterile soil. Colonization levels were
810 highly variable for both bacterial and fungal strains, with dominant seedling colonizers largely
811 originating from the soil, in accordance with previous studies [29]. This contrasts with studies on
812 younger seedlings of other plant (e.g., *Phaseolus vulgaris* [15]), and highlights the dynamic nature of
813 microbiota assembly influenced by nutrients availability [59] and the exposure to oxidative stress [60]
814 during early plant development.

815 **Evaluating SynCom design strategies: Key role of strain selection in colonization performance**

816 We next tested whether SynCom design could influence colonization success (H2), specifically whether
817 *a priori*-designed communities would outperform randomly assembled ones. Overall, only minor
818 differences were observed between the two strategies, with random SynComs showing slightly higher
819 fungal colonization. This suggests that community assembly rules alone are not sufficient to predict
820 colonization outcome. Still, within the *a priori* SynComs, some designs outperformed others at
821 colonizing seedlings. SynComs composed of naturally abundant taxa (*Cladosporium, Alternaria,*
822 *Pantoea, Pseudomonas*) in the seed or seedling microbiota were the most effective for both bacterial
823 and fungal colonization. This observation is consistent with previous studies [15] and likely reflects
824 stronger ecological adaptation of these strains to plant-associated environments [25]. Importantly,
825 these abundant taxa are not only frequently detected through sequencing but are also commonly
826 isolated in culture collections [31], supporting their naturally high prevalence. In contrast, SynComs
827 composed of rare taxa showed more variable outcomes. While some performed well, this was largely
828 driven by the presence of specific strains such as *Pseudomonas* sp. CFBP 9285 and *Vishniacozyma* sp.
829 CLIB 4449. Although rare taxa can naturally colonize seedlings [29, 62], our results suggest that their
830 efficient transmission under artificial enrichment is strain-dependent and less predictable. A mixed
831 SynCom combining taxa of different abundance levels created to mimic the natural community
832 structure of natural seed microbiota [63], and reduce niche overlap [64] did not outperform
833 communities composed solely of highly abundant taxa. This suggests that, in our system, ecological
834 compatibility with the plant environment was a stronger determinant of establishment than niche
835 complementarity. Similarly, SynComs designed to maximize phylogenetic diversity did not enhance
836 colonization, indicating that reducing intra-community competition, or potentially increasing
837 metabolic complementarity [65], is insufficient when strong competition with native microbiota
838 persists [66]. The limited performance of SynComs composed of fast-growing strains further
839 emphasizes that *in vitro* growth traits are poor predictors of *in planta* success, likely due to the
840 mismatch between artificial media and plant-associated environments [67]. Finally, a highly diverse
841 SynCom containing a large number of strains achieved strong colonization of seedling for both bacteria
842 and fungi. This might reflect facilitative processes such as niche expansion [68], cross feeding [69] and

even higher order interactions [23]. More broadly, our results suggest that native microbiota exert stronger competitive pressures than interactions within the SynCom itself. Taken together, these findings suggest that strain selection is a more critical determinant of SynCom performance than assembly strategy. Even randomly assembled communities can perform well, as long as they are drawn from a pool of ecologically relevant and well-adapted taxa. However, because randomly assembled SynComs were drawn from an ecologically relevant strain pool and overall colonization remained limited, the role of assembly criteria may be underestimated and likely depends on the environmental context of the inoculation and the desired functional outcomes.

Identification of shared and kingdom-specific traits involved in seedling colonization

Monitoring individual strains across multiple SynCom contexts revealed strong strain-dependent colonization patterns, supporting our third hypothesis (H3). Strain identity emerged as the most explanatory variable for both bacterial and fungal colonization, indicating that colonization success relies on strain-specific traits that are not easily captured by simple phenotypic descriptors. This phenomenon may emerge from interaction-driven processes, in line with the concept of phenotypic niche extension, whereby microbial strains expand or shift through niche interactions with co-occurring taxa [68]. Nevertheless, several traits were associated with improved colonization of strains. For both bacteria and fungi, higher initial abundance on seed increased colonization of seedling. This relationship was linear for bacteria in accordance with previous research [15] whereas for fungi, it reached a plateau and then decreased, indicating an inoculation threshold beyond which colonization decreased. This threshold could be explained by autoregulatory mechanisms such as *quorum sensing* controlling conidia germination [70]. Lag phase also influenced colonization in both kingdoms, although with a modest and non-linear effect. A biphasic pattern emerged, where rapidly growing strains likely benefited from early niche occupation, whereas strains with longer lag phases appeared favored at later stages (around 21 h). This might be linked to the dynamic environmental modification during oilseed rape seed germination, including exudates released in the soil [71] which could create temporal niches favoring late-establishing strains, and oxidative stress release that induce strain selection [60, 72]. Additional kingdom-specific traits were identified. For bacteria, larger genome size was positively correlated to a better colonization. Since bacterial genomes are highly dense in genes [73], higher genome size could be linked to greater metabolic versatility and adaptive capacity [74]. For fungi, natural prevalence on seed was positively linked to better colonization, suggesting that dominant seed-associated fungi are better adapted to withstand germination-related stresses and persist during early plant development.

Impact of SynCom inoculation on bacterial native communities revealing distinct profiles

We demonstrated that SynCom inoculation significantly altered the native bacterial microbiota, leading to the emergence of two distinct community profiles: weakly disturbed and strongly modified bacterial communities. In contrast, fungal microbiota remained stable. These two clusters were robustly confirmed by ASV differential abundance analyses, in line with current methodological frameworks [75, 76]. This clustering further enabled the construction of two distinct multi-kingdom co-occurrence networks, corresponding to SynCom-responsive (Cluster 1) and non-responsive (Cluster 2) communities. Differences in network topology between these clusters likely reflect the extent to which inoculated strains successfully integrate into the native microbiota and influence its assembly. A total of 82 native bacterial ASVs were identified as responsive to SynCom inoculation, most of which likely originated from the soil, indicating that SynComs influence community assembly by modulating the recruitment of environmental taxa. Importantly, these shifts were not attributable to any single SynCom composition, as the 14 SynComs associated with modified communities did not share a common set of strains. In responsive communities (Cluster 1), inoculated strains appeared more central and connected within the network, suggesting successful integration into the native microbiota and a greater capacity to reshape microbial interactions, including the recruitment of additional taxa. In contrast, non-responsive communities (Cluster 2) displayed network structures closer to the native state, indicating limited integration of introduced strains. By separating these two community response types, our approach allowed a more accurate identification of SynCom-driven dynamics and highlighted the context dependency of microbial establishment and interaction within plant-associated microbiota. At the strain level, *Pantoea agglomerans* CFBP 9280 displayed a different co-occurrence profile between clusters. This strain's relative abundance being highly enhanced in seedling of inoculated conditions, its introduction might play a pivotal role in early seedling microbial assembly through interactions with environmental taxa, as it belongs to a seed core microbiota genus with a potential high transmission in a natural context [77]. Interestingly, samples with altered bacterial communities exhibited increased interkingdom connectivity, highlighting the importance of bacteria-fungi interactions in shaping microbiota assembly [20].

Finally, four different SynCom profiles emerged from their impact on seedling, whether they shifted bacterial communities and/or fungal strains colonized the seedlings. The modulation of bacterial communities without or with low colonization of SynComs translates to a potential effect of transient interactions, a pattern already observed in soil only between bacterial inoculant and communities [78]. On the other hand, a combined fungal colonization with bacterial shift can be associated with longer-lasting inter-kingdom interactions between inoculated and native strains mediated by the installation of introduced fungi. Notably, this profile of high colonization and community shift was associated with an increase of hypocotyl length, hinting at specific design that might impact the plant more efficiently [79]. Interestingly, profiles with no bacterial community shift were observed whether SynCom

colonized or not seedlings, showing that SynCom transmission is not necessarily associated with broad community modification. Overall, these results highlight the complexity of microbiota modulation, which arises from multiple interactions within and between kingdoms, between inoculated strains, native microbiota, and the plant. Since our observations are limited to a 15-day time point, the potential role of transient or low abundance taxa remains to be investigated, and may exert a lasting effect on community assembly [80].

Conclusions:

Through the inoculation and monitoring of 20 different multi-kingdom SynComs on Brassica napus seeds, we showed that inoculated strains were partially transmitted to seedlings while 14 SynComs significantly reshaped the seedling bacterial microbiota by modifying the recruitment of 82 bacterial taxa. Our design strategy highlighted that strain identity mattered more than the SynCom assembly strategy for seedling colonization. We also demonstrated that the fungal microbiota was more resistant to both seed colonization and community modulation in contrast to bacterial communities. These modulations of the bacterial communities were explained by a better integration of microbial strains in the network community structures. Based on our findings, we distinguish four different SynComs profiles: SynComs that have high colonization and those that do not, as well as between communities that disrupt or preserve seedling bacterial recruitment. These non-disruptive profiles deserve attention given growing concerns about the ecological risks of microbial inoculants [8] by their potential effect on plant health while having reduced impact on native communities. Altogether, these findings provide actionable directions for improving SynCom design, suggesting that leveraging ecological processes such as host adaptation, optimal inoculation density, and network integration could enhance both colonization efficiency and plant phenotypic outcomes.

Declarations:

Ethics approval and consent to participate

Not applicable

Consent for publication

Not applicable

Availability of data and materials

The datasets generated and analyzed during the current study are available in the INRAE forge repository, https://forge.inrae.fr/irhs-emersys/2026_logan_inoseed

Competing interests

The authors declare that they have no competing interests

Funding

This work was funded by the 3rd Programme for Future Investments (France 2030), operated by the SUCSEED project (ANR-20-PCPA-0009) and funded by the 'Growing and Protecting crops Differently' French Priority Research Program (PPR-CPA), part of the national investment plan operated by the French National Research Agency (ANR). This research was also funded by the National Research Institute for Agriculture, Food, and the Environment' (INRAE) through the HOLOFLUX metaprogram and with the support of the French Region Pays de la Loire, Angers Loire Métropole.

Authors' contributions

LS produced the data, analyzed, interpreted and was the main contributor in writing the manuscript. CC, NG and MS provided support for experimentation, insight for analysis as well as thorough corrections and rephrasing of the manuscripts. CM helped for bacterial culture and phenotyping as well as for amplicon bank preparation and sequencing. MB assembled bacterial genomes. AH and KH helped with plant culture. KM provided help and expertise for the co-occurrence network analysis, power calculation as well as corrections and rephrasing of the manuscript. MM provided support for fungal strain culture, phenotyping and taxonomic affiliation. All authors read and approved the final manuscript.

Acknowledgements

We thank the platform PHENOTIC [81] for the plant culture, the ANAN platform for genome and amplicon sequencing, the Himic platform for the individual growth culture assay. We also thank the CIRM-CFBP [82] and CIRM-Levures for the strain conservation. We thank Elise Alix and Bernard Moulin (IGEPP) and the Experimental Unit UE La Motte for the oilseed rape seed production in the field and the CRB BrACYSol for providing the oilseed rape genetic resources. We would also like to thank Alain Sarniguet for his advice and expertise on *B. napus* seed experiments, Justin Colou for her knowledge on fungal genome assembly, Martial Briand for his expertise on bacterial genomes and Philippe Simoneau for his insight on fungal taxonomy. A special thanks for everyone who helped inoculating, sowing and harvesting the seed and seedlings: Louna Colaert-Sentenac, Thomas Chadelaud, Coralie Marais, Clara Centa, Marie-Agnès Jacques, Chrystelle Brin, Martial Briand, Nathan Kavunu, Géraldine Taghouti, Oscar Joubert and Franck Bastide.

References

1. Koch H, Clavel T, Mayr C, Coltman BL, Schloter M, Vorholt JA, et al. From "synthetic" to defined microbial communities for clearer terminology. Nat Commun. 2026;17:5283. https://doi.org/10.1038/s41467-026-74251-1.

2. Großkopf T, Soyer OS. Synthetic microbial communities. Curr Opin Microbiol. 2014;18:72–7. https://doi.org/10.1016/j.mib.2014.02.002.

3. Vannier N, Mony C, Bittebiere A-K, Michon-Coudouel S, Biget M, Vandenkoornhuyse P. A microorganisms' journey between plant generations. Microbiome. 2018;6:79. https://doi.org/10.1186/s40168-018-0459-7.

4. Portal-Gonzalez N, Wang W, He W, Santos-Bermudez R. Engineering Plant Holobionts for Climate-Resilient Agriculture. ISME J. 2025;:wraf158. https://doi.org/10.1093/ismejo/wraf158.

5. Vannier N, Agler M, Hacquard S. Microbiota-mediated disease resistance in plants. PLOS Pathog. 2019;15:e1007740. https://doi.org/10.1371/journal.ppat.1007740.

6. Kaminsky LM, Trexler RV, Malik RJ, Hockett KL, Bell TH. The Inherent Conflicts in Developing Soil Microbial Inoculants. Trends Biotechnol. 2019;37:140–51. https://doi.org/10.1016/j.tibtech.2018.11.011.

7. Russ D, Fitzpatrick CR, Teixeira PJPL, Dangl JL. Deep discovery informs difficult deployment in plant microbiome science. Cell. 2023;186:4496–513. https://doi.org/10.1016/j.cell.2023.08.035.

8. Ladau J, Fahimipour AK, Newcomer ME, Brown JB, Vora GJ, Melby MK, et al. Microbial inoculants and invasions: a call to action. Trends Microbiol. 2025;33:1064–75. https://doi.org/10.1016/j.tim.2025.04.018.

9. Rillig MC, Antonovics J, Caruso T, Lehmann A, Powell JR, Veresoglou SD, et al. Interchange of entire communities: microbial community coalescence. Trends Ecol Evol. 2015;30:470–6. https://doi.org/10.1016/j.tree.2015.06.004.

10. Russel J, Røder HL, Madsen JS, Burmølle M, Sørensen SJ. Antagonism correlates with metabolic similarity in diverse bacteria. Proc Natl Acad Sci. 2017;114:10684–8. https://doi.org/10.1073/pnas.1706016114.

11. Moyne O, Norton GJ, Al-Bassam M, Lieng C, Thiruppathy D, Kumar M, et al. Predicting competition and substrate preferences for targeted microbiome alteration. Cell. 2026;189:3324-3338.e23. https://doi.org/10.1016/j.cell.2026.03.036.

12. Garin T, Brin C, Préveaux A, Brault A, Briand M, Simonin M, et al. The type VI secretion system of Stenotrophomonas rhizophila CFBP13503 limits the transmission of Xanthomonas campestris pv. campestris 8004 from radish seeds to seedlings. Mol Plant Pathol. 2024;25. https://doi.org/10.1111/mpp.13412.

13. Colautti RI, Grigorovich IA, MacIsaac HJ. Propagule Pressure: A Null Model for Biological Invasions. Biol Invasions. 2006;8:1023–37. https://doi.org/10.1007/s10530-005-3735-y.

14. Debray R, Herbert RA, Jaffe AL, Crits-Christoph A, Power ME, Koskella B. Priority effects in microbiome assembly. Nat Rev Microbiol. 2022;20:109–21. https://doi.org/10.1038/s41579-021-00604-w.

15. Arnault G, Marais C, Préveaux A, Briand M, Poisson A-S, Sarniguet A, et al. Seedling microbiota engineering using bacterial synthetic community inoculation on seeds. FEMS Microbiol Ecol. 2024;100:fiae027. https://doi.org/10.1093/femsec/fiae027.

16. Joubert O, Arnault G, Barret M, Simonin M. Sowing success: ecological insights into seedling microbial colonisation for robust plant microbiota engineering. Trends Plant Sci. 2025;30:21–34. https://doi.org/10.1016/j.tplants.2024.09.004.

17. Rocha I, Ma Y, Souza-Alonso P, Vosátka M, Freitas H, Oliveira RS. Seed Coating: A Tool for Delivering Beneficial Microbes to Agricultural Crops. Front Plant Sci. 2019;10. https://doi.org/10.3389/fpls.2019.01357.

18. Simonin M, Préveaux A, Marais C, Garin T, Arnault G, Sarniguet A, et al. Transmission of synthetic seed bacterial communities to radish seedlings: impact on microbiota assembly and plant phenotype. Peer Community J. 2023;3. https://doi.org/10.24072/pcjournal.329.

19. Xu X, Dinesen C, Pioppi A, Kovács ÁT, Lozano-Andrade CN. Composing a microbial symphony: synthetic communities for promoting plant growth. Trends Microbiol. 2025;33:738–51. https://doi.org/10.1016/j.tim.2025.01.006.

20. Durán P, Thiergart T, Garrido-Oter R, Agler M, Kemen E, Schulze-Lefert P, et al. Microbial Interkingdom Interactions in Roots Promote Arabidopsis Survival. Cell. 2018;175:973-983.e14. https://doi.org/10.1016/j.cell.2018.10.020.

21. Liu Q, Cheng L, Zhang E, Ling L, Tan W, Liang S, et al. Cross-niche metabolite–microbiome interactions orchestrate systemic soybean resistance to *Fusarium* root rot. ISME J. 2026;20:wrag080. https://doi.org/10.1093/ismejo/wrag080.

22. Lee KK, Kim H, Lee Y-H. Cross-kingdom co-occurrence networks in the plant microbiome: Importance and ecological interpretations. Front Microbiol. 2022;13.

23. Deveau A, Bonito G, Uehling J, Paoletti M, Becker M, Bindschedler S, et al. Bacterial–fungal interactions: ecology, mechanisms and challenges. FEMS Microbiol Rev. 2018;42:335–52. https://doi.org/10.1093/femsre/fuy008.

24. Liu X, Mei S, Salles JF. Inoculated microbial consortia perform better than single strains in living soil: A meta-analysis. Appl Soil Ecol. 2023;190:105011. https://doi.org/10.1016/j.apsoil.2023.105011.

25. Sun J, Zhou H, Cheng H, Chen Z, Wang Y. Bacterial abundant taxa exhibit stronger environmental adaption than rare taxa in the Arctic Ocean sediments. Mar Environ Res. 2024;199:106624. https://doi.org/10.1016/j.marenvres.2024.106624.

26. Malard LA, Guisan A. Into the microbial niche. Trends Ecol Evol. 2023;38:936–45. https://doi.org/10.1016/j.tree.2023.04.015.

27. Mallon CA, Elsas JD van, Salles JF. Microbial Invasions: The Process, Patterns, and Mechanisms. Trends Microbiol. 2015;23:719–29. https://doi.org/10.1016/j.tim.2015.07.013.

28. Zhang X, Ma Y-N, Wang X, Liao K, He S, Zhao X, et al. Dynamics of rice microbiomes reveal core vertically transmitted seed endophytes. Microbiome. 2022;10:216. https://doi.org/10.1186/s40168-022-01422-9.

29. Rochefort A, Simonin M, Marais C, Guillerm-Erckelboudt A-Y, Barret M, Sarniguet A. Transmission of Seed and Soil Microbiota to Seedling. mSystems. 2021;6:10.1128/msystems.00446-21. https://doi.org/10.1128/msystems.00446-21.

30. Abdelfattah A, Tack AJM, Lobato C, Wassermann B, Berg G. From seed to seed: the role of microbial inheritance in the assembly of the plant microbiome. Trends Microbiol. 2023;31:346–55. https://doi.org/10.1016/j.tim.2022.10.009.

31. Simonin M, Guschinskaya N, Marchi M, Marais C, Préveaux A, Briand M, et al. Seed Microbiota Diversity and Culture Collection of Four Major Crops Covering Different Genotypes and Production Modes. 2026;:2026.04.29.721552. https://doi.org/10.64898/2026.04.29.721552.

32. Joubert A, Calmes B, Berruyer R, Pihet M, Bouchara J-P, Simoneau P, et al. Laser nephelometry applied in an automated microplate system to study filamentous fungus growth. BioTechniques. 2010;48:399–404. https://doi.org/10.2144/000113399.

33. Chesneau G, Laroche B, Préveaux A, Marais C, Briand M, Marolleau B, et al. Single Seed Microbiota: Assembly and Transmission from Parent Plant to Seedling. mBio. 2022;13:e01648-22. https://doi.org/10.1128/mbio.01648-22.

34. Association IST. International Rules Seed Testing | Official ISTA Guidelines. International Seed Testing Association. https://www.seedtest.org/en/publications/international-rules-seed-testing.html. Accessed 23 June 2026.

35. Barret M, Briand M, Bonneau S, Préveaux A, Valière S, Bouchez O, et al. Emergence Shapes the Structure of the Seed Microbiota. Appl Environ Microbiol. 2015;81:1257–66. https://doi.org/10.1128/AEM.03722-14.

36. Buée M, Reich M, Murat C, Morin E, Nilsson RH, Uroz S, et al. 454 Pyrosequencing analyses of forest soils reveal an unexpectedly high fungal diversity. New Phytol. 2009;184:449–56. https://doi.org/10.1111/j.1469-8137.2009.03003.x.

37. Möller EM, Bahnweg G, Sandermann H, Geiger HH. A simple and efficient protocol for isolation of high molecular weight DNA from filamentous fungi, fruit bodies, and infected plant tissues. Nucleic Acids Res. 1992;20:6115–6. https://doi.org/10.1093/nar/20.22.6115.

38. Kolmogorov M, Yuan J, Lin Y, Pevzner PA. Assembly of long, error-prone reads using repeat graphs. Nat Biotechnol. 2019;37:540–6. https://doi.org/10.1038/s41587-019-0072-8.

39. Parks DH, Imelfort M, Skennerton CT, Hugenholtz P, Tyson GW. CheckM: assessing the quality of microbial genomes recovered from isolates, single cells, and metagenomes. Genome Res. 2015;25:1043–55. https://doi.org/10.1101/gr.186072.114.

40. Chaumeil P-A, Mussig AJ, Hugenholtz P, Parks DH. GTDB-Tk v2: memory friendly classification with the genome taxonomy database. Bioinformatics. 2022;38:5315–6. https://doi.org/10.1093/bioinformatics/btac672.

41. Martin M. Cutadapt removes adapter sequences from high-throughput sequencing reads. EMBnet.journal. 2011;17:10–2. https://doi.org/10.14806/ej.17.1.200.

42. Pauvert C, Buée M, Laval V, Edel-Hermann V, Fauchery L, Gautier A, et al. Bioinformatics matters: The accuracy of plant and soil fungal community data is highly dependent on the metabarcoding pipeline. Fungal Ecol. 2019;41:23–33. https://doi.org/10.1016/j.funeco.2019.03.005.

43. Briand, Martial, Rué, Olivier, Barret, Matthieu, Institut national de recherche pour l'agriculture, l'alimentation et l'environnement. gyrB database for taxonomic assignment formatted for DADA2. 2025. https://doi.org/10.57745/DD7RZ8.

44. Nilsson RH, Larsson K-H, Taylor AFS, Bengtsson-Palme J, Jeppesen TS, Schigel D, et al. The UNITE database for molecular identification of fungi: handling dark taxa and parallel taxonomic classifications. Nucleic Acids Res. 2019;47:D259–64. https://doi.org/10.1093/nar/gky1022.

45. Frøslev TG, Kjøller R, Bruun HH, Ejrnæs R, Brunbjerg AK, Pietroni C, et al. Algorithm for post-clustering curation of DNA amplicon data yields reliable biodiversity estimates. Nat Commun. 2017;8:1188. https://doi.org/10.1038/s41467-017-01312-x.

46. Oksanen J, Simpson GL, Blanchet FG, Kindt R, Legendre P, Minchin PR, et al. vegan: Community Ecology Package. 2001;:2.7-5. https://doi.org/10.32614/CRAN.package.vegan.

47. McMurdie PJ, Holmes S. phyloseq: An R Package for Reproducible Interactive Analysis and Graphics of Microbiome Census Data. PLOS ONE. 2013;8:e61217. https://doi.org/10.1371/journal.pone.0061217.

48. Wood SN. Generalized Additive Models. Annu Rev Stat Its Appl. 2025;12 Volume 12, 2025:497–526. https://doi.org/10.1146/annurev-statistics-112723-034249.

49. Lai J, Tang J, Li T, Zhang A, Mao L. Evaluating the relative importance of predictors in Generalized Additive Models using the *gam.hp* R package. Plant Divers. 2024;46:542–6. https://doi.org/10.1016/j.pld.2024.06.002.

50. Russel J, Thorsen J, Brejnrod AD, Bisgaard H, Sørensen SJ, Burmølle M. DAtest: a framework for choosing differential abundance or expression method. 2018;:241802. https://doi.org/10.1101/241802.

51. Kurtz ZD, Müller CL, Miraldi ER, Littman DR, Blaser MJ, Bonneau RA. Sparse and Compositionally Robust Inference of Microbial Ecological Networks. PLOS Comput Biol. 2015;11:e1004226. https://doi.org/10.1371/journal.pcbi.1004226.

52. Aitchison J. The Statistical Analysis of Compositional Data. J R Stat Soc Ser B Methodol. 1982;44:139–77.

53. Bastian M, Heymann S, Jacomy M. Gephi: An Open Source Software for Exploring and Manipulating Networks. Proc Int AAAI Conf Web Soc Media. 2009;3:361–2. https://doi.org/10.1609/icwsm.v3i1.13937.

54. Csárdi G, Nepusz T, Müller K, Horvát S, Traag V, Zanini F, et al. igraph for R: R interface of the igraph library for graph theory and network analysis. 2026. https://doi.org/10.5281/ZENODO.7682609.

55. Newman MEJ. Mixing patterns in networks. Phys Rev E. 2003;67:026126. https://doi.org/10.1103/PhysRevE.67.026126.

56. Kruskal WH, Wallis WA. Use of Ranks in One-Criterion Variance Analysis. J Am Stat Assoc. 1952;47:583–621. https://doi.org/10.1080/01621459.1952.10483441.

57. Dunn OJ. Multiple Comparisons Using Rank Sums. Technometrics. 1964;6:241–52. https://doi.org/10.1080/00401706.1964.10490181.

58. Aleklett K, Rosa D, Pickles BJ, Hart MM. Community Assembly and Stability in the Root Microbiota During Early Plant Development. Front Microbiol. 2022;13. https://doi.org/10.3389/fmicb.2022.826521.

59. Torres-Cortés G, Bonneau S, Bouchez O, Genthon C, Briand M, Jacques M-A, et al. Functional Microbial Features Driving Community Assembly During Seed Germination and Emergence. Front Plant Sci. 2018;9. https://doi.org/10.3389/fpls.2018.00902.

60. Gerna D, Roach T, Mitter B, Stöggl W, Kranner I. Hydrogen Peroxide Metabolism in Interkingdom Interaction Between Bacteria and Wheat Seeds and Seedlings. Mol Plant-Microbe Interactions®. 2020;33:336–48. https://doi.org/10.1094/MPMI-09-19-0248-R.

61. Westerband AC, Funk JL, Barton KE. Intraspecific trait variation in plants: a renewed focus on its role in ecological processes. Ann Bot. 2021;127:397–410. https://doi.org/10.1093/aob/mcab011.

62. Chesneau G, Laroche B, Préveaux A, Marais C, Briand M, Marolleau B, et al. Single Seed Microbiota: Assembly and Transmission from Parent Plant to Seedling. mBio. 2022;13:e01648-22. https://doi.org/10.1128/mbio.01648-22.

63. Bintarti AF, Sulesky-Grieb A, Stopnisek N, Shade A. Endophytic Microbiome Variation Among Single Plant Seeds. Phytobiomes J. 2022;6:45–55. https://doi.org/10.1094/PBIOMES-04-21-0030-R.

64. Jiao S, Lu Y. Abundant fungi adapt to broader environmental gradients than rare fungi in agricultural fields. Glob Change Biol. 2020;26:4506–20. https://doi.org/10.1111/gcb.15130.

65. Shu X, Liu Y. Collaboration promotes stability: insights from SynComs study. Trends Microbiol. 2025. https://doi.org/10.1016/j.tim.2025.08.003.

66. Lemos-Costa P, Miller ZR, Allesina S. Phylogeny structures species' interactions in experimental ecological communities. Ecol Lett. 2024;27:e14490. https://doi.org/10.1111/ele.14490.

67. Hegazi NA, Patz S, Fricke F, El-Zayat AS, Ahmed MN, Hamza MA, et al. Culturomics of the plant microbiota: the emerging in situ similis cultivation strategies to meet the complexity of nutritional requirements of microbiota associated with plants of multiple species, growth stages and compartments. Plant Soil. 2026. https://doi.org/10.1007/s11104-025-08269-7.

68. Li M, Wei Z, Wang J, Jousset A, Friman V, Xu Y, et al. Facilitation promotes invasions in plant-associated microbial communities. Ecol Lett. 2019;22:149–58. https://doi.org/10.1111/ele.13177.

69. Mataigne A, Vannier N, Vandenkoornhuyse P, Hacquard S. Microbial Systems Ecology to Understand Cross-Feeding in Microbiomes. Front Microbiol. 2021;12. https://doi.org/10.3389/fmicb.2021.780469.

70. LINGAPPA BT, LINGAPPA Y. Role of Auto-inhibitors on Mycelial Growth and Dimorphism of Glomerella cingulata. Microbiology. 1969;56:35–45. https://doi.org/10.1099/00221287-56-1-35.

71. Nelson EB. MICROBIAL DYNAMICS AND INTERACTIONS IN THE SPERMOSPHERE. Annu Rev Phytopathol. 2004;42 Volume 42, 2004:271–309. https://doi.org/10.1146/annurev.phyto.42.121603.131041.

72. Schopfer P, Plachy C, Frahry G. Release of Reactive Oxygen Intermediates (Superoxide Radicals, Hydrogen Peroxide, and Hydroxyl Radicals) and Peroxidase in Germinating Radish Seeds Controlled by Light, Gibberellin, and Abscisic Acid. Plant Physiol. 2001;125:1591–602. https://doi.org/10.1104/pp.125.4.1591.

73. Kuo C-H, Moran NA, Ochman H. The consequences of genetic drift for bacterial genome complexity. Genome Res. 2009. https://doi.org/10.1101/gr.091785.109.

74. Rodríguez-Gijón A, Buck M, Andersson AF, Izabel-Shen D, Nascimento FJA, Garcia SL. Linking prokaryotic genome size variation to metabolic potential and environment. ISME Commun. 2023;3:25. https://doi.org/10.1038/s43705-023-00231-x.

75. Lin H, Peddada SD. Analysis of microbial compositions: a review of normalization and differential abundance analysis. Npj Biofilms Microbiomes. 2020;6:60. https://doi.org/10.1038/s41522-020-00160-w.

76. Nearing JT, Douglas GM, Hayes MG, MacDonald J, Desai DK, Allward N, et al. Microbiome differential abundance methods produce different results across 38 datasets. Nat Commun. 2022;13:342. https://doi.org/10.1038/s41467-022-28034-z.

77. Simonin M, Briand M, Chesneau G, Rochefort A, Marais C, Sarniguet A, et al. Seed microbiota revealed by a large-scale meta-analysis including 50 plant species. New Phytol. 2022;234:1448–63. https://doi.org/10.1111/nph.18037.

78. Mallon CA, Le Roux X, van Doorn GS, Dini-Andreote F, Poly F, Salles JF. The impact of failure: unsuccessful bacterial invasions steer the soil microbial community away from the invader's niche. ISME J. 2018;12:728–41. https://doi.org/10.1038/s41396-017-0003-y.

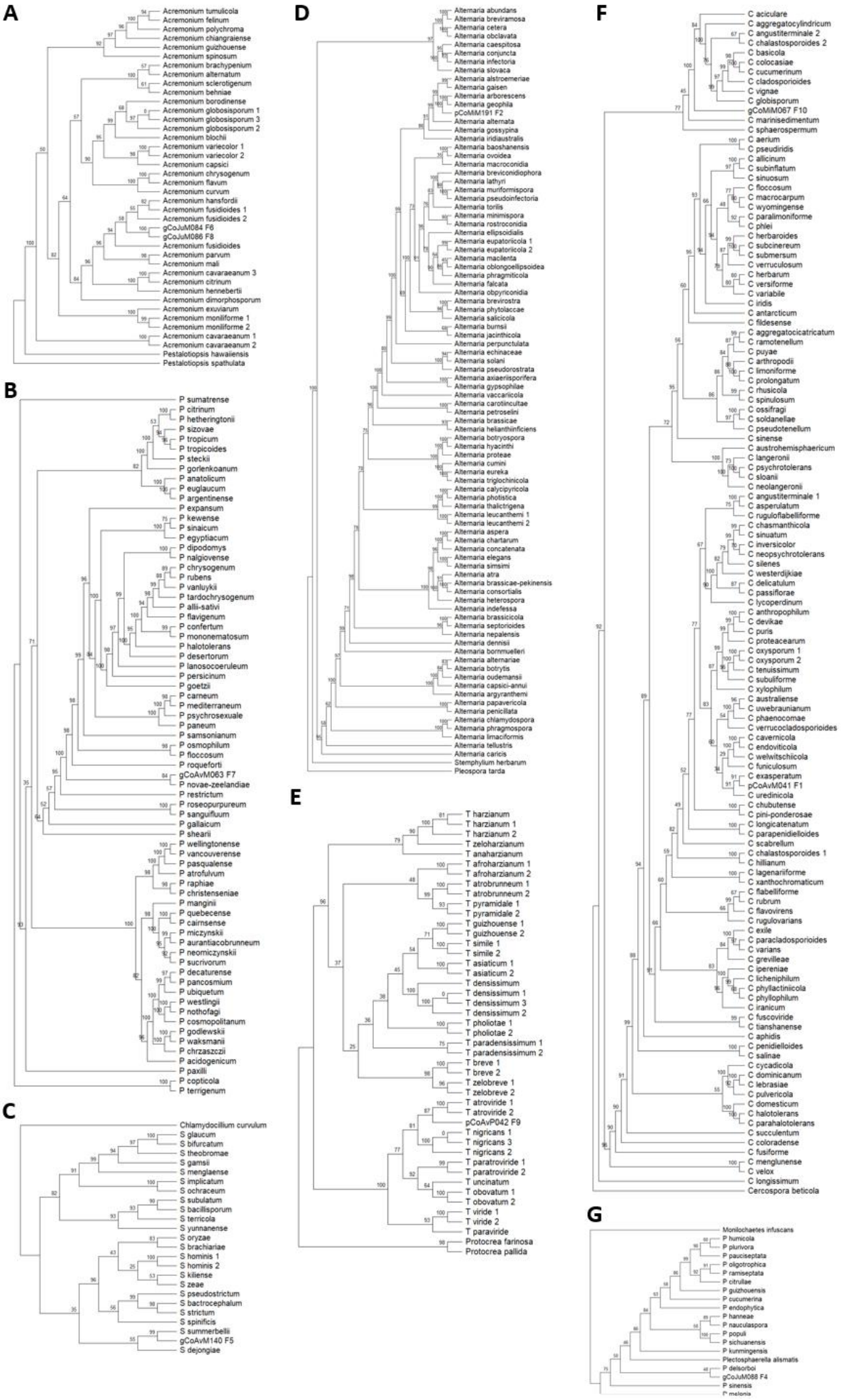
79. Newman A, Picot E, Davies S, Hilton S, Carré IA, Bending GD. Circadian rhythms in the plant host influence rhythmicity of rhizosphere microbiota. BMC Biol. 2022;20:235. https://doi.org/10.1186/s12915-022-01430-z.

80. Suteau L, Colaert-Sentenac L, Law SR, Simonin M. Transient microbial architects: tracing the legacy effects of ephemeral taxa during plant microbiome assembly. Curr Opin Microbiol. 2025;88:102664. https://doi.org/10.1016/j.mib.2025.102664.

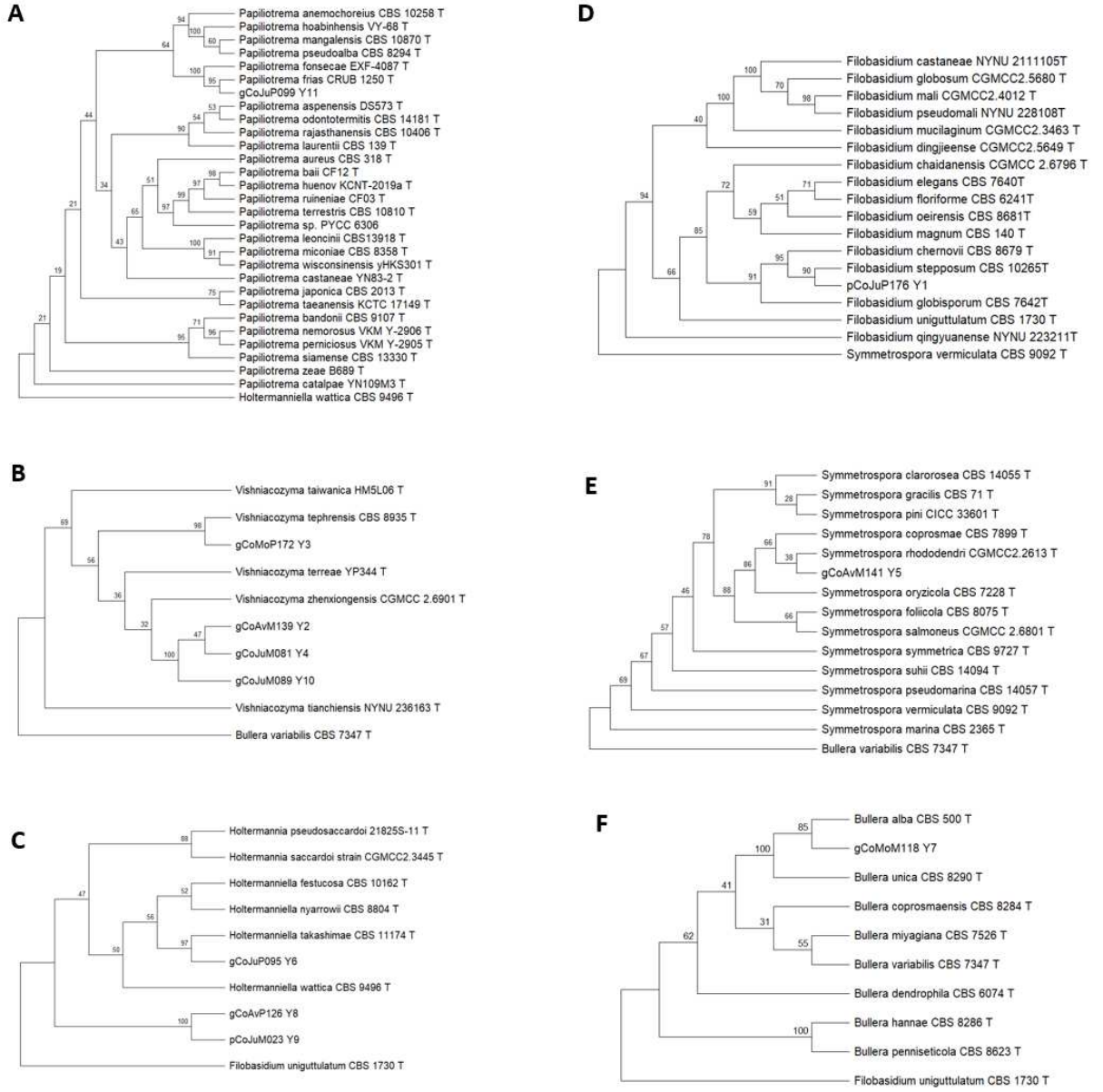
81. PHENOTIC. Angers Plant Phenotyping Facility. 2023. https://doi.org/10.17180/YKBZ-2V85.

82. CIRM-CFBP. International Centre of Microbial Resource (CIRM) - French Collection for Plant-associated Bacteria. 2021. https://doi.org/10.15454/E8XX-4Z18.

Additional files :


A
Acremonium tumulicola
Acremonium felinum
Acremonium polychroma
Acremonium chiangraiense
Acremonium guizhouense
Acremonium spinosum
Acremonium brachypenium
Acremonium alternatum
Acremonium sclerotigenum
Acremonium behniae
Acremonium borodinense
Acremonium globosisporum 1
Acremonium globosisporum 3
Acremonium globosisporum 2
Acremonium blochii
Acremonium variecolor 1
Acremonium variecolor 2
Acremonium capsici
Acremonium chrysogenum
Acremonium flavum
Acremonium curvum
Acremonium hansfordii
Acremonium fusidioides 1
Acremonium fusidioides 2
gCoJuM084 F6
gCoJuM086 F8
Acremonium fusidioides
Acremonium parvum
Acremonium mali
Acremonium cavaraeanum 3
Acremonium citrinum
Acremonium hennebertii
Acremonium dimorphosporum
Acremonium exuviarum
Acremonium moniliforme 1
Acremonium moniliforme 2
Acremonium cavaraeanum 1
Acremonium cavaraeanum 2
Pestalotiopsis hawaiiensis
Pestalotiopsis spathulata
B
P sumatrense
P citrinum
P hetheringtonii
P sizovae
P tropicum
P tropicoides
P steckii
P gorlenkoanum
P anatolicum
P euglaucum
P argentinense
P expansum
P kewense
P sinaicum
P egyptiacum
P dipodomys
P nalgiovense
P chrysogenum
P rubens
P vanluykii
P tardochrysogenum
P allii-sativi
P flavigenum
P confertum
P mononematosum
P halotolerans
P desertorum
P lanosocoeruleum
P persicinum
P goetzii
P carneum
P mediterraneum
P psychrosexuale
P paneum
P samsonianum
P osmophilum
P floccosum
P roqueforti
gCoAvM063 F7
P novae-zeelandiae
P restrictum
P roseopurpureum
P sanguifluum
P gallaicum
P shearii
P wellingtonense
P vancouverense
P pasqualense
P atrofulvum
P raphiae
P christenseniae
P manginii
P quebecense
P cairnsense
P miczynskii
P aurantiacobrunneum
P neomiczynskii
P sucrivorum
P decaturense
P pancosmium
P ubiquetum
P westlingii
P nothofagi
P cosmopolitanum
P godlewskii
P waksmanii
P chrzaszczii
P acidogenicum
P paxilli
P copticola
P terrigenum
C
Chlamydocillium curvulum
S glaucum
S bifurcatum
S theobromae
S gamsii
S menglaense
S implicatum
S ochraceum
S subulatum
S bacillisporum
S terricola
S yunnanense
S oryzae
S brachiariae
S hominis 1
S hominis 2
S kiliense
S zeae
S pseudostrictum
S bactrocephalum
S strictum
S spinificis
S summerbellii
gCoAvM140 F5
S dejongiae
D
Alternaria abundans
Alternaria breviramosa
Alternaria cetera
Alternaria obclavata
Alternaria caespitosa
Alternaria conjuncta
Alternaria infectoria
Alternaria slovaca
Alternaria alstroemeriae
Alternaria gaisen
Alternaria arborescens
Alternaria geophila
pCoMM191 F2
Alternaria alternata
Alternaria gossypina
Alternaria iridiaustralis
Alternaria baoshanensis
Alternaria ovoidea
Alternaria macroconidia
Alternaria breviconidiophora
Alternaria lathyri
Alternaria muriformispora
Alternaria pseudoinfectoria
Alternaria torilis
Alternaria minimispora
Alternaria rostroconidia
Alternaria ellipsoidialis
Alternaria eupatoricola 1
Alternaria eupatoricola 2
Alternaria macilenta
Alternaria oblongoellipsoidea
Alternaria phragmiticola
Alternaria falcata
Alternaria obpyriconidia
Alternaria brevirostra
Alternaria phytolaccae
Alternaria salicicola
Alternaria burnsii
Alternaria jacinthicola
Alternaria perpunctulata
Alternaria echinaceae
Alternaria solani
Alternaria pseudorostrata
Alternaria axiaeriisporifera
Alternaria gypsophilae
Alternaria vaccariicola
Alternaria carotiincultae
Alternaria petroselini
Alternaria brassicae
Alternaria helianthiinficiens
Alternaria botryospora
Alternaria hyacinthi
Alternaria proteae
Alternaria cumini
Alternaria eureka
Alternaria triglochinicola
Alternaria calycipyricola
Alternaria photistica
Alternaria thalictrigena
Alternaria leucanthemi 1
Alternaria leucanthemi 2
Alternaria aspera
Alternaria chartarum
Alternaria concatenata
Alternaria elegans
Alternaria simsimi
Alternaria atra
Alternaria brassicae-pekinensis
Alternaria consortialis
Alternaria heterospora
Alternaria indefessa
Alternaria brassicicola
Alternaria septorioides
Alternaria nepalensis
Alternaria dennisii
Alternaria bornmuelleri
Alternaria alternariae
Alternaria botrytis
Alternaria oudemansii
Alternaria capsici-annui
Alternaria argyranthemi
Alternaria papavericola
Alternaria penicillata
Alternaria chlamydospora
Alternaria phragmospora
Alternaria limaciformis
Alternaria tellustris
Alternaria caricis
Stemphylium herbarum
Pleospora tarda
E
T harzianum
T harzianum 1
T harzianum 2
T zeloharzianum
T anaharzianum
T afroharzianum 1
T afroharzianum 2
T atrobrunneum 1
T atrobrunneum 2
T pyramidale 1
T pyramidale 2
T guizhouense 1
T guizhouense 2
T simile 1
T simile 2
T asiaticum 1
T asiaticum 2
T densissimum
T densissimum 1
T densissimum 3
T densissimum 2
T pholiotae 1
T pholiotae 2
T paradensissimum 1
T paradensissimum 2
T breve 1
T breve 2
T zelobreve 1
T zelobreve 2
T atroviride 1
T atroviride 2
pCoAvP042 F9
T nigricans 1
T nigricans 3
T nigricans 2
T paratroviride 1
T paratroviride 2
T uncinatum
T obovatum 1
T obovatum 2
T viride 1
T viride 2
T paraviride
Protocrea farinosa
Protocrea pallida
F
C aciculare
C aggregatocylindricum
C angustiterminale 2
C chalastosporoides 2
C basicola
C colocasiae
C cucumerinum
C cladosporioides
C vignae
C globisporum
gCoMiM067 F10
C marinisedimentum
C sphaerospermum
C aerium
C pseudiridis
C allicinum
C subinflatum
C sinuosum
C floccosum
C macrocarpum
C wyomingense
C paraliminiforme
C phlei
C herbaroides
C subcinereum
C submersum
C verruculosum
C herbarum
C versiforme
C variabile
C iridis
C antarcticum
C fildesense
C aggregatocicatricatum
C ramotenellum
C puyae
C arthropodii
C limoniforme
C prolongatum
C rhusicola
C spinulosum
C ossifragi
C soldanellae
C pseudotenellum
C sinense
C austrohemisphaericum
C langeronii
C psychrotolerans
C sloanii
C neolangeronii
C angustiterminale 1
C asperulatum
C ruguloflabelliforme
C chasmanthicola
C sinuatum
C inversicolor
C neopsychrotolerans
C silenes
C westerdijkiae
C delicatulum
C passiflorae
C lycoperdinum
C anthropophilum
C devikae
C puris
C proteacearum
C oxysporum 1
C oxysporum 2
C tenuissimum
C subuliforme
C xylophilum
C australiense
C uwebraunianum
C phaenocomae
C verrucocladosporioides
C cavernicola
C endoviticola
C welwitschiicola
C funiculosum
C exasperatum
pCoAvM041 F1
C uredinicola
C chubutense
C pini-ponderosae
C longicatenatum
C parapenidielloides
C scabrellum
C chalastosporoides 1
C hillianum
C lagenariiforme
C xanthochromaticum
C flabelliforme
C rubrum
C flavovirens
C rugulovarians
C exile
C paracladosporioides
C varians
C grevilleae
C ipereniae
C licheniphilum
C phyllactiinicola
C phyllophilum
C iranicum
C fuscoviride
C tianshanense
C aphidis
C penidielloides
C salinae
C cycadicola
C dominicanum
C lebrasiae
C pulvericola
C domesticum
C halotolerans
C parahalotolerans
C succulentum
C coloradense
C fusiforme
C menglunense
C velox
C longissimum
Cercospora beticola
G
Monilochaetes infuscans
P humicola
P plurivora
P pauciseptata
P oligotrophica
P ramiseptata
P citrullae
P guizhouensis
P cucumerina
P endophytica
P hanneae
P nauculaspora
P populi
P sichuanensis
P kunmingensis
Plectosphaerella alismatis
P deliscribi
gCoJuM088 F4
P sinensis
P melonis

Supplementary Fig. 1 : Phylogenetic trees of the genus (A) *Acremonium*, (B) *Penicillium*, (C) *Sarocladium*, (D) *Alternaria*, (E) *Trichoderma*, (F) *Cladosporium* and (G) *Plectosphaerella* using the IQ-TREE Ultrafast bootstrap (1000 iterations)



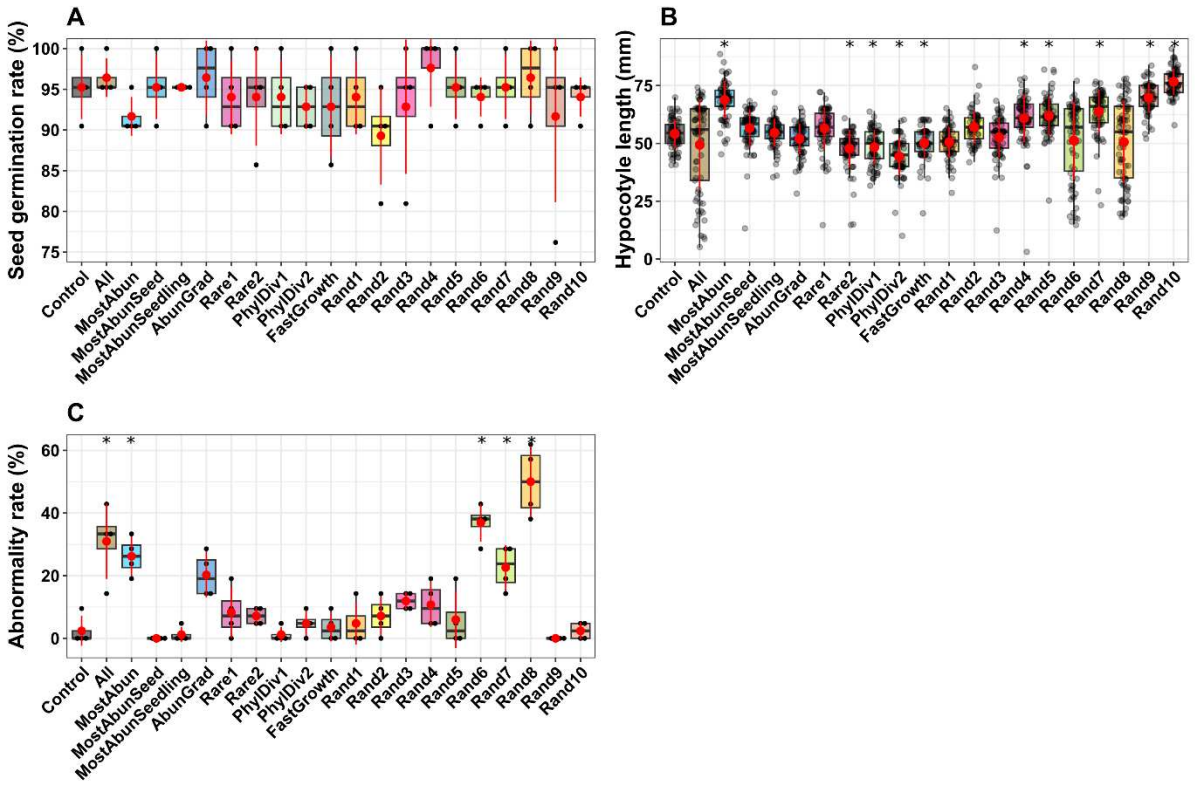
Supplementary Fig. 2: Phylogenetic tree of the genus (A) *Papiliotrema*, (B) *Vishniacozyma*, (C) *Holtermaniella*, (D) *Filobasidium*, (E) *Symmetrospora* and (F) *Bullera* using the IQ-TREE Ultrafast bootstrap (1000 iterations)



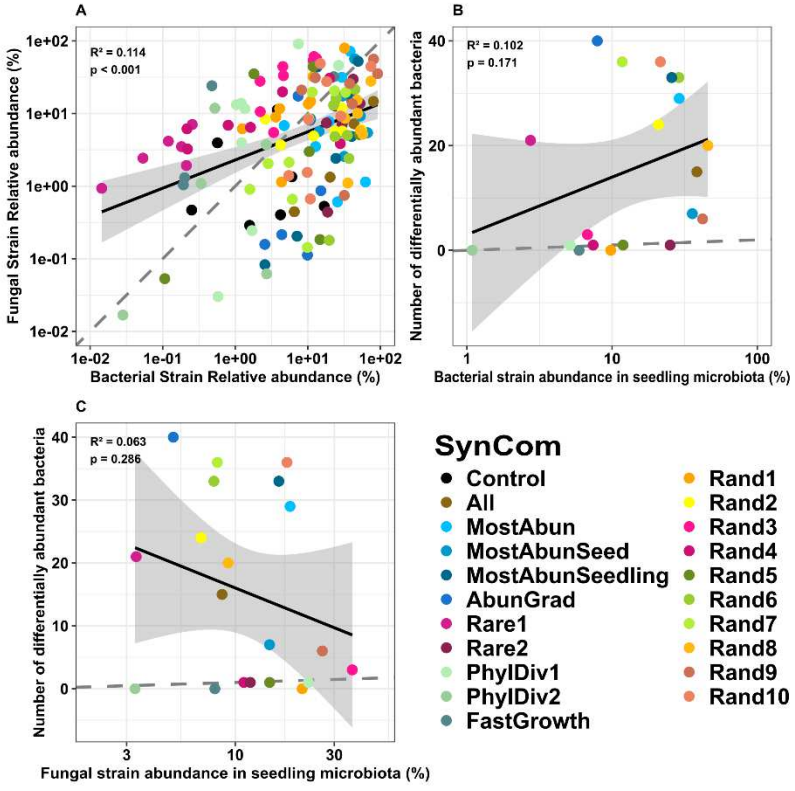
1203

1204 Supplementary Fig. 3: Assessment of microbial alpha diversity and taxonomic composition across seeds and
1205 seedlings. (A–B) Observed alpha richness (number of unique ASVs) for (A) bacterial and (B) fungal communities.
1206 For the non-inoculated control condition, each replicate point represents a pooled batch of 20 seeds, whereas
1207 all other points represent individual inoculated seeds. Asterisks denote significant differences relative to the
1208 control group (Pairwise comparisons using Dunn's many-to-one test with Benjamini-Hochberg correction, $p < 0.05$). (C–H) Taxonomic profiling of recovered inoculated strains across different experimental stages for
1210 bacterial (left panels: C, E, G) and fungal (right panels: D, F, H) communities. Panels represent relative abundances
1211 within the initial inoculum (C, D), the mature seed microbiota (E, F), and the emerged seedling microbiota (H, G).

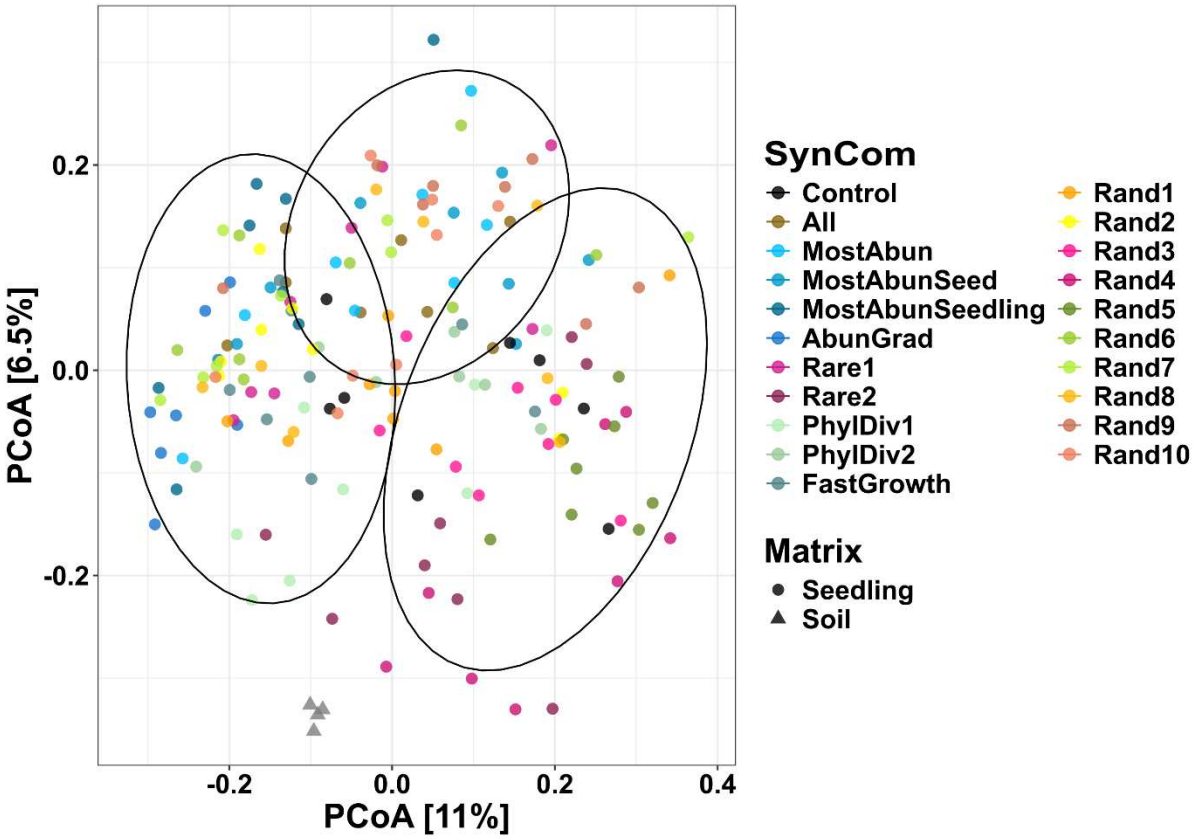
1212



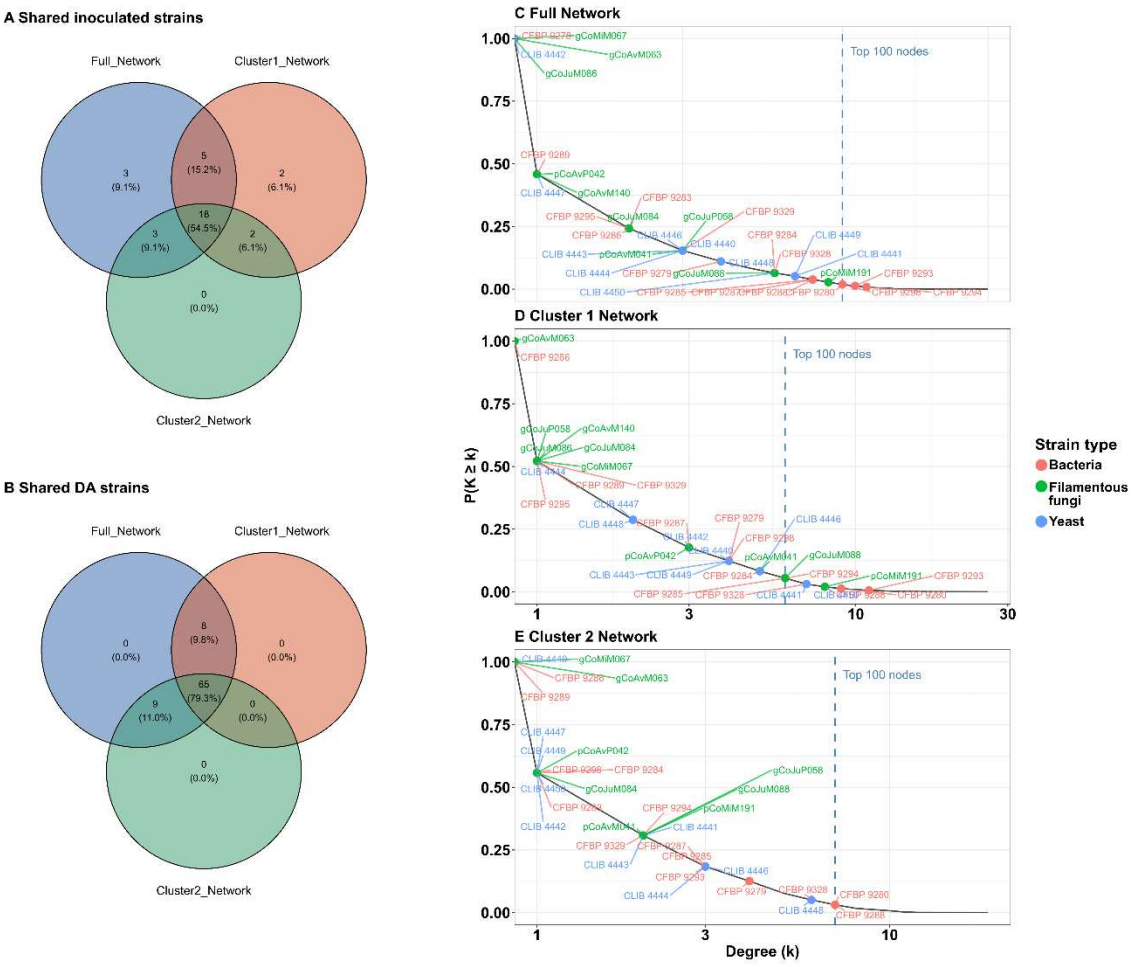
Supplementary Fig. 4: Phenotypic assessment of *Brassica napus* seedlings 15 days post-inoculation with various SynCom formulations. (A) Germination percentages, (B) hypocotyl length, and (C) proportion of morphologically normal seedlings. Asterisks (*) denote statistically significant differences relative to the non-inoculated control group (Pairwise comparisons using Dunn's many-to-one test with Benjamini-Hochberg correction, $p < 0.05$).



Supplementary Fig. 5: Correlation analyses between colonization dynamics and differential taxonomic abundance in seedlings. (A) Linear regression evaluating the relationship between the cumulative relative abundance of fungal and bacterial SynCom strains within individual seedlings. (B–C) Relationship between the number of differentially abundant host taxa and the cumulative abundance of introduced (B) bacterial or (C) fungal SynCom strains within the seedling matrix.



Supplementary Fig. 6: Principal Coordinate Analysis (PCoA) based on Bray-Curtis dissimilarity matrices (log(x+1) transformed) for fungal communities across bulk soil, non-inoculated control seedlings, and SynCom-inoculated seedlings. Cluster overlays are derived from k-means clustering partitioning using the NbClust package in R based on Euclidean distances.



Supplementary Fig. 7: (A–B) Venn diagrams illustrating the overlapping and unique (A) introduced SynCom strains and (B) differentially abundant bacterial ASVs localized within the giant components of the Full, Cluster 1 and Cluster 2 networks. (C–E) Complementary cumulative distribution function (cCDF) curves modeling the topological degree distributions within the (C) full, (D) Cluster 1 and (E) Cluster 2 network models. Individual introduced SynCom strains are highlighted by taxonomic groups: bacteria (green points), filamentous fungi (red points), and yeasts (blue points). The vertical black dashed line marks the threshold designating the top 100 most highly connected nodes within each respective network architecture.

Table S1: Strain used in SynCom inoculation and their information

Isolate_name	Exp_Name	CIRM	Fig_Name	Phylum	Class	Order	Family	Genus	Species	Sampling year	Isolated by	Recommanded_media	Recommanded_temp	Plant	Genotype	Production	Type	BioProject	BioSample	Lag_time	Relabu_all	Prev_all	Relabu_seed	Prev_seed	Relabu_seedl	Prev_seedl	Growth_rate	AUC	Genome_size	Presence_in_SynCom
P04_B9	B1	CFBP9288	Pantoea agglomerans CFBP9288	Proteobacteria	Gammaproteobacteria	Enterobacterales	Erwiniaceae	Pantoea	Pantoea agglomerans	2023	C.Marais/A.Preveaux	TSA	20°C	Rapeseed	Jupiter	Pepiniere	Seedling	PRJNA1484330	SAMN61228305	231	0,24	0,79	0,23	0,92	0,26	0,67	0,53	6,66E+03	5,10	7
P04_E9	B10	CFBP9292	Sphingomonas aerolata CFBP9292	Proteobacteria	Alphaproteobacteria	Sphingomonadales	Sphingomonadaceae	Sphingomonas	Sphingomonas aerolata	2023	C.Marais/A.Preveaux	TSA	20°C	Rapeseed	Jupiter	Pepiniere	Seedling	PRJNA1484336	SAMN61228525	487	0,00	0,52	0,00	0,79	0,00	0,25	0,34	1,91E+03	4,50	4
P03_A3	B11	CFBP9289	Frigoribacterium sp. CFBP9289	Actinobacteria	Actinobacteria	Micrococcales	Microbacteriaceae	Frigoribacterium	Frigoribacterium sp.	2023	C.Marais/A.Preveaux	TSA	20°C	Rapeseed	Jupiter	Minicage	Seed	PRJNA1484333	SAMN61228341	758	0,00	0,42	0,00	0,71	0,00	0,13	1,07	4,75E+03	3,50	4
P04_F7	B12	CFBP9329	Sphingomonas sp. CFBP9329	Proteobacteria	Alphaproteobacteria	Sphingomonadales	Sphingomonadaceae	Sphingomonas	Shingomonas sp.	2023	C.Marais/A.Preveaux	TSA	20°C	Rapeseed	Jupiter	Pepiniere	Seedling	PRJNA1484347	SAMN61228699	1207	0,00	0,50	0,00	0,79	0,00	0,21	0,49	5,39E+03	4,40	4
P08_H11	B13	CFBP9286	Sanguibacter inulinus CFBP9286	Actinobacteria	Actinobacteria	Micrococcales	Sanguibacteraceae	Sanguibacter	Sanguibacter inulinus	2023	C.Marais/A.Preveaux	TSA	20°C	Rapeseed	Mohican	Pepiniere	Seedling	PRJNA1484352	SAMN61229059	454	0,00	0,25	0,00	0,50	0,00	0,00	0,70	6,23E+03	4,40	6
P05_B9	B14	CFBP9278	Saccharibacillus sp. CFBP9278	Firmicutes	Bacilli	Bacillales	Paenibacillaceae	Saccharibacillus	Saccharibacillus sp.	2023	C.Marais/A.Preveaux	TSA	20°C	Rapeseed	Milena	Minicage	Seedling	PRJNA1484355	SAMN61229108	725	0,00	0,08	0,00	0,13	0,00	0,04	0,33	4,04E+03	5,50	4
P07_B4	B15	CFBP9327	Brachybacterium sp. CFBP9327	Actinobacteria	Actinobacteria	Micrococcales	Dermabacteraceae	Brachybacterium	Brachybacterium sp.	2023	C.Marais/A.Preveaux	TSA	20°C	Rapeseed	Mohican	Minicage	Seed	PRJNA1484356	SAMN61229109	1350	0,00	0,19	0,00	0,38	0,00	0,00	0,89	7,66E+03	4,00	3
P01_B4	B16	CFBP9283	Luteimonas sp. CFBP9283	Proteobacteria	Gammaproteobacteria	Xanthomonadales	Xanthomonadaceae	Luteimonas	Luteimonas sp.	2023	C.Marais/A.Preveaux	TSA	20°C	Rapeseed	Aviso	Minicage	Seed	PRJNA1484358	SAMN61229216	599	0,00	0,00	0,00	0,00	0,00	0,00	1,01	9,52E+03	3,70	6
P03_D3	B17	CFBP9282	Nocardioides alkalitolerans CFBP9282	Actinobacteria	Actinobacteria	Propionibacteriales	Nocardioidaceae	Nocardioides	Nocardioides alkalitolerans	2023	C.Marais/A.Preveaux	TSA	20°C	Rapeseed	Jupiter	Minicage	Seed	PRJNA1484371	SAMN61230061	585	0,00	0,00	0,00	0,00	0,00	0,00	0,60	5,51E+03	4,70	3
P03_D9	B18	CFBP9299	Bacillus pumilus CFBP9299	Firmicutes	Bacilli	Bacillales	Bacillaceae	Bacillus	Bacillus pumilus	2023	C.Marais/A.Preveaux	TSA	20°C	Rapeseed	Jupiter	Minicage	Seedling	PRJNA1484376	SAMN61230140	208	0,00	0,00	0,00	0,00	0,00	0,00	0,98	5,70E+03	3,80	4
P04_G6	B19	CFBP9295	Agreia sp. CFBP9295	Actinobacteria	Actinobacteria	Micrococcales	Microbacteriaceae	Agreia	Agreia sp.	2023	C.Marais/A.Preveaux	TSA	20°C	Rapeseed	Jupiter	Pepiniere	Seed	PRJNA1484381	SAMN61230350	2118	0,00	0,00	0,00	0,00	0,00	0,00	0,43	4,55E+03	3,60	4
P07_G7	B2	CFBP9298	Pseudomonas coleoptericum CFBP9298	Proteobacteria	Gammaproteobacteria	Pseudomonadales	Pseudomonadaceae	Pseudomonas	Pseudomonas coleoptericum	2023	C.Marais/A.Preveaux	TSA	20°C	Rapeseed	Mohican	Minicage	Seedling	PRJNA1484382	SAMN61230362	288	0,05	0,15	0,00	0,13	0,09	0,17	0,88	5,88E+03	4,80	5
P05_B3	B20	CFBP9330	Pedobacter sp. CFBP9330	Bacteroidetes	Sphingobacteriia	Sphingobacteriales	Sphingobacteriaceae	Pedobacter	Pedobacter sp.	2023	C.Marais/A.Preveaux	TSA	20°C	Rapeseed	Milena	Minicage	Seed	PRJNA1484383	SAMN61230387	739	0,00	0,00	0,00	0,00	0,00	0,00	0,38	2,95E+03	4,80	3
P06_F5	B21	CFBP9296	Chryseobacterium indoltheticum CFBP9296	Bacteroidetes	Flavobacteriia	Flavobacteriales	Flavobacteriaceae	Chryseobacterium	Chryseobacterium indoltheticum	2023	C.Marais/A.Preveaux	TSA	20°C	Rapeseed	Milena	Pepiniere	Seed	PRJNA1484385	SAMN61230500	248	0,00	0,00	0,00	0,00	0,00	0,00	0,72	8,38E+03	4,40	5
P07_A5	B22	CFBP9285	Pseudomonas sp. CFBP9285	Proteobacteria	Gammaproteobacteria	Pseudomonadales	Pseudomonadaceae	Pseudomonas	Pseudomonas sp.	2023	C.Marais/A.Preveaux	TSA	20°C	Rapeseed	Mohican	Minicage	Seed	PRJNA1484395	SAMN61230534	203	0,00	0,00	0,00	0,00	0,00	0,00	0,21	6,52E+03	6,60	4
P07_C6	B23	CFBP9281	Arthrobacter sp. CFBP9281	Actinobacteria	Actinobacteria	Micrococcales	Micrococcaceae	Arthrobacter	Arthrobacter sp.	2023	C.Marais/A.Preveaux	TSA	20°C	Rapeseed	Mohican	Minicage	Seed	PRJNA1484399	SAMN61230543	722	0,00	0,00	0,00	0,00	0,00	0,00	0,22	5,18E+03	3,70	3

P05_E5	B24	CFBP9297	Devosia sp. CFBP 9297	Proteobacteria	Alphaproteobacteria	Rhizobiales	Hyphomicrobiaceae	Devosia	Devosia sp.	2023	C.Marais/A.Preveaux	TSA	20°C	Rape seed	Milena	Minicage	Seed	PRJNA1484402	SAMN61230566	492	0,00	0,00	0,00	0,00	0,00	0,00	0,26	2,51E+03	4,10	2
P01_A6	B3	CFBP9279	Pantoea agglomerans CFBP 9279	Proteobacteria	Gammaproteobacteria	Enterobacterales	Erwiniaceae	Pantoea	Pantoea agglomerans	2023	C.Marais/A.Preveaux	TSA	20°C	Rape seed	Aviso	Minicage	Seed	PRJNA1484412	SAMN61231321	214	0,03	0,08	0,06	0,13	0,00	0,04	0,26	5,15E+03	4,90	4
P03_H9	B4	CFBP9293	Leclercia tamurae CFBP 9293	Proteobacteria	Gammaproteobacteria	Enterobacterales	Enterobacteriaceae	Leclercia	Leclercia tamurae	2023	C.Marais/A.Preveaux	TSA	20°C	Rape seed	Jupiter	Minicage	Seedling	PRJNA1484415	SAMN61231363	174	0,03	0,13	0,00	0,00	0,06	0,25	0,43	8,84E+03	4,90	4
P05_C11	B5	CFBP9280	Pantoea agglomerans CFBP 9280	Proteobacteria	Gammaproteobacteria	Enterobacterales	Erwiniaceae	Pantoea	Pantoea agglomerans	2023	C.Marais/A.Preveaux	TSA	20°C	Rape seed	Milena	Minicage	Seedling	PRJNA1484417	SAMN61231392	216	0,02	0,06	0,00	0,08	0,04	0,04	0,61	6,55E+03	4,80	4
P04_A5	B6	CFBP9294	Erwinia persicina CFBP 9294	Proteobacteria	Gammaproteobacteria	Enterobacterales	Erwiniaceae	Erwinia	Erwinia persicina	2023	C.Marais/A.Preveaux	TSA	20°C	Rape seed	Jupiter	Pepiniere	Seed	PRJNA1484428	SAMN61231470	286	0,02	0,35	0,03	0,67	0,01	0,04	0,64	7,26E+03	5,30	4
P02_A5	B7	CFBP9328	Neorhizobium soli CFBP 9328	Proteobacteria	Alphaproteobacteria	Rhizobiales	Rhizobiaceae	Neorhizobium	Neorhizobium soli	2023	C.Marais/A.Preveaux	TSA	20°C	Rape seed	Aviso	Pepiniere	Seed	PRJNA1484432	SAMN61231472	709	0,01	0,46	0,01	0,67	0,02	0,25	1,32	6,17E+03	4,90	5
P04_A9	B8	CFBP9287	Stenotrophomonas sp. CFBP 9287	Proteobacteria	Gammaproteobacteria	Xanthomonadales	Xanthomonadaceae	Stenotrophomonas	Stenotrophomonas sp.	2023	C.Marais/A.Preveaux	TSA	20°C	Rape seed	Jupiter	Pepiniere	Seedling	PRJNA1484434	SAMN61231519	436	0,01	0,50	0,02	0,88	0,00	0,13	1,23	1,01E+04	4,50	5
P04_B3	B9	CFBP9284	Xanthomonas campestris CFBP 9284	Proteobacteria	Gammaproteobacteria	Xanthomonadales	Xanthomonadaceae	Xanthomonas	Xanthomonas campestris	2023	C.Marais/A.Preveaux	TSA	20°C	Rape seed	Jupiter	Pepiniere	Seed	PRJNA1484436	SAMN61231621	1403	0,00	0,17	0,01	0,29	0,00	0,04	0,63	6,64E+03	5,20	3
pCoAvM041	F1		Cladosporium sp. pCoAvM041	Ascomycota	Dothideomycetes	Capnodiales	Cladosporiaceae	g__Cladosporium	Cladosporium sp.	2023	N.Guschinskaya/M.Marchi	MA	20°C	Rape seed	Aviso	Minicage	Seedling	PRJNA1489507	SAMN61385471	823	0,51	0,67	0,43	1,00	0,59	1,00	0,37	3,40E+09	34,00	11
gCoMiM067	F10		Cladosporium sp. gCoMiM067	Ascomycota	Dothideomycetes	Capnodiales	Cladosporiaceae	Cladosporium	Cladosporium sp.	2023	N.Guschinskaya/M.Marchi	MA	20°C	Rape seed	Milena	Minicage	Seed	PRJNA1489508	SAMN61385472	909	0,00	0,00	0,00	0,00	0,00	0,00	0,28	3,11E+09	35,08	9
pCoMiM191	F2		Alternaria arborescens pCoMiM191	Ascomycota	Dothideomycetes	Pleosporales	Pleosporaceae	Alternaria	Alternaria arborescens	2023	N.Guschinskaya/M.Marchi	MA	20°C	Rape seed	Milena	Minicage	Seedling	PRJNA1489510	SAMN61385885	552	0,01	0,42	0,00	0,96	0,02	0,29	0,40	4,31E+09	33,74	11
gCoJuP058	F3		Mycosphaerella sp. gCoJuP058	Ascomycota	Dothideomycetes	Capnodiales	Mycosphaerellaceae	Mycosphaerella	Mycosphaerella sp.	2023	N.Guschinskaya/M.Marchi	MA	20°C	Rape seed	Jupiter	Pepiniere	Seed	PRJNA1489514	SAMN61385887	635	0,07	0,38	0,13	1,00	0,00	0,13	0,21	3,97E+09	30,97	10
gCoJuM088	F4		Plectosphaerella sp. gCoJuM088	Ascomycota	Sordariomycetes	Glomerellales	Plectosphaerellaceae	Plectosphaerella	Plectosphaerella sp.	2023	N.Guschinskaya/M.Marchi	MA	20°C	Rape seed	Jupiter	Minicage	Seed	PRJNA1489515	SAMN61385902	864	0,01	0,33	0,01	0,46	0,02	0,54	0,11	3,97E+09	34,31	8
gCoAvM140	F5		Sarocladium sp. gCoAvM140	Ascomycota	Sordariomycetes	Hypocreales	Hypocreales_fam_Incertae_sedis	Sarocladium	Sarocladium sp.	2023	N.Guschinskaya/M.Marchi	MA	20°C	Rape seed	Aviso	Minicage	Seed	PRJNA1489517	SAMN61385963	1254	0,00	0,19	0,00	0,42	0,00	0,17	0,13	2,88E+09	33,03	6
gCoJuM084	F6		Acremonium sp. gCoJuM084	Ascomycota	Sordariomycetes	Hypocreales	Hypocreales_fam_Incertae_sedis	Acremonium	Acremonium sp.	2023	N.Guschinskaya/M.Marchi	MA	20°C	Rape seed	Jupiter	Minicage	Seed	PRJNA1489519	SAMN61386030	1301	0,00	0,08	0,00	0,08	0,00	0,17	0,11	3,06E+09	28,13	8
gCoAvM063	F7		Penicillium novae-zeelandiae gCoAvM063	Ascomycota	Eurotiomycetes	Eurotiales	Didymosphaeriaceae	Penicillium	Penicillium novae-zeelandiae	2023	N.Guschinskaya/M.Marchi	MA	20°C	Rape seed	Aviso	Minicage	Seed	PRJNA1489520	SAMN61386031	781	0,00	0,00	0,00	0,00	0,00	0,00	0,12	4,23E+09	32,72	8
gCoJuM086	F8		Acremonium sp. gCoJuM086	Ascomycota	Sordariomycetes	Hypocreales	Pleosporaceae	Acremonium	Acremonium sp.	2023	N.Guschinskaya/M.Marchi	MA	20°C	Rape seed	Jupiter	Minicage	Seed	PRJNA1489521	SAMN61386035	1221	0,00	0,00	0,00	0,00	0,00	0,00	0,07	3,07E+09	34,28	7

pCoAvP042	F9		Trichoderma sp. pCoAvP042	Ascomycota	Sordariomycetes	Hypocreales	Hypocreaceae	Trichoderma	Trichoderma sp.	2023	N.Guschinskaya/M.Marchi	MA	20°C	Rapeseed	Aviso	Pepiniere	Seedling	PRJNA1489523	SAMN61386056	773	0,00	0,00	0,00	0,00	0,00	0,00	3,00	4,55 E+09	38,00	8
pCoJuP176	Y1	CLIB 4440	Filobasium sp. CLIB 4440	Basidiomycota	Tremellomycetes	Filobasidiales	Filobasidiaceae	Filobasidium	Filobasium sp.	2023	N.Guschinskaya/M.Marchi	MA	20°C	Rapeseed	Jupiter	Pepiniere	Seedling	PRJNA1484526	SAMN61241740	1105	0,03	0,40	0,00	0,67	0,06	0,54	40,90	2,21 E+09	25,00	10
gCoJuM089	Y10	CLIB 4449	Vishniacozyma sp. CLIB 4449	Basidiomycota	Tremellomycetes	Tremellales	Bulleribasidiaceae	Vishniacozyma	Vishniacozyma sp.	2023	N.Guschinskaya/M.Marchi	MA	20°C	Rapeseed	Jupiter	Miniciage	Seed	PRJNA1484568	SAMN61243599	497	0,00	0,00	0,00	0,00	0,00	0,00	32,94	2,83 E+09	19,79	6
gCoJuP099	Y11	CLIB 4450	Papiliotrema sp. CLIB 4450	Basidiomycota	Tremellomycetes	Tremellales	Rhynchogastremataceae	Papiliotrema	Papiliotrema sp.	2023	N.Guschinskaya/M.Marchi	MA	20°C	Rapeseed	Jupiter	Pepiniere	Seed	PRJNA1484574	SAMN61243604	743	0,00	0,00	0,00	0,00	0,00	0,00	50,74	2,81 E+09	19,46	8
gCoAvM139	Y2	CLIB 4441	Vishniacozyma sp. CLIB 4441	Basidiomycota	Tremellomycetes	Tremellales	Bulleribasidiaceae	Vishniacozyma	Vishniacozyma sp.	2023	N.Guschinskaya/M.Marchi	MA	20°C	Rapeseed	Aviso	Miniciage	Seed	PRJNA1484537	SAMN61241850	1762	0,00	0,28	0,00	0,71	0,00	0,13	36,60	1,84 E+09	17,85	9
gCoMoP172	Y3	CLIB 4442	Vishniacozyma sp. CLIB 4442	Basidiomycota	Tremellomycetes	Tremellales	Bulleribasidiaceae	Vishniacozyma	Vishniacozyma sp.	2023	N.Guschinskaya/M.Marchi	MA	20°C	Rapeseed	Mohican	Pepiniere	Seed	PRJNA1484539	SAMN61242542	769	0,00	0,21	0,00	0,58	0,00	0,04	41,03	2,79 E+09	19,00	8
gCoJuM081	Y4	CLIB 4443	Vishniacozyma sp. CLIB 4443	Basidiomycota	Tremellomycetes	Tremellales	Bulleribasidiaceae	Vishniacozyma	Vishniacozyma sp.	2023	N.Guschinskaya/M.Marchi	MA	20°C	Rapeseed	Jupiter	Miniciage	Seed	PRJNA1484542	SAMN61242599	666	0,00	0,13	0,00	0,29	0,00	0,08	52,61	2,79 E+09	20,05	7
gCoAvM141	Y5	CLIB 4444	Symmetrospora sp. CLIB 4444	Basidiomycota	Cystobasidiomycetes	Erythrobasidiales	Erythrobasidiaceae	Symmetrospora	Symmetrospora sp.	2023	N.Guschinskaya/M.Marchi	MA	20°C	Rapeseed	Aviso	Miniciage	Seed	PRJNA1484545	SAMN61242672	813	0,00	0,10	0,00	0,25	0,00	0,04	48,98	3,05 E+09	20,00	9
gCoJuP095	Y6	CLIB 4445	Holtermanniella sp. CLIB 4445	Basidiomycota	Tremellomycetes	Holtermanniales	Holtermanniales_fam_Incertae_sedis	Holtermanniella	Holtermanniella sp.	2023	N.Guschinskaya/M.Marchi	MA	20°C	Rapeseed	Jupiter	Pepiniere	Seed	PRJNA1484547	SAMN61242684	933	0,00	0,00	0,00	0,00	0,00	0,00	75,23	3,36 E+09	16,50	9
gCoMoM118	Y7	CLIB 4446	Bullera sp. CLIB 4446	Basidiomycota	Tremellomycetes	Tremellales	Tremellaceae	Bullera	Bullera sp.	2023	N.Guschinskaya/M.Marchi	MA	20°C	Rapeseed	Mohican	Miniciage	Seed	PRJNA1484554	SAMN61242687	730	0,00	0,00	0,00	0,00	0,00	0,00	52,66	3,44 E+09	19,81	8
gCoAvP126	Y8	CLIB 4447	Holtermanniella sp. CLIB 4447	Basidiomycota	Tremellomycetes	Holtermanniales	Holtermanniales_fam_Incertae_sedis	Holtermanniella	Holtermanniella sp.	2023	N.Guschinskaya/M.Marchi	MA	20°C	Rapeseed	Aviso	Pepiniere	Seed	PRJNA1484565	SAMN61243549	810	0,00	0,00	0,00	0,00	0,00	0,00	73,84	4,02 E+09	15,87	5
pCoJuM023	Y9	CLIB 4448	Holtermanniella sp. CLIB 4448	Basidiomycota	Tremellomycetes	Holtermanniales	Holtermanniales_fam_Incertae_sedis	Holtermanniella	Holtermanniella sp.	2023	N.Guschinskaya/M.Marchi	MA	20°C	Rapeseed	Jupiter	Miniciage	Seedling	PRJNA1484567	SAMN61243556	882	0,00	0,00	0,00	0,00	0,00	0,00	77,18	3,74 E+09	16,50	8

Each strain used is described in a line, “relabu” columns indicate natural relative abundance and “prev “natural prevalence in seeds, seedling or both (all). Lag time is in min, growth rate in min^{-1}, genome size in Mb and last column indicates the number of SynComs a strain belongs to.

1242 Table S2: Loci used for taxonomic identification of fungal strains

Locus/target gene	Marker	Reference	DOI	Forward	Reverse	Target species
D1/D2 region of the large 26S rDNA subunit	D1D2	Vilgalys & Hester, 1990	https://doi.org/10.1128/jb.172.8.4238-4246.1990	ACCCGCTGAACTTAAGC	TCCTGAGGGAAACTTCG	Yeast
internal transcribed spacer (ITS) region	NS7_ITS4	White et al 1990	https://doi.org/10.1016/B978-0-12-372180-8.50042-1	GAGGCAATAACAGGTCTGTGATGC	TCCTCCGCTTATTGATATGC	Yeast
internal transcribed spacer (ITS) region	ITS1-4	White et al 1990	https://doi.org/10.1016/B978-0-12-372180-8.50042-1	TCCGTAGGTGAACCTGCGG	TCCTCCGCTTATTGATATGC	Fungi
internal transcribed spacer (ITS) region	ITS1-2	White et al 1990	https://doi.org/10.1016/B978-0-12-372180-8.50042-1	TCCGTAGGTGAACCTGCGG	GGTTGGTTTCTTTTCCT	*Mycosphaerella*
small subunit rDNA (SSU) NS1/NS4	SSU_NS1-NS4	White et al 1990	https://doi.org/10.1016/B978-0-12-372180-8.50042-1	GTAGTCATATGCTTGTCTC	CTTCCGTCAATTCCTTTAAG	*Acremonium*
Partial actin gene (act)	act	Carbone & Kohn 1999	https://doi.org/10.1080/00275514.1999.12061051	ATGTGCAAGGCCGGTTTCGC	TACGAGTCCTTCTGGCCCAT	*Cladosporium, Mycosphaerella*
Translation elongation factor 1- α (tef1)	tef1	Carbone & Kohn 1999	https://doi.org/10.1080/00275514.1999.12061051	CATCGAGAAGTTCGAGAAGG	TACTTGAAGGAACCCTTACC	*Cladosporium, Alternaria, Mycosphaerella*
Glyceraldehyde-3-phosphate dehydrogenase (gapdh)	gadph	Berbee et al 1999	https://doi.org/10.1080/00275514.1999.12061106	CAACGGCTTCGGTCGCATTG	GCCAAGCAGTTGGTTGTG	*Alternaria*
RNA polymerase II second largest subunit (rpb2)	rpb2	Sung et al 2007, Liu et al 1999	https://doi.org/10.1016/j.ympev.2007.03.011 ; https://doi.org/10.1093/oxfordjournals.molbev.a026092	GGGGWGAYCAGAAGAAGGC	CCCATRGCTTGTYYRCCCAT	*Alternaria, Trichoderma*
Alternaria major allergen (alt a 1)	alta1	Hong et al 2005	10.1016/j.fgb.2004.10.009	ATGCAGTTCACCACCATCGC	ACGAGGGTGAYGTAGGCGTC	*Alternaria*
A portion of the LSU (including domains D1–D3) of the rRNA operon	LSU_D1-D3	Moncalvo et al 1995, Vilgalys & Hester 1990	https://doi.org/10.1016/S0953-7562(09)80798-3 ; https://doi.org/10.1128/jb.172.8.4238-4246.1990	ACCCGCTGAACTTAAGC	TACTACCACCAAGATCT	*Mycosphaerella*
28S large subunit nuclear ribosomal RNA (LSU rRNA) LROR/LR5	LSU_LROR-LR5	Vilgalys & Hester 1990	https://doi.org/10.1128/jb.172.8.4238-4246.1990	GGTTGGTTTCTTTTCCT	ATCCTGAGGGAAACTTC	*Plectosphaerella, Acremonium*
Translation elongation factor 1-alpha (TEF-1α) EF-1251R/EF-688F	tef1_EF688F-EF1251R	Alvers et al 2008	http://www.fungaldiversity.org/fdp/sfdp/28-1.pdf	CGGTCACTTGATCTACAAGTGC	CCTCGAACTCACCAGTACCG	*Plectosphaerella*
partial β-tubulin (TUB2)	TUB2	Glass & Donaldson 1995	https://doi.org/10.1128/aem.61.4.1323-1330.1995	GGTAACCAAATCGGTGCTGCTTTC	ACCCTCAGTGTAGTGACCCTTGGC	*Plectosphaerella*
β-tubulin (BenA)	BenA	Glass & Donaldson 1995	https://doi.org/10.1128/aem.61.4.1323-1330.1995	GGTAACCAAATCGGTGCTGCTTTC	ACCCTCAGTGTAGTGACCCTTGGC	*Penicillium*
Calmodulin (CaM)	CaM	Hong et al. 2006	https://doi.org/10.1099/ijs.0.63980-0	CCGAGTACAAGGARGCCTTC	CCGATRGAGGTCATRACGTGG	*Penicillium*
Translation elongation factor 1- α (tef1) EF1/EF2	tef1_EF1-EF2	O'Donnell et al. 1998	https://doi.org/10.1073/pnas.95.5.2044	ATGGGTAAGGAAGACAAGAC	GGAAGTACCAGTGATCATGTT	*Trichoderma*
A portion of the LSU (including domains Nl1–NL4) of the rRNA operon	LSU_NL1-NL4	Kurtzman and Robnett 1997	https://doi.org/10.1128/jcm.35.5.1216-1223.1997	GCATATCAATAAGCGGAGGAAAAG	GGTCCGTGTTTCAAGACGG	*Sarocladium*
RNA polymerase II second largest subunit (*RPB2*)	rpb2_5-7	Liu et al. 1999	https://doi.org/10.1093/oxfordjournals.molbev.a026092	GAYGAYMGWGATCAYTTYGG	CCCATRGCTTGYTTRCCCAT	*Penicillium*

1243

1244 Table S3: Strains used for the taxonomic identification within the *Acremonium* genus

Strains	Culture accession number	GenBank_LSU	GenBank_ITS
Acremonium tumulicola	CBS 127532 T	AB540478	AB540552
Acremonium felinum	CBS 147.81 T	AB540488	AB540562
Acremonium polychroma	CBS 181.27 T	HQ232091	AB540567
Acremonium brachypenium	CBS 866.73 T	HQ232004	AB540570
Acremonium hansfordii	CBS 390.73	HQ232043	AB540578
Acremonium exuviarum	UAMH 9995 T	HQ232036	AY882946
Acremonium fusidioides	CBS 840.68 T	HQ232039	FN706542
Acremonium sclerotigenum	CBS 124.42 T	HQ232126	FN706552
Acremonium borodinense	CBS 101148 T	HQ232003	HE608635
Acremonium blochii	CBS 993.69	HQ232002	HE608636
Acremonium spinosum	CBS 136.33 T	HQ232137	HE608637
Acremonium variecolor	CBS 130360 T	HE608651	HE608647
Acremonium variecolor	CBS 130361	HE608652	HE608648
Acremonium alternatum	CBS 407.66 T	HQ231988	HE798150
Acremonium parvum	CBS 381.70A	HQ231986	HF680219
Acremonium cavaraeanum	CBS 101149 T	HF680202	HF680220

Acremonium cavaraeanum	CBS 111656	HF680203	HF680221
Acremonium cavaraeanum	CBS 758.69	HQ232012	HF680222
Acremonium fusidioides	CBS 109069	HF680204	HF680223
Acremonium fusidioides	CBS 991.69	HF680211	HF680230
Acremonium citrinum	CBS 384.96 T	HF680217	HF680236
Acremonium hennebertii	CBS 768.69 T	HQ232044	HF680238
Pestalotiopsis spathulata	CBS 356.86 T	KM116236	KM199338
Pestalotiopsis hawaiiensis	CBS 114491 T	KM116239	KM199339
Acremonium dimorphosporum	CBS 139050 T	LN810506	LN810515
Acremonium moniliforme	CBS 139051 T	LN810507	LN810516
Acremonium moniliforme	FMR 10363	LN810508	LN810517
Acremonium mali	ACCC 39305 T	MF993114	MF987658
Acremonium chrysogenum	CBS 401.65	MH870276	MH858636
Acremonium flavum	CBS 316.72	MH872204	MH860487
Acremonium chiangraiense	MFLUCC 14-0397 T	MN648329	MN648324
Acremonium behniae	CBS 146824 T	MW175400	MW175360
Acremonium curvum	CGMCC 3.20954 T	ON041050	ON041034

Acremonium globosisporum	CGMCC 3.20955 T	ON041051	ON041035
Acremonium globosisporum	GZUIFR 22.037	ON041052	ON041036
Acremonium globosisporum	GZUIFR 22.038	ON041053	ON041037
Acremonium capsici	SQT01 T	OP740978	OP703286
Acremonium guizhouense	SQT04 T	OP740981	OP703289
gCoJuM084_F6			
gCoJuM086_F8			

1245

1246 Table S4: Strains used for the taxonomic identification within the *Alternaria* genus

Strains	**Strain voucher**	**GenBank_ITS**	**GenBank_gapdh**	**GenBank_rpb2**	**GenBank_tef1**
Alternaria helianthiinficiens	CBS 208.86 T	JX101649	KC584120	KC584403	EU130548
Alternaria alternata	CBS 916.96 T	AF347031	AY278808	KC584375	KC584634
Alternaria arborescens	CBS 102605 T	AF347033	AY278810	KC584377	KC584636
Alternaria argyranthemi	CBS 116530 T	KC584181	KC584098	KC584378	KC584637
Alternaria axiaeriisporifera	CBS 118715 T	NR_136037	KC584101	KC584381	KC584640
Alternaria brassicae	CBS 116528	KC584185	KC584102	KC584382	KC584641
Alternaria brassicicola	CBS 118699	JX499031	KC584103	KC584383	KC584642
Alternaria calycipyricola	CBS 121545 T	KC584186	KC584104	KC584384	KC584643
Alternaria capsici-annui	CBS 504.74	KC584187	KC584105	KC584385	KC584644
Alternaria carotiincultae	CBS 109381 T	KC584188	KC584106	KC584386	KC584645
Alternaria chlamydospora	CBS 491.72 T	KC584189	KC584108	KC584388	KC584647
Alternaria conjuncta	CBS 196.86 T	FJ266475	AY562401	KC584390	KC584649

Alternaria cumini	CBS 121329 T	KC584191	KC584110	KC584391	KC584650
Alternaria elegans	CBS 109159 T	KC584195	KC584114	KC584395	KC584654
Alternaria gypsophilae	CBS 107.41 T	KC584199	KC584118	KC584401	KC584660
Alternaria infectoria	CBS 210.86 T	DQ323697	AY278793	KC584404	KC584662
Alternaria limaciformis	CBS 481.81 T	KC584203	KC584123	KC584407	KC584665
Alternaria nepalensis	CBS 118700 T	KC584207	KC584126	KC584414	KC584672
Alternaria perpunctulata	CBS 115267 T	KC584210	KC584129	KC584418	KC584676
Alternaria petroselini	CBS 112.41 T	KC584211	KC584130	KC584419	KC584677
Alternaria photistica	CBS 212.86 T	KC584212	KC584131	KC584420	KC584678
Alternaria pseudorostrata	CBS 119411 T	JN383483	AY562406	KC584422	KC584680
Alternaria septorioides	CBS 106.41 T	KC584216	KC584136	KC584427	KC584685
Alternaria simsimi	CBS 115265 T	JF780937	KC584137	KC584428	KC584686
Alternaria thalictrigena	CBS 121712 T	EU040211	KC584144	KC584436	KC584694
Alternaria triglochinicola	CBS 119676 T	KC584222	KC584145	KC584437	KC584695
Alternaria vaccariicola	CBS 118714 T	KC584224	KC584147	KC584439	KC584697
Alternaria penicillata	CBS 116608 T	FJ357311	FJ357299	KC584440	KC584698
Alternaria cetera	CBS 121340 T	JN383482	AY562398	KC584441	KC584699
Alternaria breviramosa	CBS 121331 T	FJ839608	KC584148	KC584442	KC584700
Alternaria obclavata	CBS 124120 T	KC584225	KC584149	KC584443	KC584701
Alternaria slovaca	CBS 567.66 T	KC584226	KC584150	KC584444	KC584702
Alternaria papavericola	CBS 116606 T	FJ357310	FJ357298	KC584446	KC584705
Alternaria abundans	CBS 534.83 T	JN383485	KC584154	KC584448	KC584707
Alternaria dennisii	CBS 476.90 T	JN383488	JN383469	KC584454	KC584713

Alternaria eureka	CBS 193.86 T	JN383490	JN383471	KC584456	KC584715
Alternaria hyacinthi	CBS 416.71 T	KC584233	KC584158	KC584457	KC584716
Alternaria indefessa	CBS 536.83 T	KC584234	KC584159	KC584458	KC584717
Alternaria botryospora	CBS 478.90 T	AY278844	AY278831	KC584461	KC584720
Alternaria phragmospora	CBS 274.70 T	JN383493	JN383474	KC584462	KC584721
Alternaria proteae	CBS 475.90 T	AY278842	KC584161	KC584464	KC584723
Alternaria tellustris	CBS 538.83 T	FJ357316	AY562419	KC584465	KC584724
Alternaria caricis	CBS 480.90 T	AY278839	AY278826	KC584467	KC584726
Pleospora tarda	CBS 714.68 T	KC584238	AF443881	AF107804	KC584729
Alternaria alternariae	CBS 126989 T	AF229485	AY278815	KC584470	KC584730
Stemphylium herbarum	CBS 191.86 T	KC584239	AF443884	KC584471	KC584731
Alternaria leucanthemi	CBS 421.65 T	KC584240	KC584164	KC584472	KC584732
Alternaria leucanthemi	CBS 422.65	KC584241	KC584165	KC584473	KC584733
Alternaria aspera	CBS 115269 T	KC584242	KC584166	KC584474	KC584734
Alternaria atra	CBS 195.67 T	AF229486	KC584167	KC584475	KC584735
Alternaria botrytis	CBS 197.67 T	KC584243	KC584168	KC584476	KC584736
Alternaria brassicae-pekinensis	CBS 121493 T	KC584244	KC584170	KC584478	KC584738
Alternaria concatenata	CBS 120006 T	KC584246	AY762950	KC584480	KC584740
Alternaria chartarum	CBS 200.67 T	AF229488	KC584172	KC584481	KC584741
Alternaria consortialis	CBS 104.31 T	KC584247	KC584173	KC584482	KC584742
Alternaria oudemansii	CBS 114.07 T	FJ266488	KC584175	KC584486	KC584746
Alternaria heterospora	CBS 123376 T	KC584248	KC584176	KC584488	KC584748
Alternaria bornmuelleri	DAOM231361 T	FJ357317	FJ357305	KC584491	KC584751
Alternaria caespitosa	CBS 177.80 T	MH861255	KC584178	KC584492	KC584752

Alternaria echinaceae	CBS 489.92 T	NR_136089	KJ718015	KJ718343	KJ718518
Alternaria solani	CBS 116651 T	Y17070	KJ718068	KJ718412	KJ718584
Alternaria alstroemeriae	CBS 118809 T	NR_163686	KP124154	KP124765	KP125072
Alternaria geophila	CBS 101.13 T	KP124392	KP124244	KP124862	KP125170
Alternaria burnsii	CBS 107.38 T	NR_136119	JQ646305	JQ646457	KP125198
Alternaria gaisen	CBS 118488 T	KP124427	KP124278	KP124897	KP125206
Alternaria gossypina	CBS 102601 T	MH862801	KP124282	KP124903	KP125212
Alternaria iridiaustralis	CBS 118486 T	NR_136120	KP124284	KP124905	KP125214
Alternaria jacinthicola	CBS 133751 T	KP124438	KP124287	KP124908	KP125217
Alternaria oblongoellipsoidea	MFLUCC 22-0074 T	MZ621967	OK236574	OK236621	OK236668
Alternaria rostroconidia	MFLUCC 21-0136 T	MZ621969	OK236576	OK236623	OK236670
Alternaria macilenta	MFLUCC 21-0138 T	MZ621972	OK236579	OK236626	OK236673
Alternaria lathyri	MFLUCC 21-0140 T	MZ621974	OK236581	OK236628	OK236675
Alternaria muriformispora	MFLUCC 21-0784 T	MZ621976	OK236583	OK236630	OK236677
Alternaria obpyriconidia	MFLUCC 21-0121 T	MZ621978	OK236585	OK236633	OK236680
Alternaria minimispora	MFLUCC 21-0127 T	MZ621980	OK236587	OK236634	OK236681
Alternaria eupatoriicola	MFLUCC 21-0122 T	MZ621982	OK236589	OK236636	OK236683
Alternaria eupatoriicola	MFLU 21-0319	MZ621983	OK236589	OK236637	OK236684
Alternaria pseudoinfectoria	MFLUCC 21-0126 T	MZ621984	OK236591	OK236638	OK236685
Alternaria torilis	MFLUCC 14-0433 T	MZ621988	OK236594	OK236641	OK236688
Alternaria ellipsoidialis	MFLUCC 21-0132 T	MZ621989	OK236596	OK236643	OK236690
Alternaria falcata	MFLUCC 21-0123 T	MZ621992	OK236599	OK236649	OK236693

Alternaria phragmiticola	MFLUCC 21-0125 T	MZ621994	OK236602	OK236649	OK236696
Alternaria breviconidiophora	MFLUCC 21-0786 T	MZ621997	OK236604	OK236651	OK236698
Alternaria salicicola	MFLUCC 22-0072 T	MZ621999	OK236606	OK236653	OK236700
Alternaria macroconidia	MFLUCC 21-0134 T	MZ622001	OK236610	OK236657	OK236704
Alternaria baoshanensis	MFLUCC 21-0124 T	MZ622003	OK236613	OK236659	OK236706
Alternaria ovoidea	MFLUCC 21-0782 T	MZ622005	OK236614	OK236661	OK236708
Alternaria brevirostra	MFLUCC 21-0129 T	MZ622015	OK236619	OK236666	OK236717
Alternaria phytolaccae	MFLUCC 21-0135 T	MZ622013	OK236616	OK236663	OK236719
pCoMiM191_F2					

1247

1248 Table S5: Strains used for the taxonomic identification within the *Cladosporium* genus

Strains	**Culture accession number**	**GenBank_ITS**	**GenBank_tef1**	**GenBank_act**
C. aciculare	CBS 140488*	KT600411	KT600509	KT600607
C. aerium	CBS 143356*	MF472897	MF473324	MF473747
C. aggregatocicatricatum	CBS 140493*	KT600448	KT600547	KT600645
Cladosporium aggregatocylindricum	CBS 126352	HM148239	HM148503	HM148371
C. allicinum	CBS 121624*	EF679350	EF679425	EF679502
C. angustiterminale	CBS 140480*	KT600379	KT600476	KT600575
Cladosporium angustiterminale	CBS 126353	HM148241	HM148505	HM148373
C. antarcticum	CBS 690.92*	EF679334	EF679405	EF679484
C. anthropophilum	CBS 140685*	LN834437	LN834533	LN834621
C. aphidis	CBS 132182**	JN906978	JN906984	JN906997
C. arthropodii	CBS 124043**	JN906979	JN906985	JN906998
C. asperulatum	CBS 126340*	HM147998	HM148239	HM148485
C. australiense	CBS 125984*	HM147999	HM148240	HM148486

C. austrohemisphaericum	CBS 140482*	KT600382	KT600479	KT600578
Cladosporium basicola	CBS 126356	HM148247	HM148511	HM148379
C. cavernicola	URM 8389*	MZ518829	MZ555733	MZ555746
C. chalastosporoides	CBS 125985*	HM148001	HM148242	HM148488
Cladosporium chalastosporoides	CBS 125995	HM148248	HM148512	HM148380
C. chasmanthicola	CBS 142612*	KY646221	KY646227	KY646224
C. chubutense	CBS 124457*	FJ936158	FJ936161	FJ936165
Cladosporium cladosporioides	CBS 112333	HM148240	HM148504	HM148372
Cladosporium colocasiae	CBS 386.63	HM148252	HM148516	HM148384
C. coloradense	CBS 143357*	MF472945	MF473372	MF473795
Cladosporium cucumerinum	CBS 171.52	HM148253	HM148517	HM148385
C. cycadicola	CBS 137970*	KJ869122	KJ869236	KJ869227
C. delicatulum	CBS 126344*	HM148081	HM148325	HM148570
C. devikae	BRIP 72278a*	MZ303808	MZ344193	MZ344212
C. domesticum	CBS 143358*	MF472955	MF473382	MF473805
C. dominicanum	CBS 119415*	DQ780353	JN906986	KJ596641
C. endoviticola	JZB390018*	MN654960	MN984228	MN984220
Cladosporium exasperatum	CBS 125987	HM148203	HM148467	HM148335
C. exile	CBS 125987*	HM148091	HM148335	HM148580
C. fildesense	F09-T12-1*	JX845290	MN233633	MN233632
C. flabelliforme	CBS 126345*	HM148092	HM148336	HM148581
C. flavovirens	CBS 140462*	LN834440	LN834536	LN834624
C. floccosum	CBS 140463*	LN834416	LN834512	LN834600
C. funiculosum	CBS 122129*	HM148094	HM148338	HM148583
C. fuscoviride	FMR 16385*	LR813200	LR813212	LR813206
C. fusiforme	CBS 119414*	DQ780388	JN906988	KJ596640
Cladosporium globisporum	CBS 126359	HM148259	HM148523	HM148391
C. grevilleae	CBS 114271*	JF770450	JF770472	JF770473
C. halotolerans	CBS 119416*	DQ780364	JN906989	KJ596633

C. herbaroides	CBS 121626*	EF679357	EF679432	EF679509
C. herbarum	CBS 121621**	EF679363	EF679440	EF679516
C. hillianum	CBS 125988*	HM148097	HM148341	HM148586
C. inversicolor	CBS 401.80*	HM148101	HM148345	HM148590
C. ipereniae	CBS 140483*	KT600394	KT600491	KT600589
C. iranicum	CBS 126346*	HM148110	HM148354	HM148599
C. iridis	CBS 138.40**	EF679370	EF679447	EF679523
C. lagenariiforme	SFC20230103-M23*	OQ186119	OQ185128	OQ185167
C. langeronii	CBS 189.54*	DQ780379	JN906990	EF101357
C. lebrasiae	CBS 138283*	KJ596568	KJ596583	KJ596631
C. licheniphilum	CBS 125990*	HM148111	HM148355	HM148600
C. limoniforme	CBS 140484*	KT600397	KT600494	KT600592
C. longicatenatum	CBS 140485*	KT600403	KT600500	KT600598
C. longissimum	CBS 300.96*	DQ780352	EU570259	EF101385
C. lycoperdinum	CBS 574.78C	HM148115	HM148359	HM148604
C. macrocarpum	CBS 121623*	EF679375	EF679453	EF679529
C. marinisedimentum	SFC20230103-M28*	OQ186124	OQ185133	OQ185172
C. menglunense	**Psp2-7a1***	PV737441	PV759135	PV759127
C. neolangeronii	CBS 109868	DQ780377	MF473571	EF101362
C. neopsychrotolerans	CGMCC 3.18031*	KX938383	KX938400	KX938366
C. ossifragi	CBS 842.91*	EF679381	EF679459	EF679535
C. oxysporum	CBS 125991	HM148118	HM148362	HM148607
C. oxysporum	CBS 126351	HM148119	HM148363	HM148608
C. paracladosporioides	CBS 171.54*	HM148120	HM148364	HM148609
C. parahalotolerans	CBS 139585*	KP701955	KP701832	KP702077
C. paralimoniforme	CGMCC 3.18103*	KX938392	KX938409	KX938375
C. parapenidielloides	CBS 140487*	KT600410	KT600508	KT600606

C. passiflorae	COAD 2135*	MH682175	MH724943	MH729795
C. penidielloides	CBS 140489*	KT600412	KT600510	KT600608
C. phaenocomae	CBS 128769*	JF499837	JF499875	JF499881
C. phlei	CBS 358.69**	JN906981	JN906991	JN907000
C. phyllactiniicola	CBS 126352*	HM148150	HM148394	HM148639
C. phyllophilum	CBS 125992*	HM148154	HM148398	HM148643
C. pini-ponderosae	CBS 124456*	FJ936160	FJ936164	FJ936167
C. prolongatum	CGMCC 3.18036*	KX938394	KX938411	KX938377
C. proteacearum	BRIP 72301a*	MZ303809	MZ344194	MZ344213
C. pseudiridis	CBS 116463*	EF679383	EF679461	EF679537
C. pseudotenellum	FMR 16231*	LR813145	LR813196	LR813146
C. psychrotolerans	CBS 119412*	DQ780386	JN906992	KJ596632
C. pulvericola	CBS 143362*	MF473226	MF473648	MF474075
C. puris	COAD 2494	MK253338	MK293778	MK249981
C. puyae	CBS 274.80A*	KT600418	KT600516	KT600614
C. ramotenellum	CBS 121628*	EF679384	EF679462	EF679538
C. rhusicola	CBS 140492*	KT600440	KT600539	KT600637
C. rubrum	CMG 28*	MN053018	MN066644	MN066639
C. ruguloflabelliforme	CBS 140494*	KT600458	KT600557	KT600655
C. rugulovarians	CBS 140495*	KT600459	KT600558	KT600656
C. salinae	CBS 119413*	DQ780374	JN906993	EF101390
C. scabrellum	CBS 126358*	HM148195	HM148440	HM148685
C. silenes	CBS 109082*	EF679354	EF679429	EF679506
C. sinense	CBS 143363*	MF473252	MF473675	MF474102
C. sinuatum	CGMCC 3.18096*	KX938385	KX938402	KX938368
C. sinuosum	CBS 121629*	EF679386	EF679464	EF679540
C. sloanii	CBS 143364*	MF473253	MF473676	MF474103
C. soldanellae	CBS 132186*	JN906982	JN906994	JN907001

C. sphaerospermum	CBS 193.54*	DQ780343	EU570261	EU570269
C. spinulosum	CBS 119907*	EF679388	EF679466	EF679542
C. subcinereum	CBS 140465*	LN834433	LN834529	LN834617
C. subinflatum	CBS 121630*	EF679389	EF679467	EF679543
C. submersum	FMR 17264*	LR813144	LR813197	LR813195
C. subuliforme	CBS 126500*	HM148196	HM148441	HM148686
C. succulentum	CBS 140466*	LN834434	LN834530	LN834618
C. tenuissimum	CPC 22398	MF473285	MF473708	MF474135
C. tianshanense	CGMCC 3.18033*	KX938381	KX938398	KX938364
C. uredinicola	CPC 5390	AY251071	HM148467	HM148712
C. uwebraunianum	CBS 143365*	MF473306	MF473729	MF474156
C. variabile	CBS 121635**	EF679403	EF679481	EF679557
C. varians	CBS 126362*	HM148224	HM148470	HM148715
C. velox	CBS 119417*	DQ780361	JN906995	EF101388
C. verrucocladosporioides	CBS 126363*	HM148226	HM148472	HM148717
C. verruculosum	CGMCC 3.18099*	KX938388	KX938405	KX938371
C. versiforme	CBS 140491*	KT600417	KT600515	KT600613
Cladosporium vignae	CBS 126371	HM148281	HM148545	HM148413
C. welwitschiicola	CBS 142614*	KY646223	KY646229	KY646226
C. westerdijkiae	CBS 113746*	HM148061	HM148303	HM148548
C. wyomingense	CBS 143367*	MF473315	MF473738	MF474165
C. xanthochromaticum	CBS 140691*	LN834415	LN834511	LN834599
C. xylophilum	CBS 125997*	HM148230	HM148476	HM148721
Cercospora beticola	CBS 116456	AY840527	AY840494	AY840458
gCoMiM067_F10				
pCoAvM041_F1				

1249

1250 Table S6: Strains used for the taxonomic identification within the *Mycosphaerella* genus

Strains	Culture accession number	GenBank_ITS	GenBank_LSU_D1-D3	GenBank_act
M. colombiensis	CBS 110969	AY752149	DQ204744	DQ147639
M. crystallina	CBS 681.95	AY490757	DQ204747	DQ147636
M. gracilis	CBS 243.94	DQ267582	DQ204750	DQ147616
M. heimii	CBS 110682	AF309606	DQ204751	DQ147638
M. heimioides	CBS 111364	DQ267586	DQ204752	DQ147632
M. irregulariramosa	CBS 114774	AF309607	DQ204754	DQ147634
M. madeirae	CBS 112895	AY725553	DQ204756	DQ147641
M. lateralis	CBS 110748	AF173315	DQ204768	DQ147651
M. aurantia	CBS 110500	AY725531	DQ246256	DQ147610
M. africana	CBS 116155	DQ267577	DQ246258	DQ147608
M. keniensis	CBS 111001	AF309601	DQ246259	DQ147611
M. suberosa	CBS 436.92	AY626985	DQ246235	DQ147656
M. ambiphylla	CBS 110499	AY725530	DQ246219	DQ147669
M. molleriana	CBS 111164	AF309620	DQ246220	DQ147671
M. vespa	CBS 117924	DQ267590	DQ246221	DQ147668
M. parva	CBS 110503	AY626980	DQ246243	DQ147645
M. nubilosa	CBS 116005	AF309618	DQ246228	DQ147666
M. readeriellophora	CBS 114240	AY725577	DQ246238	DQ147658
M. cryptica	CBS 110975	AF309623	DQ246222	DQ147674
M. toledana	CBS 113313	AY725580	DQ246230	DQ147672
M. tasmaniensis	CBS 111687	DQ267591	DQ246233	DQ147676
M. mexicana	CBS 110502	AY725558	DQ246237	DQ147660
M. flexuosa	CBS 111012	AF309603	DQ246232	DQ147653
M. gregaria	CBS 110501	DQ267585	DQ246251	DQ147650
M. endophytica	CBS 111519	DQ267579	DQ246255	DQ147646
M. intermedia	CBS 114415	AY725547	DQ246248	DQ147627
M. marksii	CBS 682.95	DQ267587	DQ246249	DQ147624
M. parkii	CBS 387.92	AY626979	DQ246245	DQ147612
M. communis	CBS 114238	AY725541	DQ246262	DQ147655
Botryosphaeria ribis	N/A	DQ267604	DQ246263	DQ267605
gCoJuP058_F3				

1251 Table S7: Strains used for the taxonomic identification within the *Penicillium* genus

Strains	Culture accession number	GenBank_ITS	GenBank_BenA	GenBank_CaM	GenBank_RPB2
P. sumatrense	CBS 281.36T	GU944578	JN606639	MN969301	EF198541
P. citrinum	CBS 139.45T	AF033422	GU944545	MN969245	JF417416
P. expansum	CBS 325.48T	AY373912	AY674400	DQ911134	JF417427
P. kewense	CBS 344.61T	AF033466	KU896816	JX996973	JF417428
P. dipodomys	CBS 110412T	MN431359	AY495991	JX996950	JF909932
P. shearii	CBS 290.48T	GU944606	JN606840	EU644068	JN121482
P. chrysogenum	CBS 306.48T	AF033465	JF909955	JX996273	JN121487
P. restrictum	CBS 367.48T	AF033457	KJ834486	KP016803	JN121506
P. osmophilum	NRRL 5922T	EU427295	MN969391	KU896846	JN121518
P. flavigenum	CBS 419.89T	JX997105	AY495993	JX996281	JN406551
P. sinaicum	CBS 279.82T	JX997090	KU896818	JX996970	JN406587
P. roqueforti	CBS 221.30T	KC411724	MN969397	MN969295	JN406588
P. egyptiacum	CBS 244.32T	AF033467	KU896810	JX996969	JN406598
P. carneum	CBS 112297T	HQ442338	AY674386	HQ442322	JN406642
P. persicinum	CBS 111235T	JX997072	JF909951	JX996954	JN406644
P. anatolicum	CBS 479.66T	AF033425	JN606849	JN606571	JN606593
P. euglaucum	CBS 323.71T	JN617699	JN606856	JN606564	JN606594
P. copticola	CBS 127355T	JN617685	JN606817	JN606553	JN606599
P. terrigenum	CBS 127354T	JN617684	JN606810	JN606583	JN606600
P. gorlenkoanum	CBS 408.69T	GU944581	GU944520	MN969259	JN606601
P. steckii	CBS 260.55T	GU944597	GU944522	MN969300	JN606602
P. sizovae	CBS 413.69T	GU944588	GU944535	MN969298	JN606603
P. hetheringtonii	CBS 122392T	GU944558	GU944538	MN969263	JN606606
P. tropicum	CBS 112584T	GU944582	GU944532	MN969304	JN606607
P. tropicoides	CBS 122410T	GU944584	GU944531	MN969303	JN606608
P. gallaicum	CBS 167.81T	JN617690	JN606837	JN606548	JN606609
P. paxilli	CBS 360.48T	GU944577	JN606844	JN606566	JN606610
P. roseopurpureum	CBS 226.29T	GU944605	JN606838	JN606556	JN606613
P. wellingtonense	CBS 130375T	JN617713	JN606670	MN969311	JN606616
P. pasqualense	CBS 126330T	JN617676	JN606673	MN969286	JN606617
P. manginii	CBS 253.31T	GU944599	JN606651	MN969274	JN606618
P. raphiae	CBS 126234T	JN617673	JN606657	MN969292	JN606619
P. atrofulvum	CBS 109.66T	JN617663	JN606677	JN606387	JN606620
P. decaturense	CBS 117509T	GU944604	GU944604	MN969252	JN606621
P. quebecense	CBS 101623T	JN617661	JN606700	JN606509	JN606622
P. miczynskii	CBS 220.28T	GU944600	JN606706	MN969277	JN606623
P. christenseniae	CBS 126236T	JN617674	JN606680	MN969243	JN606624
P. westlingii	CBS 231.28T	GU944601	JN606718	MN969312	JN606625
P. godlewskii	CBS 215.28T	JN617692	JN606768	MN969258	JN606626
P. waksmanii	CBS 230.28T	GU944602	JN606779	MN969310	JN606627
P. chrzaszczii	CBS 217.28T	GU944603	JN606758	MN969244	JN606628
P. vanluykii	CBS 131539T	JX997007	JX996879	JX996220	JX996615
P. allii-sativi	DTO 149-A8T	JX997021	JX996891	JX996232	JX996627
P. tardochrysogenum	CBS 132200T	JX997028	JX996898	JX996239	JX996634

P. rubens	CBS 129667T	JX997057	JF909949	JX996263	JX996658
P. halotolerans	DTO 148-H9T	JX997005	JX996816	JX996935	JX996680
P. desertorum	DTO 148-I6T	JX997011	JX996818	JX996937	JX996682
P. confertum	CBS 171.87T	JX997081	AY674373	JX996963	JX996708
P. mononematosum	CBS 172.87T	JX997082	AY495997	JX996964	JX996709
P. goetzii	CBS 285.73T	JX997091	KU896815	JX996971	JX996716
P. nalgiovense	CBS 352.48T	AY371617	KU896811	JX996974	JX996719
P. lanosocoeruleum	CBS 215.30T	JX997110	KU896817	JX996967	JX996723
P. samsonianum	CBS 138919T	KJ668590	KJ668582	KJ668586	KT698899
P. paneum	CBS 101032T	HQ442346	AY674387	HQ442331	KU904361
P. psychrosexuale	CBS 128137T	HQ442345	HQ442356	HQ442330	KU904362
P. mediterraneum	FMR 15188T	LT899784	LT898291	LT899768	LT899802
P. argentinense	CBS 130371T	JN831361	JN606815	JN606549	MN969105
P. aurantiacobrunneum	CBS 126228T	JN617670	JN606702	MN969238	MN969106
P. cairnsense	CBS 124325T	JN617669	JN606693	MN969240	MN969108
P. cosmopolitanum	CBS 126995T	JN617691	JN606733	MN969249	MN969113
P. neomiczynskii	CBS 126231T	JN617671	JN606705	MN969278	MN969128
P. nothofagi	CBS 130383T	JN617712	JN606732	JN606507	MN969129
P. pancosmium	CBS 276.75T	JN617660	JN606790	MN969284	MN969130
P. sanguifluum	CBS 127032T	JN617681	JN606819	JN606555	MN969135
P. sucrivorum	DTO 183-E5T	JX140872	JX141015	JX141506	MN969140
P. ubiquetum	CBS 126437T	JN617680	JN606800	MN969306	MN969142
P. vancouverense	CBS 126323T	JN617675	JN606663	MN969307	MN969143
P. floccosum	CGMCC3.25422T = CC-2	OR512914	OR594640	OR594641	OR538540
P. acidogenicum	CGMCC3.25421T = CC-1	OR512884	OR531524	OR538539	OR538541
gCoAvM063_F7					
Aspergillus_fumigatus_Af293	CBS 101355				
P_novae-zeelandiae	CBS 137.41	MH856089.1	KJ834477.1	KJ866996.1	JN406628.1

1252

1253 Table S8: Strains used for the taxonomic identification within the *Plectospaerella* genus

Strains	**Culture accession number**	**GenBank_ITS**	**GenBank_LSU_LROR-LR5**	**GenBank_TUB2**	**GenBank_tef1**
Monilochaetes infuscans	CBS 379.77	LR026764	GU180645	–	–
P. humicola	CBS 423.66^{T}	LR026811	LR025949	–	–
P. hanneae	CBS 144925	LR590201	LR590378	–	–
P. nauculaspora	CGMCC 3.19656^{T}	MK880439	MK880424	–	–
P. guizhouensis	CGMCC 3.19658^{T}	MK880441	MK880431	–	–
P. kunmingensis	KUMCC 18-0181	MK993014	MK993015	–	–

P. oligotrophica	CGMCC 3.15078^{T}	KY399817	JX508806	KY421309	KY421315
P. ramiseptata	CBS 131743	KY399819	KY662252	KY421306	KY421318
P. citrullae	CBS 131741^{T}	KY399822	KY662255	KY421308	KY421320
P. plurivora	CBS131742^{T}	KY399826	KY662248	KY421298	KY421324
P. sinensis	ACCC 39144	KX527889	KX527892	KY421313	KY421326
Plectosphaerella alismatis	CBS 113362^{T}	KY399815	KY662261	KY421304	KY421328
P. melonis	CBS 489.96^{T}	KY399813	KY662260	KY421295	KY421329
P. cucumerina	3F17	KY401602	KY399831	KY421300	KY421331
P. populi	CBS139623^{T}	KY399828	KY662257	KY421311	KY421336
P. delsorboi	CBS 116708^{T}	KY499237	EF543843	KY499240	KY499238
P. endophytica	YMF 1.04701	MW024054	MW024052	MW029608	MW029607
P. sichuanensis	YMF 1.05081	MW027539	MW027535	MW441780	MW309880
P. pauciseptata	YMF 1.04725	MW024104	MW466575	MW441784	MW441779
gCoJuM088_F4					

1254

1255 Table S9: Strains used for the taxonomic identification within the *Sarocladium genus*

Strains	**Culture accession number**	**GenBank_ITS**	**GenBank_LSU**
Chlamydocillium curvulum	CBS 430.66*	HE608638	HE608656
S. glaucum	CBS 796.69*	OQ429841	HE608657
S. oryzae	CBS 180.74*	HG965026	HG965047
S. bifurcatum	UTHSC 05-3311*	HG965009	HG965057
S. hominis	UTHSC 04-1034*	HG965012	HG965060
S. hominis	UTHSC 04-3464	HG965013	HG965061
S. gamsii	CBS 707.73*	HG965015	HG965063
S. implicatum	CBS 959.72*	HG965023	HG965072
S. pseudostrictum	UTHSC 02-1892*	HG965029	HG965073
S. subulatum	MUCL 9939*	HG965031	HG965075
S. summerbellii	CBS 430.70*	HG965034	HG965078

S. bactrocephalum	CBS 749.69*	HG965006	HQ231994
S. kiliense	CBS 122.29*	AJ621775	HQ232052
S. ochraceum	CBS 428.67*	HG965025	HQ232070
S. strictum	CBS 346.70*	FN691453	HQ232141
S. zeae	CBS 800.69*	FN691451	HQ232152
S. spinificis	Z0106 Ex-type	KF269096	JQ954463
S. brachiariae	CGMCC 2192*	EU880834	KP715271
S. terricola	CBS 243.59*	MH857853	MH869389
S. bacillisporum	CBS 425.67*	HE608639	MH870718
S. dejongiae	CBS 144929*	MK069419	MK069415
S. theobromae	CBS 113440 Ex-type	OQ429856	OQ430108
***S. menglaense* sp. nov.**	**KO1-8***	PV737445	PV737452
***S. yunnanense* sp. nov.**	**WF8-2a1***	PV737449	PV737456
gCoAvM140_F5			

1256

1257 Table S10: Strains used for the taxonomic identification within the *Trichoderma genus*

Strains	Culture accession number	GenBank_rpb2	GenBank_tef1
T. harzianum	CBS 226.95 ET	AF545549	AF348101
T. atroviride	CBS 142.95 ET	EU341801	AY376051
T. viride	CBS 119325 ET	EU711362	DQ672615
Protocrea farinosa	CBS 121551 T	OP357962	EU703889
Protocrea pallida	CBS 299.78 ET	EU703948	EU703900
T. afroharzianum	GJS 04–193	FJ442709	FJ463298
T. afroharzianum	CBS 124620 ET	FJ442691	FJ463301
T. atrobrunneum	GIS 04–67	FJ442724	FJ463360
T. atrobrunneum	GJS 05–101	FJ442745	FJ463392
T. atroviride	CBS 119499	FJ860518	FJ860611
T. guizhouense	CBS 131803 T	JQ901400	JN215484
T. guizhouense	HGUP 0039	JQ901401	JX089585
T. paratroviride	CBS 136489 T	KJ665321	KJ665627
T. paratroviride	S489	KJ665322	KJ665628
T. pyramidale	CBS 135574 ET	KJ665334	KJ665699
T. harzianum	TRS94	KP009120	KP008802
T. harzianum	TRS55	KP009121	KP008803
T. viride	TRS575	KP009081	KP008931
T. pyramidale	T20	KX632570	KX632627

T. breve	CGMCC 3.18398 T	KY687983	KY688045
T. breve	HMAS 248845	KY687984	KY688046
T. zeloharzianum	YMF 1.00268 ET	MH158996	MH183181
T. anaharzianum	YMF 1.00383 T	MH158995	MH183182
T. asiaticum	YMF 1.00352 T	MH158994	MH183183
T. asiaticum	YMF 1.00168	MH262575	MH236492
T. paraviride	YMF 1.04628 T	MK775513	MK775508
T. uncinatum	YMF 1.04622 T	MK795990	MK795986
T. zelobreve	CGMCC 3.19695 T	MN605872	MN605883
T. zelobreve	CGMCC 3.19696	MN605873	MN605884
T. obovatum	YMF 1.6190	MT038433	MT070143
T. obovatum	YMF 1.06211 T	MT038432	MT070144
T. simile	YMF1.6180	MT052185	MT070153
T. simile	YMF 1.06201 T	MT052184	MT070154
T. pholiotae	JZBQH11	ON649971	ON649918
T. pholiotae	JZBQH12 T	ON649972	ON649919
T. densissimum	T31818	OP357965	OP357967
T. paradensissimum	T31823 = CGMCC 3.24125 T	OP357962	OP357968
T. paradensissimum	T31824	OP357961	OP357969
T. densissimum	T32353	OP357964	OP357970
T. densissimum	T32434 = CGMCC 3.24126 T	OP357966	OP357971
T. densissimum	T32465	OP357963	OP357972
T. nigricans	T32450	OP357958	OP357973
T. nigricans	T32781 = CGMCC40314 T	OP357959	OP357974
T. nigricans	T32794	OP357960	OP357975
pCoAvP042_F9			

1258 Table S11: Strains used for the taxonomic identification within the different yeast genus

Strains	**Culture accession number**	**GenBank_ITS**	**GenBank_LSU**
Vishniacozyma alagoana CBS15966 T	CBS15966	MH885328	MH909005
Vishniacozyma carnescens CBS 973 T	CBS973	NR130695	KY110023
Vishniacozyma catalpae CGMCC 2.6902 T	CGMCC2.6902	OP470302	OP470206
Vishniacozyma changhuana HM6L11 T	HM6L11	MT906456	MT906468
Vishniacozyma dimennae CBS 5770 T	CBS5770	KY105820	KY110025
Vishniacozyma diospyri NYNU 221044 T	NYNU221044	OP954624	OP954569
Vishniacozyma ellesmerensis JCM 32573 T	JCM32573	LC335796	LC335796

Vishniacozyma equisetis VKM Y-2979 T	VKMY-2979	HM749321	HM749316
Vishniacozyma eriobotryae NYNU 229203 T	NYNU229203	OP566897	OP566895
Vishniacozyma europaea CGMCC2.3099 T	CGMCC2.3099	MK050335	MK050335
Vishniacozyma floricola NCAIM Y.02320 T	NCAIMY.02320	PP337022	PP261370
Vishniacozyma foliicola CBS 9920 T	CBS9920	KY105821	KY110026
Vishniacozyma guiyangensis NYNU 22831 T	NYNU22831	OP566869	OP566870
Vishniacozyma marinae MLWB11-2 T	MLWB11-2	OP470294	OP470198
Vishniacozyma melezitolytica CGMCC2.3472 T	CGMCC2.3472	MK050330	MK050330
Vishniacozyma paravictoriae NYG10-6 T	NYG10-6	OP470300	OP470204
Vishniacozyma peneaus CBS 2409 T	CBS2409	KY105826	KY110032
Vishniacozyma phoenicis KBP Y-6564 T	KBPY-6564	MN449981	MN449981
Vishniacozyma pingtangensis NYNU 23281 T	NYNU23281	OQ851896	OQ851894
Vishniacozyma pini XZY496-1 T	XZY496-1	OP470296	OP470200
Vishniacozyma pseudocarnescens CGMCC 2.6457 T	CGMCC2.6457	OR077051	OR077057
Vishniacozyma pseudodimennae CGMCC 2.6790 T	CGMCC2.6790	OM417179	OM417179
Vishniacozyma pseudopenaeus CGMCC2.3165 T	CGMCC2.3165	MK050333	MK050333
Vishniacozyma pyri T1-6-1 T	T1-6-1	OP470298	OP470202
Vishniacozyma siamensis DMKU- SG26 T	DMKU-SG26	LC786857	LC797015
Vishniacozyma sinopodophylli XZY87M1 T	XZY87M1	OP470297	OP470201
Vishniacozyma taibaiensis CBS 9919 T	CBS9919	KY105827	KY110033
Vishniacozyma taiwanica HM5L06 T	HM5L06	MT906464	MT906477
Vishniacozyma tephrensis CBS 8935 T	CBS8935	NR144812	KX507032
Vishniacozyma terreae YP344 T	YP344	MZ734447	MZ734225
Vishniacozyma tianchiensis NYNU 236163 T	NYNU236163	OR426458	OR426457
Vishniacozyma zhenxiongensis CGMCC 2.6901 T	CGMCC2.6901	OP470301	OP470205
Vishnicozyma paraequisetis VKM Y-2980 T	VKMY-2980	HM749319	HM749318
gCoAvM139_Y2			
gCoMoP172_Y3			
gCoJuM081_Y4			
gCoJuM089_Y10			
Bullera alba CBS 500 T	CBS500	KY101811	KY106260
Bullera coprosmaensis CBS 8284 T	CBS8284	KY103497	KY107778
Bullera dendrophila CBS 6074 T	CBS6074	KY103932	KY108198
Bullera hannae CBS 8286 T	CBS8286	KY101788	KY106238
Bullera miyagiana CBS 7526 T	CBS7526	KY105560	KY109797
Bullera penniseticola CBS 8623 T	CBS8623	KY101792	KY106242
Bullera unica CBS 8290 T	CBS8290	KY101799	KY106248
Bullera variabilis CBS 7347 T	CBS7347	KY101808	AF189855
gCoMoM118_Y7			
Filobasidium castaneae sp. nov. NYNU 2111105T	NYNU2111105	OM049430	OM049431
Filobasidium chaidanensis CGMCC 2.6796 T	CGMCC2.6796	OM417191	OM417191
Filobasidium chernovii CBS 8679 T	CBS8679	KY103413	KY107701
Filobasidium dingjieense CGMCC2.5649 T	CGMCC2.5649	MK050342	MK050342
Filobasidium elegans CBS 7640T	CBS7640	AF190006	AF181548
Filobasidium floriforme CBS 6241T	CBS6241	NR119429	NG069409
Filobasidium globisporum CBS 7642T	CBS7642	NR119453	NG070553

Filobasidium globosum CGMCC2.5680 T	CGMCC2.5680	MK050344	MK050344
Filobasidium magnum CBS 140 T	CBS140	KY103433	KY107722
Filobasidium mali CGMCC2.4012 T	CGMCC2.4012	MK050346	MK050346
Filobasidium mucilaginum CGMCC2.3463 T	CGMCC2.3463	MK050349	MK050349
Filobasidium oeirensis CBS 8681T	CBS8681	NR077106	NG070508
Filobasidium pseudomali sp. nov. NYNU 228108T	NYNU228108	OP581930	OP566876
Filobasidium qingyuanense sp. nov. NYNU 223211T	NYNU223211	OP278683	OP278680
Filobasidium stepposum CBS 10265T	CBS10265	NR111207	KY107724
Filobasidium uniguttulatum CBS 1730 T	CBS1730	KY103442	KY107727
pCoJuP176_Y1			
Holtermannia pseudosaccardoi 21825S-11 T	21825S-11	OP470257	OP470161
Holtermannia saccardoi strain CGMCC2.3445 T	CGMCC2.3445	MK050336	MK050336
Holtermanniella festucosa CBS 10162 T	CBS10162	KY102693	KY107040
Holtermanniella nyarrowii CBS 8804 T	CBS8804	KY103594	KY107873
Holtermanniella takashimae CBS 11174 T	CBS11174	FM246501	FM242574
Holtermanniella wattica CBS 9496 T	CBS9496	KY103595	KY107874
gCoJuP095_Y6			
gCoAvP126_Y8			
pCoJuM023_Y9			
Papiliotrema anemochoreius CBS 10258 T	CBS10258	KY104455	KY108727
Papiliotrema aspenensis DS573 T	DS573	KC485500	KC469778
Papiliotrema aureus CBS 318 T	CBS318	LK023832	LK023771
Papiliotrema baii CF12 T	CF12	LK023827	LK023766
Papiliotrema bandonii CBS 9107 T	CBS9107	NR121465	AF416642
Papiliotrema castaneae YN83-2 T	YN83-2	OP470272	OP470176
Papiliotrema catalpae YN109M3 T	YN109M3	OP470271	OP470175
Papiliotrema fonsecae EXF-4087 T	EXF-4087	JN193468	JN193447
Papiliotrema frias CRUB 1250 T	CRUB1250	GU997162	GU560004
Papiliotrema hoabinhensis VY-68 T	VY-68	AB110695	AB193347
Papiliotrema huenov KCNT-2019a T	KCNT-2019a	MN535049	MN539617
Papiliotrema japonica CBS 2013 T	CBS2013	AF444666	AF444760
Papiliotrema laurentii CBS 139 T	CBS139	KY104469	KY108739
Papiliotrema leoncinii CBS13918 T	CBS13918	KP203864	KJ608554
Papiliotrema mangalensis CBS 10870 T	CBS10870	KY102795	KY107130
Papiliotrema miconiae CBS 8358 T	CBS8358	AF444387	AF444698
Papiliotrema nemorosus VKM Y-2906 T	VKMY-2906	AF472628	AF472625
Papiliotrema odontotermitis CBS 14181 T	CBS14181	KU883277	KU883278
Papiliotrema perniciosus VKM Y-2905 T	VKMY-2905	AF472627	AF472624
Papiliotrema pseudoalba CBS 8294 T	CBS8294	KY101794	KY106243
Papiliotrema rajasthanensis CBS 10406 T	CBS10406	KY104474	KY108743
Papiliotrema ruineniae CF03 T	CF03	LK023825	LK023764
Papiliotrema siamense CBS 13330 T	CBS13330	AB915387	AB909023
Papiliotrema sp. PYCC:6306	PYCC:6306	LK023830	LK023769
Papiliotrema taeanensis KCTC 17149 T	KCTC17149	AY686645	AY422719
Papiliotrema terrestris CBS 10810 T	CBS10810	KY104476	KY108747
Papiliotrema wisconsinensis yHKS301 T	yHKS301	KM384105	KM408131
Papiliotrema zeae B689 T	B689	MH718306	MH718306

gCoJuP099_Y11			
Symmetrospora clarorosea CBS 14055 T	CBS14055	KJ701231	KJ701232
Symmetrospora coprosmae CBS 7899 T	CBS7899	KY105570	KY109807
Symmetrospora foliicola CBS 8075 T	CBS8075	KY105571	KY109808
Symmetrospora gracilis CBS 71 T	CBS71	AF444578	AF189985
Symmetrospora marina CBS 2365 T	CBS2365	KY105572	KY109809
Symmetrospora oryzicola CBS 7228 T	CBS7228	KY105520	KY109758
Symmetrospora pini CICC 33601 T	CICC33601	OQ851927	OQ851926
Symmetrospora pseudomarina CBS 14057 T	CBS14057	KJ701216	KJ701217
Symmetrospora rhododendri CGMCC2.2613 T	CGMCC2.2613	MK050388	MK050388
Symmetrospora salmoneus CGMCC 2.6801 T	CGMCC2.6801	OM417187	OM417187
Symmetrospora suhii CBS 14094 T	CBS14094	KJ701206	AY520389
Symmetrospora symmetrica CBS 9727 T	CBS9727	KY105573	KY109810
Symmetrospora vermiculata CBS 9092 T	CBS9092	KY105574	AF460176
gCoAvM141_Y5			
Acremonium aerium	CBS:189.70	OQ429441	OQ055352.1

Table S12: Output of the NbClust R package used to choose the optimal number of clusters of seedling bacterial communities

Method	Number_clusters	Value_Index
Hubert	0	0.0000
Dindex	0	0.0000
CH	2	519.9080
CCC	2	6.5011
DB	2	0.5717
Silhouette	2	0.6698
Beale	2	1.4637
PtBiserial	2	0.8521
Frey	2	4.5388
McClain	2	0.3072
Dunn	2	0.3109
SDindex	2	15.0654
TrCovW	3	0.2779
Duda	3	1.1009
PseudoT2	3	-5.3151
Ratkowsky	3	0.4492
Ball	3	0.5761
Hartigan	4	107.9825
KL	5	14.4125
Scott	5	200.8912
Marriot	5	5.0808
TraceW	5	0.5400
Friedman	5	18.6690
Rubin	5	-2.6809
Cindex	5	0.2221

SDbw	10	0.1308

Table S13: Main metrics of the three co-occurrence networks, divided between entire networks and giant and peripheral components.

Network	Component	Total node number	Inoculated strain number	Differentially abundant ASVs number	Node degree	Normalized node degree	Density
Full	Total	6890	36	82	4443	0.64	1.87E-04
Full	Giant	2400	29	82	4017	1.67	1.40E-03
Full	Periph	4490	7	0	426	0.09	4.23E-05
Cluster1	Total	3189	34	77	2135	0.67	4.20E-04
Cluster1	Giant	1220	27	73	1885	1.55	2.53E-03
Cluster1	Periph	1969	7	4	250	0.13	1.29E-04
Cluster2	Total	3211	32	81	2213	0.69	4.29E-04
Cluster2	Giant	1263	23	74	1903	1.51	2.39E-03
Cluster2	Periph	1948	9	7	310	0.16	1.63E-04

265

Supplementary material and methods: SynCom Composition Space Analysis

Strain Pool and Experimental Design

The synthetic community (SynCom) strain pool comprised 45 microbial isolates distributed across three kingdoms: 24 bacteria (B1–B24), 10 fungi (F1–F10), and 11 yeasts (Y1–Y11). Each SynCom was assembled under a balanced combinatorial constraint of exactly 4 bacteria, 4 fungi, and 4 yeasts (4B+4F+4Y), yielding a total theoretical design space of:

$$\binom{24}{4} \times \binom{10}{4} \times \binom{11}{4} = 10.626 \times 210 \times 330 = 736.164.600\ possible\ combinations$$

Nineteen SynComs were experimentally designed, including randomly assembled communities (Rand1–Rand10), ecologically informed assemblages (MostAbun, MostAbunSeed, MostAbunSeedling, FastGrowth, Rare1, Rare2, AbunGrad), and phylogenetically diverse assemblages (PhylDiv1, PhylDiv2).

Theoretical Space Sampling

To represent the full theoretical composition space, 5,000 communities were generated by random sampling without replacement of 4 strains from each kingdom pool (set.seed = 42), representing approximately 0.00068% of all possible combinations. This Monte Carlo approach served as a tractable proxy for the full combinatorial space in all subsequent analyses.

Compositional Dissimilarity and Ordination

Pairwise compositional dissimilarity between all communities (theoretical and effective) was quantified using the binary Jaccard distance: $d_j(A, B) = 1 - \frac{|A \cap B|}{|A \cup B|}$

computed via the *vegdist* function (vegan; Oksanen et al, 2007). For two 12-member communities sharing s strains, this simplifies to $d_j = (24 - 2s)/(24 - s)$, yielding distances anchored to discrete integer strain-sharing levels (*e.g.*, $d_j = 0.5$ at $s = 8$; $d_j = 0.667$ at $s = 6$).

Pairwise Jaccard distances were first computed among the 19 experimentally designed SynComs alone, and subsequently on a combined presence–absence matrix constructed by row-binding the 5,000 theoretical communities and the 19 designed SynComs (5,019 × 45). Both distance matrices were subjected to Principal Coordinates Analysis (PCoA) using the pcoa function (ape package) with Cailliez correction for negative eigenvalues, retaining the first two axes for visualisation. Designed SynComs were overlaid on the theoretical space point cloud using the combined PCoA ordination.

Dispersion of Designed SynComs Relative to Random Sets

To assess whether the 19 designed SynComs collectively span more compositional space than expected by chance, their mean pairwise Jaccard dissimilarity was computed as an observed dispersion statistic. A permutation null distribution was generated by repeatedly drawing 19 random 4B+4F+4Y communities from the full strain pool (n = 5,000 permutations; set.seed = 42) and computing their mean pairwise Jaccard dissimilarity. A one-sided p-value was estimated as the proportion of permuted sets yielding a mean pairwise Jaccard dissimilarity greater than or equal to the observed value.

Nearest-Neighbour Distance to Theoretical Composition Space

To quantify how well each designed SynCom was embedded within the theoretical composition space, the Jaccard distance from each of the 19 designed SynComs to its nearest neighbour among the 5,000 theoretical communities was extracted from the full cross-distance submatrix. Lower nearest-neighbour (NN) distances indicate greater compositional representativeness of the theoretical space. As a null reference, the self-NN

distance distribution of the theoretical space was computed by identifying, for each of the 5,000 random communities, the distance to its closest neighbour among all remaining random communities. The two distributions were compared visually, and a one-sided p-value was estimated as the proportion of theoretical self-NN distances greater than or equal to the mean NN distance of the designed SynComs. Individual NN distances were additionally ranked per SynCom and stratified by design strategy (A priori vs. Random) to identify which communities occupied peripheral versus representative regions of the composition space, using the mean theoretical self-NN distance as a reference threshold.